FABRICATION AND CHARACTERIZATION OF Al, AlMgSi AND AlSi FOAMS

by

Nazım Mahmutyazıcıoğlu

B.S., Mechanical Engineering, Istanbul Technical University, 1998

M.S., Mechanical Engineering, Boğaziçi University, 2002

Submitted to the Institute for Graduate Studies in
Science and Engineering in partial fulfillment of
the requirements for the degree of
Doctor of Philosophy

Graduate Program in Mechanical Engineering

Boğaziçi University

2010

ACKNOWLEDGEMENTS

First, I would like to thank my thesis supervisor Prof. Dr. Sabri ALTINTAŞ for his continuous support during my Ph.D. work. He was always there to listen and to give advice. I am grateful for his invaluable guidance and help during the preparation of this dissertation which could not have been completed without his patience, encouragement and motivation. I am also grateful to the members of my thesis committee, Prof. Dr. Mahmut Ahsen SAVAŞ and Prof. Dr. Turan ÖZTURAN for their encouraging support and guidance. They have been kind to give their valuable time and have always been positive about the progress and outcomes of my study in our regular meetings.

Besides my supervisor and other members of the thesis committee, I would like to thank to my colleagues Önder ALBAYRAK and Mehmet İPEKOĞLU. They made Materials Science and Manufacturing Techniques Laboratory a wonderful workplace and home for the past six years by indulging my absence in some of the laboratory work in order to complete this dissertation. I also would like to thank to all my friends very much for being with me and helping me to have fun even in the bad times.

I am greatly indebted to the professors of Mechanical Engineering Department of Boğaziçi University for teaching me how to be persistent to accomplish the goals of the courses I have taken. Let me also say “thank you” to the staff of Mechanical Engineering Department Hicran KIRILMAZ and Seher YILDIZ for their positive motivation and help in preparing the necessary documents for our regular meetings with the thesis committee.

I would also like to thank to the following people; İbrahim MUTLU for his help in preparation of my experimental set-up and specimens, Hasan Cem ÇİTAK for the extrusion press, Adil GÜREL from Gürel Makina A.Ş. and Talar HİSARLI from Hisarlı Ltd. for providing the aluminum powders, Aydın GÜRLER from Chemetall A.Ş. for providing the titanium hydride powder, S. Burhan YILDIZ from Yıldız Isıl İşlem San. Ve Tic. A.Ş., Satı ŞİMŞİR from Hidro Pno Market A.Ş. and Cem OCAKÇI from Dalgıç Kalıp Metal ve Plastik San. Tic. Ltd. Şti.

Lastly, but not least, I thank my family. My parents Neslihan and Nizam MAHMUTYAZICIOĞLU, for raising me as I am and for their unconditional support both financially and morally. They have always encouraged me to follow my interests, even when they were sometimes not reasonable. My brother Murat MAHMUTYAZICIOĞLU, for listening to my complaints and frustrations with patience, and for reminding me that I was getting old and had to work harder. I also thank to all the other members of my family, for their encouragement and for believing in me.

This work was supported in part by the Turkish State Planning Agency (DPT-03K120250) and Boğaziçi University Scientific Research Project (BAP-07A603D). I would like to thank Boğaziçi Üniversitesi Vakfı (BÜVAK) and Fen Bilimleri Enstitüsü (FBE) for their financial support, which helped me presenting my work at the conferences held in Canada and Germany.

ABSTRACT

FABRICATION AND CHARACTERIZATION OF Al, AlMgSi AND AlSi FOAMS

Manufacturing of metal foams by using powder compact melting (PCM) method, with the most important considerations like material and method selection, powder blending, cold compaction, hot compaction and hot extrusion and foaming is explained briefly. The effects of Al_2O_3 particle addition on the heat treatment, cell structure and mechanical properties of AlMgSi foams were studied. Alloy and composite foams were manufactured by powder compact melting (PCM) method. A pre-blended mixture of Al, Mg, Si and Cu representing the wrought AlMgSi alloy (6061) were mixed with heat treated TiH_2 and Al_2O_3 ceramic particles, hot compacted and foamed at temperatures between 750 and 800 °C. The amount of <20μm sized Al_2O_3 particles in the composite foams were 3, 5 and 10 per cent by volume. The effects of different heat treatments on the microhardness of the foams were investigated. Foams that were fully heat treated had the highest hardness values and they performed best with an increase in collapse strength up to 100 per cent over the untreated samples. It was found that the addition of Al_2O_3 did not affect the hardenability but the strength and the compression stiffness of the composite foams were increased with 3 and 5 vol. per cent Al_2O_3 addition. This was attributed to the improved cell structure and decreased drainage when the ceramic amount is not more than 5 per cent. The compression test results were interpreted in terms of the foam's microstructure and correlations were made relating the unloading modulus and compression strength of the foams with the relative density. It was found that the foams were inhomogeneous and their mechanical properties were close to those expected from open cell foams.

An important phenomenon in Al foam production is stabilization of the structure. Especially it is very difficult to obtain highly expanded foams made from pure Al powder. In this study, an improvement in the stabilization was achieved by Al_2O_3 and B_4C ceramic powder addition to the Al-TiH_2 mixtures. Compaction of the mixture was achieved by hot

extrusion. Extruded dense semi-products (precursors) were foamed at 800 °C and the macro and microstructures of the foams were analyzed. It was found that both of the ceramics increased the number of cells and cell size homogeneity of Al foams. The stabilization seems to be enhanced with the presence of solid constituents but the mechanism acting could not be understood clearly. Most of the ceramic particles were partially wetted and segregation between the metal and gas interface was observed. The wetting of B_4C particles by the aluminum matrix was relatively better and this resulted in smoother foam cell walls when compared with the cell walls of pure and Al_2O_3 added Al foams.

Finally, a different matrix alloy, hypereutectic AlSi (AlSi14Cu2.5Mg0.6) was used for foam manufacturing by PCM method. The alloy has some advantages over the Mg, Cu and Zn added alloys like good wear resistance, high mechanical strength without aging heat treatment and dimensional stability. Foams manufactured were heat treated, in order to analyze the changes in the microstructure and the mechanical properties. The results showed that, heat treatment caused spheroidizing of eutectic Si phases and depending on the density, the compression strength of the foams could be increased up to 50 per cent. The deformation of the foam was similar to brittle foams and densification strain was higher than ductile foams which makes it a good candidate for energy absorption applications.

ÖZET

Al, AlMgSi ve AlSi KÖPÜKLERİN ÜRETİMİ VE KARAKTERİZASYONU

Sıkıştırılmış toz ergitme yöntemi (STE) ile metal köpüklerin üretimi ve üretim esnasında dikkate alınması gereken işlemlerden malzeme ve metot seçimi, tozların karıştırılması, soğuk sıkıştırma, sıcak sıkıştırma, sıcak ekstrüzyon ve köpürtme kısaca açıklanmıştır. Al_2O_3 seramik parçacıkları katılmasının AlMgSi matrisli köpüklerde ısıl işleme, hücre yapısına ve mekanik özelliklere etkisi incelenmiştir. Alüminyum alaşımı ve kompozit köpükler STE metoduyla üretilmiştir. AlMgSi (6061) alaşımını temsilen önceden hazırlanmış Al, Mg, Si ve Cu toz karışımı ile ısıl işlemden geçmiş TiH_2 tozu ve Al_2O_3 seramik parçacıkları karıştırılmış, karışım sıcak şekilde sıkıştırılmış ve çıkan ürün 750 ile 800 °C arası sıcaklıklarda köpürtülmüştür. Kompozit köpüklerde kullanılan <20 μm Al_2O_3 miktarı hacmen 3, 5 yüzde 10 olarak seçilmiştir. Köpüklerin farklı ısıl işlemlerden geçirilmesinin mikrosertlik değerlerine etkileri incelenmiştir. Tam bir ısıl işlemden geçen köpükler en yüksek basma dayanımını göstermiş ve ısıl işlemden geçmeyen köpüklere kıyasla yüzde yüzlere kadar varan artışlar ölçülmüştür. Al_2O_3 parçacıkların ısıl işlemle sertleşme kabiliyetini etkilemediği görülürken, hacmen yüzde 3 ve 5 katıldığında basma rijitliği ve dayanımda artma tespit edilmiştir. Bu artışın seramik tozun katılması sonucunda köpüğün hücre yapısındaki iyileşme ve azalan drenajdan olduğu düşünülmektedir. Basma testi sonuçları köpüklerin mikroyapısı ile birlikte yorumlanmış ve ölçülen elastikiyet modülleri ve basma dayanımları ile bağıl yoğunluk arasında ilişkiyi veren eşitlikler elde edilmiştir. Sonuç olarak köpüklerin genel olarak homojen olmadıkları ve elde edilen eşitliklerden köpüklerin mekanik özelliklerinin açık hücreli bir köpükten beklenen değerlere yakın olduğu bulunmuştur.

Alüminyum köpük üretiminde önemli bir kavram da köpürme sırasındaki yapısal kararlılıktır. Özellikle saf alüminyumla yüksek köpürme oranlarını elde etmek çok güçtür. Bu çalışmada, Al-TiH_2 toz karışımına Al_2O_3 ve B_4C seramik parçacıklar ilave edilerek

köpürmede bir iyileştirme sağlanmıştır. Karışımın sıkıştırılması sıcak ekstrüzyon işlemiyle gerçekleştirilmiştir. Extrüzyondan elde edilen ara-ürünler 800 °C de köpürtülmüş ve makro ile mikro yapıları incelenmiştir. Her iki seramik katkısının da Al köpüklerin hücre sayısını ve hücre boyutlarının homojenliğini arttırdığı görülmüştür. Köpürme sırasındaki kararlılığının katı bileşenler sayesinde artıyor göründüğü tespit edilmekle birlikte bunu sağlayan mekanizma tam olarak anlaşılamamıştır. Seramik parçacıklarının birçoğunun sıvı Al matris tarafından kısmi olarak ıslatıldığı ve katılaşma sonrasında metal ile gaz arasında ayrışarak hücre duvarlarında konumlandıkları gözlemlenmiştir. B_4C parçacıklarının Al_2O_3 parçacıklarına göre Al matris tarafından daha iyi ıslatıldıkları görülmüş ve bunun sonucunda saf Al ve Al_2O_3 eklenmiş Al köpüklerin hücre duvarlarına göre daha düzgün bir hücre duvarı yüzeyine sahip köpükler elde edilmiştir.

Son olarak STE metoduyla farklı bir matris alaşımı ötektik-üstü bir AlSi (AlSi14Cu2.5Mg0.6) kullanılarak köpük üretilmiştir. Bu yüksek Si içeren alaşımın Mg, Cu veya Zn içeren diğer Al alaşımlarına göre yüksek aşınma direnci, yaşlandırma yapılmadan elde edilebilen yüksek mekanik dayanım ve boyutsal kararlılık gibi bazı avantajları vardır. Üretilen köpükler ısıl işlemden geçirilmiş ve mikroyapı ile mekanik özellikleri incelenmiştir. Sonuçlar ısıl işlem ile ötektik Si tanelerinde küreselleşme olduğunu ve yoğunluğa bağlı olarak köpüklerin basma dayanımının yüzde 50'lere kadar arttırılabileceğini göstermektedir. Köpüklerin deformasyonu gevrek köpüklere benzer şekilde olmuş ve köpüğü sabit yük altında enerji emme uygulamalarına aday yapacak bir özellik olarak yoğunlaşma birim uzamasının sünek bir köpüğe göre daha yüksek olduğu görülmüştür.

TABLE OF CONTENTS

LIST OF FIGURES

LIST OF TABLES

LIST OF SYMBOLS/ABBREVIATIONS

ε_D	Densification strain
ρ	Density
ρ^*	Foam density
ρ_r	Relative density
ρ_s	Solid density
σ	Surface tension
σ_{cs}	Compression strength
σ_{ts}	Tensile strength
σ_{ys}	Yield strength
υ	Poisson's ratio
Φ	Fraction of solid in the foam cell edges
E	Young's modulus
E^*	Modulus of the foam
E_l	Lower bound elastic modulus
E_m	Elastic modulus of the matrix
E_r	Elastic modulus of the reinforcement
E_s	Modulus of the solid
f	Volume fraction of reinforcement
G	Shear modulus
H	Hardness
K	Bulk modulus
P_a	Ambient pressure
P_B	Bubble pressure
R	Radius of the bubble
R^2	Coefficient of determination
A231	AlSi blend
A321	AlMgSi blend

AC	Alternating current
AF	As foamed
AISI	American Iron and Steel Institute
CIP	Cold isostatic pressing
DIN	Deutsche Industrial Norms
EDM	Electro discharge machining
EDX	Energy dispersive X-ray
EPS	Endogenous particle stabilization
HRC	Rockwell C hardness
HT	Heat treated
HV	Vickers hardness
MMC_p	Particle reinforced metal matrix composite
ONS	Oxide network particle stabilization
PCM	Powder compact melting
PM	Powder metallurgy
SEM	Scanning electron microscopy
SHT	Solution heat treatment
SPS	Solid particle stabilization
TEM	Transmission electron microscopy
TGA	Thermo-gravimetric analysis
XRD	X-ray diffraction

1. INTRODUCTION

Rigid porous or cellular products offer unique mechanical and physical properties. There is a wide range of engineering applications of these materials. They can be open cell or closed cell with respect to their cell topology. In filtration industry open cell products are used for liquid filtration. These products consist of a network of interconnected voids. This pore structure is also called “through pore”. Ceramics, plastics and metals can be engineered for this service. In ceramic industry open cell plastic molds are commonly used in slip casting of sanitarywares and dinnerwares as an alternative to gypsum (plaster) molds. Open cell cellular metals have high surface area over volume ratio which makes them candidates for catalytic surfaces and electrodes. These materials are also called open cell foams although they look like sponges. When the cells are not interconnected or each cell is sealed from each other by the cell walls the foam is said to be closed cell. The high specific strength, structural rigidity and insulating properties of closed cell foams produced from a polymer matrix are well known in the industry. Such polymeric foams are used extensively in a wide range of applications including construction, packaging and transportation. They are also used as core materials clad with metals as in a sandwich beam, which gives the structure a high flexural rigidity and high buckling strength at relatively low weight.

While polymeric foams have a wide market success, metal foams have seen only limited applications. Metallic foams offer many of the attractive attributes of polymeric foams like mechanical and thermal properties. In addition, the inherently higher bulk modulus of metals compared to polymers provides higher specific rigidity. This higher modulus makes metal foams attractive as core materials in laminate panels and sandwich beams where rigidity and resistance to deflection are important performance measures. Due to its cellular structure the metal foam can be compressed to very large strains. The force remains nearly constant up to high level of strains and when it is compared with the force in compression of its polymer counterparts the energy absorption is much higher.

In the subsequent section, the physical properties and important attributes of metal foams with attractive application potentials are summarized. Since the physical properties

and structure of metal foams are related to their production, a short survey on the principle manufacturing methods is also presented.

1.1. Metal Foams

Metal foams have a cellular structure, just like polymer foams but with cells made out of metal. Most of the metal foams are made of aluminum (Al) and its alloys, but they can also be made of another metal, for example copper (Cu), magnesium (Mg), nickel (Ni), steel, titanium (Ti) or zinc (Zn). The relative density of metal foams, which is found by dividing the density of metal foam by the density of solid metal, is less than 0.3, and it can even be as low as 0.02-0.10 [1]. Two types of metal foams can be distinguished, closed cell (foam like) or open cell (sponge like). In the closed cell foam the cells are sealed off from its neighbors and it looks like Figure 1.1a [2]. In the open cell foams the cells are interconnected and it has an appearance as in Figure 1.1b [2]. The connections in open cell foam are called struts, which meet in nodes. For closed cell foams the cells are closed by faces, which meet in cell edges, which in turn meet in nodes. Metal foams whether they are sponge like or foam like have many potential application areas. Table 1.1 [3] summarizes some potential application areas with engineering importance.

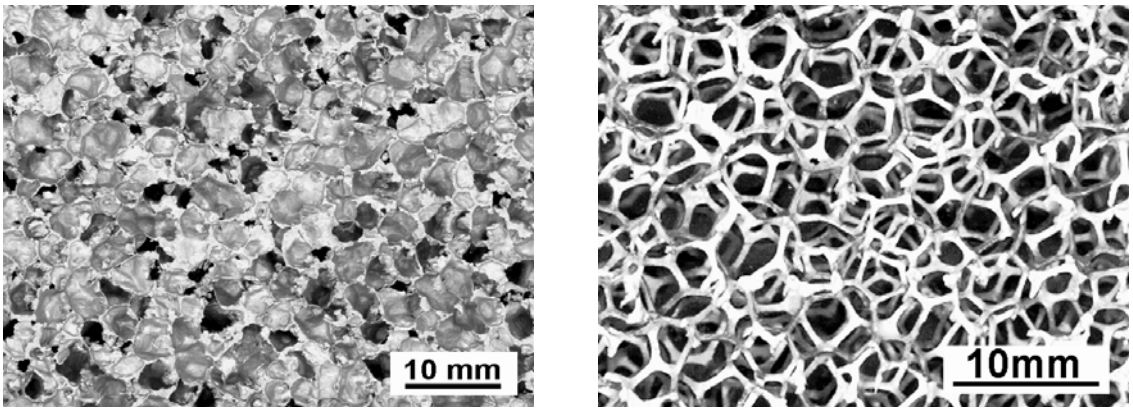

(a) (b)

Figure 1.1. Al foams: (a) Open cell, (b) Closed cell [2]

Table 1.1. Potential application areas for metal foams [3]

Application	Advantages
Lightweight structures	Excellent stiffness-to-weight ratio when loaded in bending
Sandwich cores	Metal foams have low density with good shear and fracture strength
Strain isolation	Metal foams can take up strain mismatch by crushing at controlled pressure
Mechanical damping	The damping capacity of metal foams is larger than that of solid metals
Vibration control	Foamed panels have higher natural frequency vibration frequencies than solid sheet of the same mass per unit area
Acoustic absorption	Reticulated metal foams have sound absorbing capacity
Energy management	Metal foams have exceptional ability to absorb energy at almost constant stress
Packaging with high-temperature capability	Ability to absorb impact at constant load, with thermal stability above room temperature
Artificial wood (furniture, wall panels)	Metal foams have some wood-like characteristics: light, stiff, and ability to be joined with wood screws
Thermal management: heat exchangers	Open cell foams have a large accessible surface area and high cell-wall conduction giving exceptional heat transfer ability
Thermal management: flame arresters	High thermal conductivity of cell edges together with high surface area quenches combustion
Thermal management: heat shields	Metal foams are non-flammable; oxidation of cell faces of closed cell aluminum foams appears to impart exceptional resistance to direct flame
Consumable cores for castings	Metal foams, injection molded to complex shapes, are used as consumable cores for aluminum castings
Biocompatible inserts	The cellular texture of biocompatible metal foams such as titanium stimulate cell growth
Filters	Open cell foams with controlled pore size have potential for fluid filtration
Electrical screening	Good electrical conduction, mechanical strength and low density make metal foams attractive for screening
Electrodes, and catalyst carriers	High surface/volume ratio allows compact electrodes with high reaction surface area
Buoyancy	Low density and good corrosion resistance suggests possible floatation applications

1.2. Manufacturing of Metal Foams

The first attempt to make metal foam was in early 1940's. In 1948 Benjamin Sosnick melted a mixture of aluminum and mercury (Hg) in a high pressure chamber. When the pressure was released at the melting temperature of aluminum, the mercury evaporated and formed the foam [4, 5]. From 1950's to 1970's new techniques were developed, but it was still very hard to control the cell structure of the foam [6-10]. Improvements in the manufacturing processes, as well as increasing interest and demand of industry in high performance and low weight materials have revived the interest in metal foams in 1990's. This has led to more research and resulted in additional manufacturing techniques, more applications and a better understanding of metal foams [11-20]. Today metal foams are made by a range of novel processing techniques, many of which are still under development. Main manufacturing processes and the name of the manufacturers are listed below [3, 21]:

- Blowing gas through molten Al-SiC or Al-Al_2O_3 to form bubbles and then stabilize them. Foams of this type are made by Cymat, Canada and Hütte Klein-Reichenbach G.m.b.H, Austria.
- By stirring a foaming agent (TiH_2) into a molten alloy (again aluminum alloys are the most common) and controlling the pressure while cooling. The foaming agent is dispersed by stirring, releases gas and expands the metal. The foam made by Shinko Wire, Japan with the trade name, Alporas.
- Consolidation of a metal powder (typically an aluminum alloy) with a particulate foaming agent (typically TiH_2) followed by heating into the mushy state upon which the foaming agent releases hydrogen, expanding the material. The expansion can be done in a closed mold giving structures of complex shape with a dense outer skin. Such foams are manufactured by Alulight, Austria and Fraunhofer Institute, Germany.
- Pressure infiltration of a ceramic mold made from a polymer foam precursor, which is burned out before material is injected. The process has considerable flexibility and enables the fabrication of foams from many different metals. The resulting structure is regular and reproducible, has open cells, and a typical relative density of 0.1. The foams available from ERG Materials and Aerospace Corporation, USA.

- Vapor phase or electro-deposition onto a polymer foam precursor, which is subsequently burned out. The result is an open cell metal foam with hollow cell edges. The process developed by Inco, Canada works in this way.
- Expansion of an inert gas trapped in pores at high pressure when a powder compact is hot isostatically pressed. In the Boeing process, for example, Ti-alloy powder is HIPed in a sealed can with argon in the pores. The HIPed product is rolled into a sheet with the can material forming dense faces. The sheet is reheated to expand the trapped gas in the original powder layer giving a sandwich structure with a core porosity of 30 per cent. The porosity is limited by physical constraints of solid state foaming.
- Sintering of hollow spheres made by either a modified atomization process or by the sintering of a metal oxide (hydride), followed by reduction to the metal. Hollow Cu, stainless steel and Ti-6Al-4V spheres can be produced by this method.
- Co-pressing of a metal powder with a leachable powder, or pressure infiltration of a bed of leachable particles by a liquid metal, followed by leaching to leave a metal foam skeleton (for example aluminum and salt).
- Dissolution of gas (typically hydrogen) in a liquid metal under pressure allowing it to be released in a controlled way during subsequent solidification. Copper, nickel and aluminum foams can be processed with this method.

Metal foams processed by the first five methods are commercially available. Each method is suitable for a certain subset of metals and manufactured porous materials have a limited range of relative density and cell sizes. The properties of metal foams depend upon the properties of the metal, the relative density and cell topology. Each of the method listed above can result in a different cell topology (open cell, closed cell, cell size, cell shape) which will give a different property. Control of the structure e.g., cell formation is important in this respect. A successful product must have manufacturing-process-controlled cell morphology, a homogeneous distribution of cells, and a minimum anisotropy in structure with minimum defects.

1.3. Scope of the Thesis

In this thesis, aluminum and aluminum alloys were selected as the matrix material of the metal foams. Aluminum has low melting point, it is a light and abundant metal. It is not surprising that this metal has been one of the first metals to be foamed. When aluminum is foamed it has a relative density of 0.3 or lower. Considering the density of the aluminum (2.7 gr/cm^3) it will be seen that it is lighter than water (1.0 gr/cm^3). It has a high stiffness to density ratio, and absorbs high amount of energy during compression. When compared with polymeric foams, aluminum foams have high temperature resistance and are non-flammable. They are also electrical and thermal conductive. Additionally, aluminum foams are non-toxic and corrosion resistant. They can be shaped or machined with conventional methods [22, 23]. Finally, they have low cost when compared with metals like titanium and nickel.

The powder compact melting (PCM) method that was first patented by Fraunhofer Research Institute of Germany is an interesting method for making of aluminum foams [5, 14]. It offers the possibilities of using wide range of aluminum alloys, addition of different ceramics in order to obtain composite foams and enables well known powder metallurgy techniques for making of the aluminum foams. Aluminum foams used in this study were manufactured by using PCM method. A manufacturing setup was constructed in the laboratory for this purpose. The details of foam manufacturing are explained in the following chapters. The foaming process is very fast and the structure and density of the foam changes considerably with time. The foam expansion and collapse and the intrinsic stochastic nature of pore formation in the material makes it difficult to obtain a reproducible structure. Especially, production of foams from pure aluminum powder compacts is not preferred because of the difference in the melting temperature of aluminum and the decomposition temperature of the blowing agent. This problem is addressed and the effects of ceramic particle addition are discussed.

Compression behavior of aluminum foams is important because it describes the energy absorbing capacity of the material. A typical stress-strain curve for compression of aluminum foam is shown in Figure 1.2 [3]. The area under the stress-strain curve shows the high capacity of energy absorption at relatively low strength level. The mechanical

response of metal foams can be influenced by several factors [3]. First one is the properties of the sample like relative density, shape, size and anisotropy. Second one is the topology of the sample, whether it is closed cell or open cell. Finally, microstructure of the sample, the metallurgical condition of the material is important. In order to investigate the effects of the microstructure, AlMgSi (≈6061) and AlSi (≈A390) alloy foams were manufactured and characterized by metallography, scanning electron microscopy (SEM), microhardness measurements and compression tests.

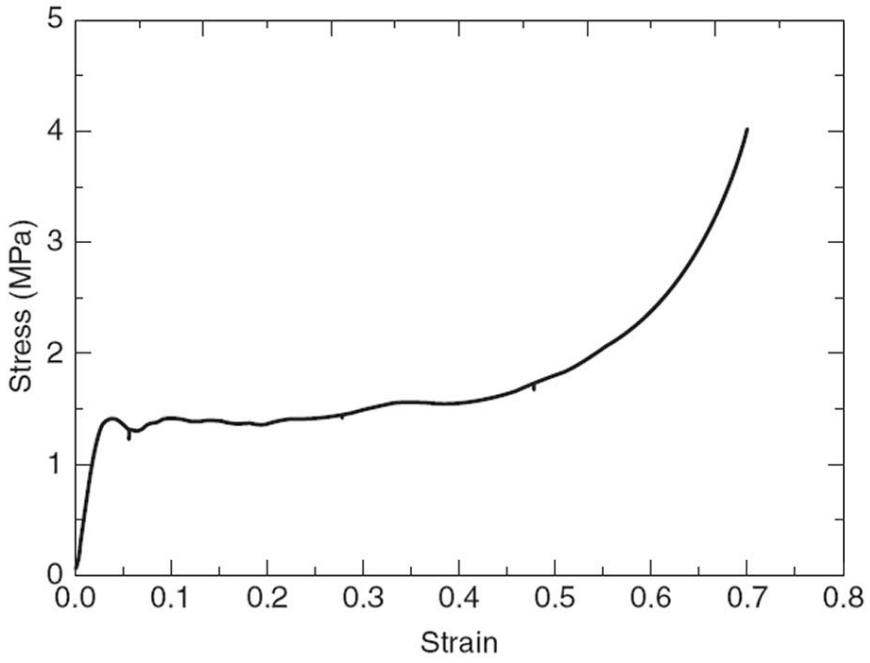

Figure 1.2. Stress–strain curve from a uniaxial compression test on a cubic specimen of a closed cell aluminum foam with 0.08 relative density [3]

2. LITERATURE SURVEY

2.1. Manufacturing of Aluminum Foams

Banhart [5] classifies metal foam manufacturing processes according to the state of metal during processing which defines four "families" of processes, metal vapor, liquid metal, powdered metal and metal ions. Liquid state processing of metals can be done in various ways. The molten metal can be foamed directly with gas (Figure 2.1) [12, 13, 15-17] or a blowing agent can be stirred into the melt which releases gas at that temperature to foam the material (Figure 2.2) [6, 9-11]. The resulting solid foam in former is in principle as long as desired, as wide as the vessel containing the liquid metal allows it, and typically 10 cm thick. The porosities of aluminum foams produced this way range from 80 to 98 per cent, corresponding to densities between 0.069 and 0.54 gr/cm^3, average pore sizes from 25 down to 3 mm, and wall thickness from 50 to 85 μm. In the latter, the resulting foam structure is more homogeneous with a careful adjustment of process parameters [5]. Foamed aluminum is produced in batches with dimensions up to 2050×650×405 mm. Typical densities are between 0.18 and 0.24 gr/cm^3, with the average pore size ranging from 2 to 10 mm.

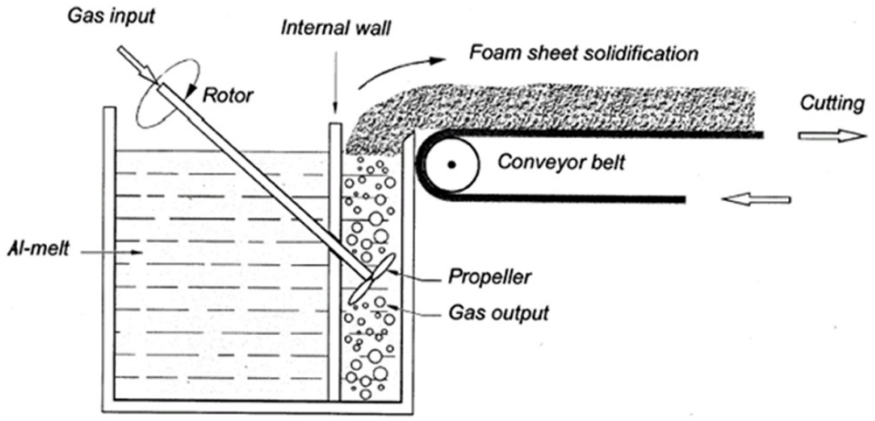

Figure 2.1. Direct foaming of melts by gas injection [5]

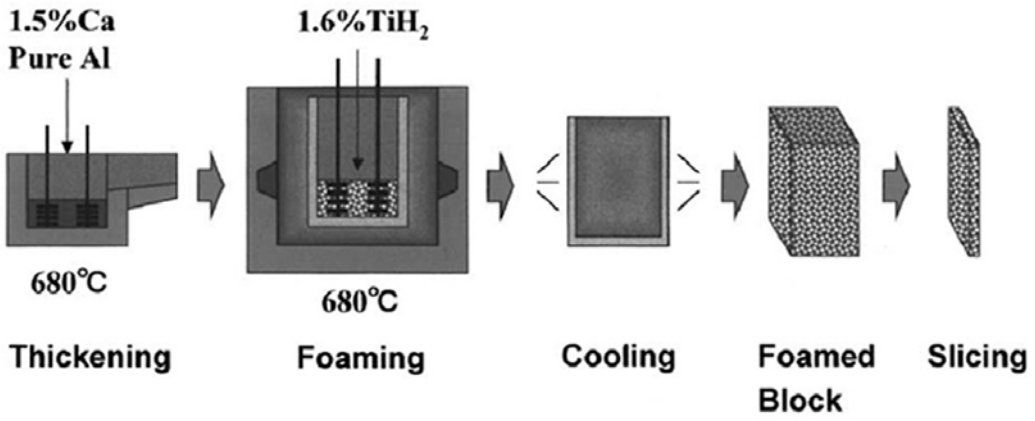

Figure 2.2. Direct foaming of melts with blowing agents [5]

In the PCM method, metal powders are mixed and compacted. After a forming process the semi-product is heated in a mold and foamed (Figure 2.3) [14, 18]. Because the heating temperature is near or higher the melting point of the parent material this process is also listed as a liquid state process. Foaming process is aid by the blowing agent metal powder, which decomposes at temperature close to the melting temperature of the parent material and expands the pre-form (precursor). The density of the solid metal foam can be controlled by adjusting the content of blowing agent and several other foaming parameters, such as temperature and heating rates. Details of the manufacturing method are explained in the next section. Quite complicated parts can be manufactured by a modification in the process like injecting the still expanding foam into suitable molds. Sandwich panels consisting of a foamed metal core and two metal face sheets can be easily obtained by bonding the face sheets to a piece of foam with adhesives. Alternatively, if pure metallic bonding is required, conventional sheets of metal-aluminum or steel are roll-clad to a sheet of foamable precursor material. The resulting composite can be deformed in an optional step, e.g., by deep drawing [20]. Tubes or other shapes of columns can be filled with pre-foamed material and foamed in furnace to give foam-filled structures. Again, bonding can be achieved by adhesives or by extrusion of the pre-foamed material and outer metallic tube [22, 23].

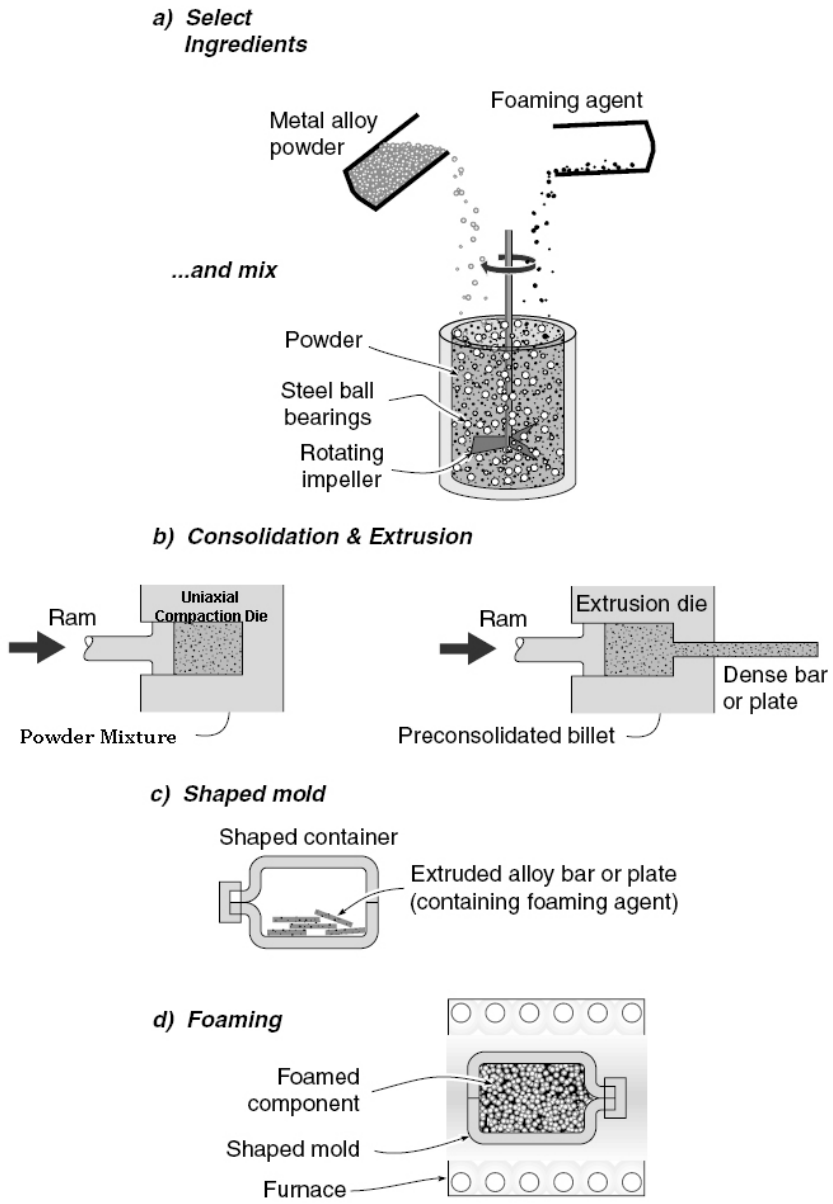

Figure 2.3. Powder compact melting (foaming) process [3]

Another liquid state processing method is casting. Investment casting using polymer foams is done by first filling an open cell foam with a heat resistant material slurry. After curing polymer foam is removed by thermal treatment and aluminum is cast with pressure. Removal of the mold material gives a metallic structure, which is an exact replicate of the original polymer foam. This method gives an open cell metal foam which can have pores 2 to 16 per cm with porosities typically between 80 to 97 per cent [24].

Another method is casting metal around inorganic or even organic granules or hollow spheres of low density, or by introducing such materials into a metallic melt [5]. The granules either remain in the metallic product after casting yielding what is called a "syntactic foam" or are removed by leaching in suitable solvents or acids or by thermal treatment (Figure 2.4). Parts of a predefined shape can be fabricated by designing a mold of the desired geometry. In all cases, the morphology of the materials created can be characterized as "sponge-like".

In spray forming process aluminum melt is continuously atomized and a spray of fast flying small metal droplets is created. The droplets are collected on a substrate where they grow to a dense deposit in a given shape, e.g., a billet, sheet or tube, provided the process parameters are appropriately chosen [25]. The characteristics of spray-formed materials include low oxide content, fine grain size or a high content of metastable alloy phases.

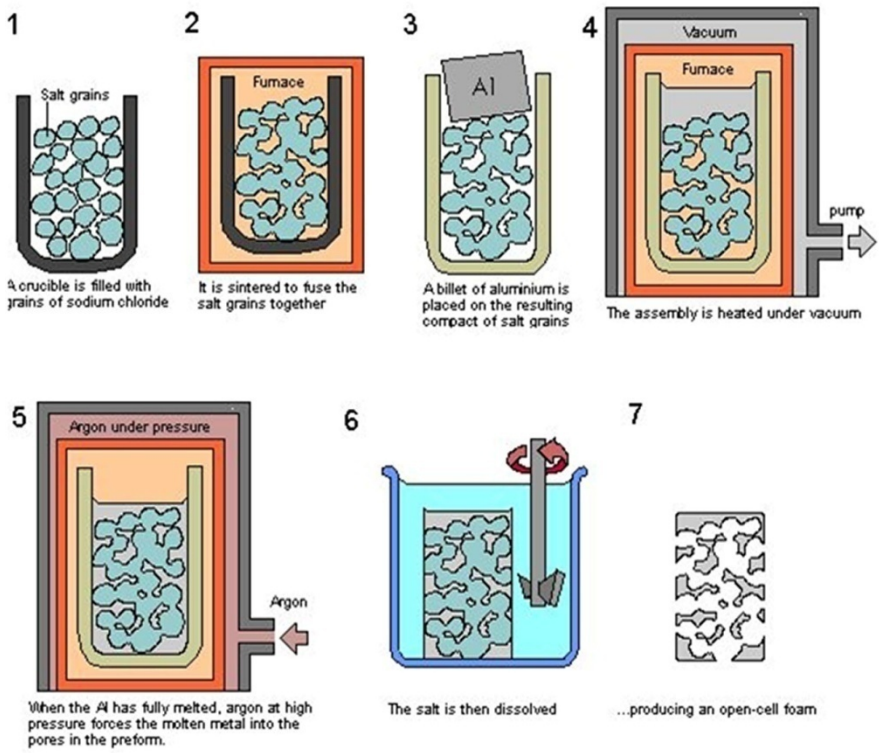

Figure 2.4. Pressure infiltration of a bed of leachable particles by a liquid metal [2]

2.2. Foaming by Powder Compact Melting (PCM)

Manufacturing of metallic foams from metal powders (typically aluminum and its alloys) and particulate foaming agents (typically TiH_2 and ZrH_2) was first patented in 1963 by Allen *et al.* [7]. The process consists of mixing metal powder and a powder blowing agent and compacting the mix to a dense semi-finished product (called "foamable precursor material"). The semi-finished product is fabricated at about 400-480 °C [5, 26]. By meaning dense, it should be noted that the powder compact must reach higher values than 90 per cent of its solid form. The foaming agent thus becomes uniformly distributed and gas-tightly embedded in the metal matrix. This way after heating the entrapped gas coming from powdered blowing agent cannot escape out from the compact and volume expansion occurs. If metal hydrides are used as foaming agents a content of less than one per cent is sufficient in most cases [5, 27-30].

The compaction can be done by any technique that ensures that the blowing agent is embedded into the metal matrix without any notable residual open porosity. Examples of such compaction methods are cold pressing, hot pressing, extrusion, powder rolling or similar other methods. The manufacture of the precursor has to be carried out very carefully because residual porosity or other defects will lead to poor results during further processing. Matijasevic and Banhart [29] have shown that using impure powders or the presence of adsorbed water, dirt or gases entrapped in the precursor during compaction have an adverse effect on foaming. The impurities can act as nuclei for big voids in early stages of gas evolution from the blowing agent. The voids then grow to large pores.

Heating the precursor at temperatures near the melting point of the matrix material is the next step. The blowing agent, which is homogeneously distributed within the dense metallic matrix, decomposes [26, 28, 30] and the released gas forces the melting precursor material to expand, thus forming its highly porous structure. The time needed for full expansion depends on temperature and the size of the precursor and ranges from a few seconds to several minutes.

2.3. Process Variables in PCM Foaming Technique

Similar to other foaming techniques, foaming of aluminum and aluminum alloys by PCM technique requires high degree of control on the process conditions. The most important variable is temperature, which affects the physical condition of the foamable precursor and the foam. For example, if the expansion takes place while the metal powders surrounding the blowing agent powders are still solid the foaming is called “solid state foaming”. Elzey and Wadley [31] have studied and showed the limits of this foaming technique. In solid state foaming expansion is by plastic expansion mechanism (creep). It has been shown that the porosity is limited by the reduction in pore pressure as voids expand and ultimately by the loss of gas accompanying void coalescence. Achievable porosities during solid state foaming have shown to be limited to less than 50 per cent; much less than that of metals foamed in liquid state. The mechanism limiting the solid state foaming is shown in Figure 2.5. If the material is foamed in semi-solid state much higher porosities can be achievable because void coalescence can be avoided. A simple model has been developed to identify the achievable porosity as a function of the temperature time history, the initial gas pressure and the initial relative density for any material for which the creep constants are known. Finally, a comparison between solid state and semi-solid state foaming has been done. In solid-state creep flow dominates the expansion whereas in semi-solid-state flow is modeled as viscous fluid. Figure 2.6 illustrates schematically the limiting achievable porosity during solid, semi-solid and liquid state foaming.

Considering the results of this work it can be concluded that for higher porosity and expansion, the powder compact must be foamed at temperatures very close or higher than its melting temperature. This way metal will be transferred into a semi liquid viscous state and by decomposition of the blowing agent simultaneously a highly porous structure will be obtained.

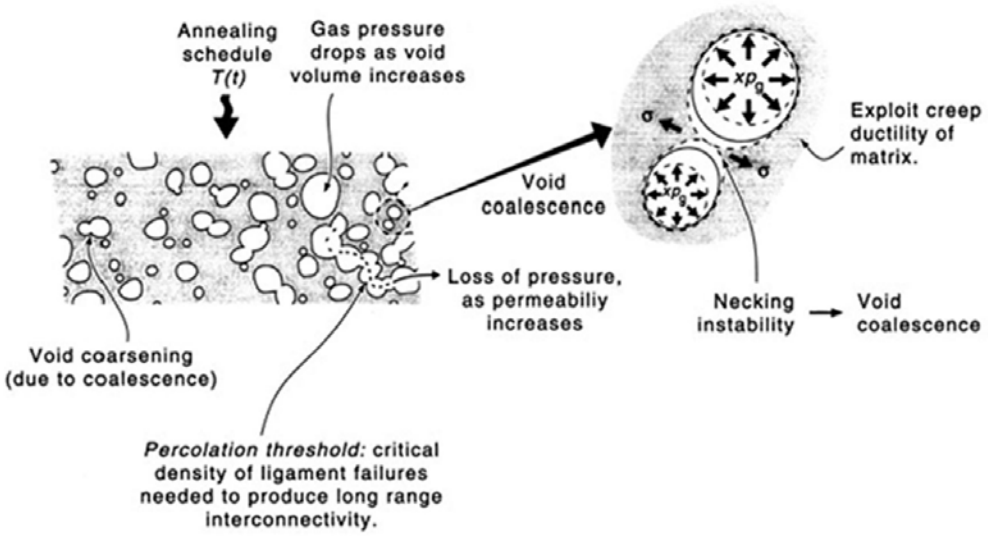

Figure 2.5. The mechanisms limiting the solid state foaming of a metal [31]

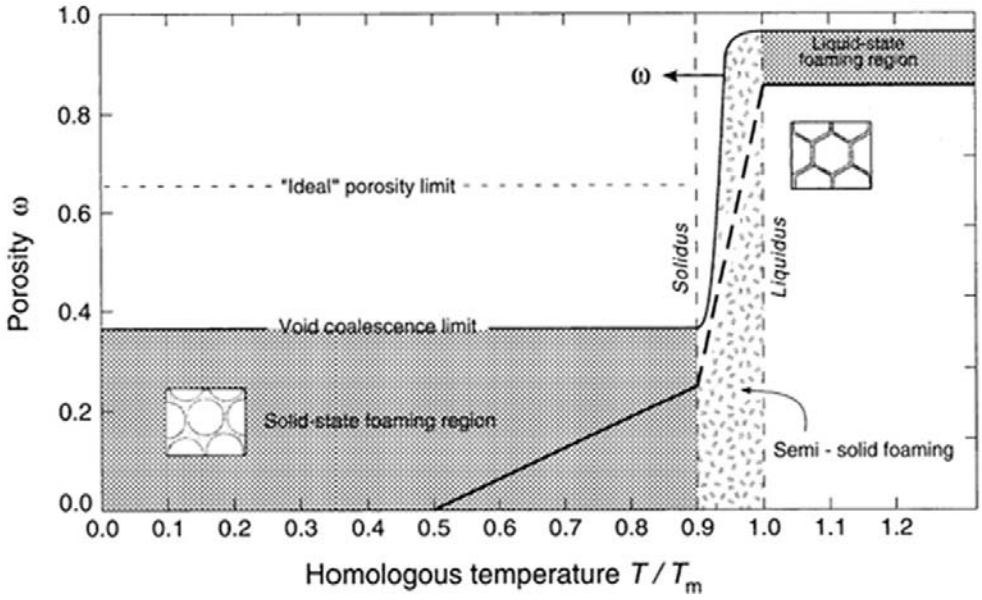

Figure 2.6. The transition to much higher porosity levels during semi-solid and liquid state foaming relative to the solid state [31]

In PCM technique, the process of foaming metal powders is very rapid taking only a few minutes, and the structure and density of the foam changes dramatically with time. Therefore, under normal gravity, the creation of solid metal foam is a race against time. Once formed in the liquid state, it must be frozen quickly to avoid drainage, which would lead to inhomogeneity and collapse. To overcome this difficulty various tricks are used including the use of additives [32-38]. In addition, phase separations and oxides are thought to play important roles in making metal foam fabrication possible in practice [39-42]. However, there is still a little understanding of their effects, acting as surfactants, acting as mechanical barriers by creating a disjoining pressure or acting as viscosity modifiers.

The rapid nature of the process makes reproducibility of the pore structure difficult to obtain. A number of different foaming configurations can be used, including the use of either free or constrained foaming. Kennedy [43] has investigated the effects of such configuration on foaming behavior and reproducibility. His results indicate that significantly improved reproducibility in density is achieved when foaming was in constrained conditions for example in a steel tube. When foaming in the tube, the area of the expanding surface is smaller than unconstrained foaming, and is invariant with foam expansion, thus reducing the work required to produce a change in volume. During expansion the surface area across which gas can burst through the surface skin and cause cell collapse is also reduced, enabling larger expansion to be realized. Beyond the maximum expansion, and when large-scale collapse occurs for free foaming, the tube mechanically supports the foam. The work of adhesion between the liquid metal and the tube, which is positive even for non-wetting systems, supports the weight of the foam enabling larger expansions to be maintained after long holding times. Reducing the influence of processes that contribute to large-scale foam collapse reduces the variability in foam density, improving the reproducibility.

Monitoring the foaming process of metals is much more difficult than doing the same with for example, aqueous foams. Many of the observation techniques used for such foams cannot be applied owing to specific properties of metals: they are hot, opaque, very reactive with oxygen and have a high electrical conductivity. These rules out optical or resistometric methods, which are often used for investigating aqueous foams [27].

Therefore, there is not much work on how the metal foam emerges from the liquid, how it changes with time and what mechanisms are responsible for its formation. Most of the work is carried out is relied on so-called “ex-situ” investigations. A foam is produced by heating up foamable precursor material; after a given time the foaming process is interrupted and the resulting solid foam is analyzed. By varying the time between the beginning of the experiment and the interruption of foaming one can obtain a set of samples that reflect the evolution of the foam and can analyze these samples by macro analyses, microscopy or metallography. An example is given in Figure 2.7, which shows typical expansion curves and foam structure for the PCM AlMg1SiCu alloy (6061). The points marked with capital letters A-K indicate the different foaming stages that were photographed. In Figure 2.7b the corresponding macrographs of the various foaming stages are shown (the foamable precursor material is identified by “P”). The macrographs show:

- The initiation and evolution of porosity; pores elongated perpendicular to the compaction direction (which was from top to bottom) are formed (phase A).
- Pore growth; the pores are initiated by the evolving hydrogen and are increasingly rounded of as the foam expands (phase B-G). The initial anisotropy starts to vanish until only a slight asphericity remains. Moreover, initially round pores are deformed to more polyhedral pores as the level of porosity increases and no more space can be filled by spherical pores.
- Collapse; after maximum expansion, no more hydrogen gas is released and the foam begins to decay. This decay leads to foams with large and irregular pores, collapsed and oxidized pores especially at the top of the sample and a solid metal layer at the bottom.

The foams owe their collapse to two mechanisms, drainage and coalescence. Drainage is the flow of molten metal from the cell walls into the cell edges and through cell edges downwards driven by gravity (see H-K in Figure 2.7b) [27]. A thick layer of metal at the bottom of the samples is the result of this process. Coalescence occurs whenever two cells merge to form one large one. It is thought that cell rupture is the reason for such processes. It seems that metal membranes are not as stretchable as, e.g., the membranes in soap foams and rupture as soon as their thickness has fallen below a certain critical limit.

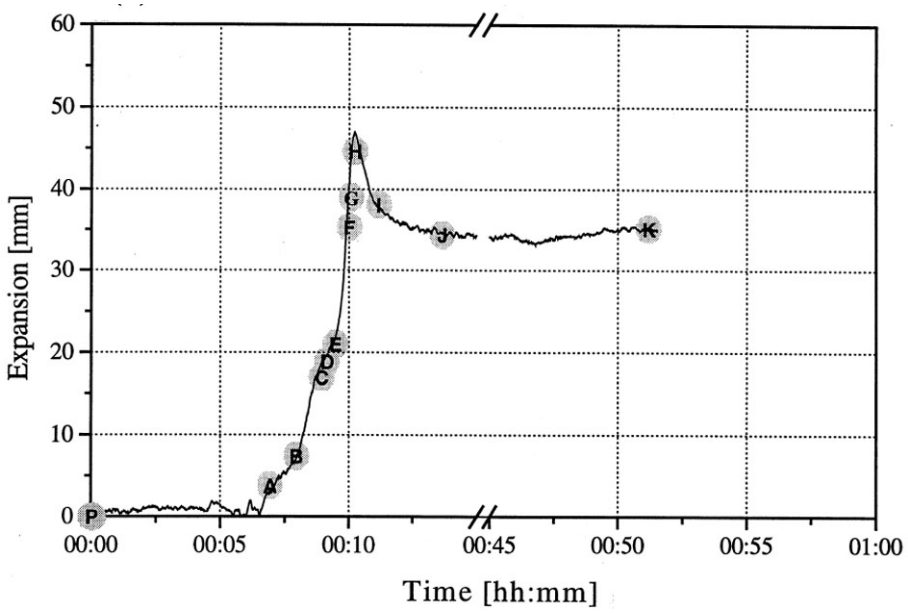

(a)

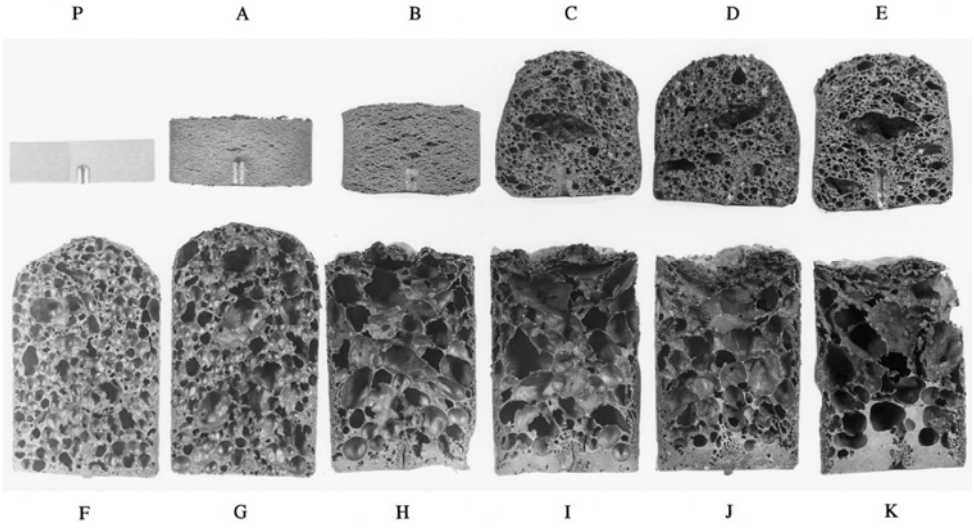

(b)

Figure 2.7. Monitoring the foaming process ex-situ: (a) expansion curve for 6061 foam using a preheated furnace at 800 ^{o}C, (b) structure of 6061 foams at different stages [27]

2.3.1. Selection of Powders

Selection of powders automatically determines the system to be foamed. Banhart [44] indicates that the appropriate selection of the raw powders in terms of purity, particle size and distribution, alloying elements and other powder properties is essential for a successful foaming. The most important selection criterion is the composition of the foaming system. AlSi systems are frequently used due to their low melting point and broad solidification range. AlMgSi (6000 series) systems are also common and selected whenever heat treatable alloys combining medium strength and moderate costs are required. Other compositions have also been used. Al alloy could be pre-alloyed powder or obtained from elemental powders. Although there are examples, foaming of pure Al is not common due to its low viscosity and high melting point. Table 2.1 shows the melting ranges of some of the important Al alloys [45].

Table 2.1. The melting temperature ranges for some cast and wrought Al alloys [45]

Chemical Designation	**Temperature (°C)**		
	Liquidus	**Solidus**	**Melting range**
Al 99.5	635	659	24
AlSi12	567	579	12
AlSi11MgCu	538	560	22
AlSi7Mg	550	615	65
AlSi17Cu4Mg	505	650	145
AlMg5	575	630	55
AlMg1SiCu	575	640	45
AlMgSi	605	650	50

Selection of foaming agent is usually done by comparing decomposition temperature of metal hydride and melting temperature of base metal. Baumgartner *et al.* [28] have shown that presently TiH_2 seems to be the best choice for the blowing agent for foaming of Al and Al alloys. Other hydrides, e.g., ZrH_2 and MgH_2, have also proved to be practical, but more expensive than TiH_2, and no technical advantage has been seen. Zeppelin [46] have shown that foam expansion is highest for TiH_2 followed by ZrH_2 and MgH_2, which decompose at lower temperatures and are therefore less effective for foaming.

The decomposition of hydrogen from the TiH_2 powder starts at about 400 °C [29, 46-50]. Considering the melting temperature of aluminum it was seen that the earlier release of the hydrogen gas from the blowing agent had an important effect on foamability of aluminum. Kennedy [47] heat treated TiH_2 and concluded that heat treating in air delays hydrogen evolution to higher temperatures. Heat treatment did not however, prevent gas being released before the melting point of the pure aluminum precursor. Particle sizes, shapes and surface properties of both base metal and foaming agent can be crucial. Generally, average particle sizes up to 160 μm are used for both pre-alloyed and elemental powder systems [27]. TiH_2 is mostly used in the as-received form, in which the particle size is generally close to 50 μm.

2.3.2. Mixing of Powders

Homogeneity of powder mixtures is crucial to obtain homogenous pore distribution in foam product. The homogenous mixture of powders should be attained to obtain high quality foams with uniform pore distribution [44]. Commonly, tumbling mixers are used as a method of mixing in the laboratory-scale productions [28]. The mixing procedure should yield a homogeneous distribution of alloying elements and the blowing agent to ensure that high-quality foams with uniform pore size distributions are obtained. Excessive mixing can result in work hardening of metal powders or alter the shapes of particles. In industry-scale productions usually powders are blended by blowing inert gases in a closed volume.

Blending of powders can be done for several reasons. Because same metal powders made by various processes vary in shape and sizes, one can obtain uniformity or homogeneity by mixing. Another reason is mixing of different metal and different material

powders to import special physical and mechanical properties and characteristics to the product. Finally, to enhance mold filling or flow characteristics and lubrication during pressing lubricants like stearic acid or zinc stearate can be blended. In PCM route of Al foaming, mixing of Al powder with blowing agent is an important step. After compaction a uniform distribution of TiH_2 is required for uniform cell structure of foamed metal.

2.3.3. Compaction of Powder Mixtures

Powder consolidation can be performed using various techniques. To obtain high amounts of foaming, compaction should yield almost full compact structure, which makes Cold Isostatic Pressing (CIP) a candidate method. Other methods are cold uniaxial pressing and hot uniaxial pressing. By these methods, tablets in square, rectangular or cylindrical geometry can be compacted. Hot extrusion or hot rolling can be subsequently applied to semi-compact structure. After the CIP, compacts have 70-80 per cent relative densities whereas after extrusion or rolling it approaches to theoretical value. It should be noted that in the case of rolling, foamable sheets or sandwiches could be obtained which makes the process more flexible.

Duarte and Banhart [27] carried out a detailed study on the effect of compaction on foaming. It was found that in the case of hot pressing, the temperature of compaction is very crucial. As seen in Figure 2.8a, up to 450 °C, increase in compaction temperature increases the degree of foaming. However, if compaction temperature exceeds this value, the degree of foaming decreases with temperature. It was concluded by authors that up to 450 °C, the amount of compaction increases with time and hydrogen release from TiH_2 does not occur. Above this temperature, hydrogen release occurs extensively and less hydrogen remains for subsequent foaming process. Figure 2.8b demonstrates that the compaction time is a fairly uncritical parameter for hot pressing temperature and pressure chosen. The expansion curves are all quite similar, the remaining differences being within the normal statistical fluctuations.

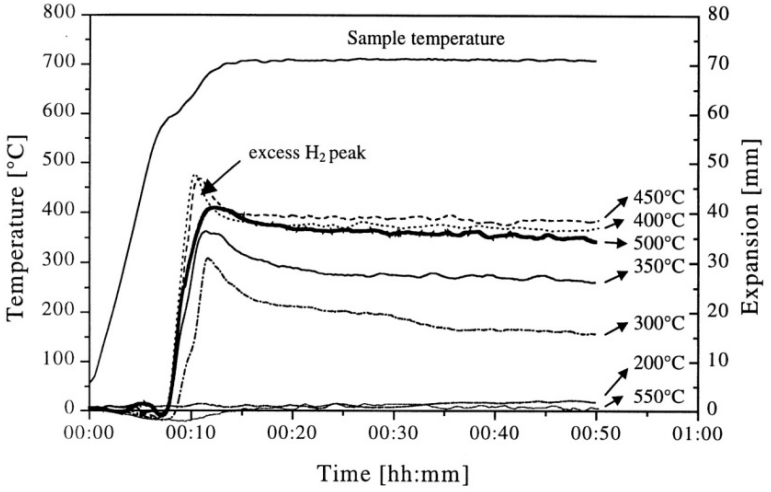

$T_{hot\ pressing}$ [°C]	200	300	350	400	450	500	550
$\rho_{average}$ [g/cm^3]	2.46	2.58	2.61	2.65	2.66	2.66	2.68
$\rho_{average}$ [%]	91.79	96.27	97.39	98.98	99.25	99.25	≈100

(a)

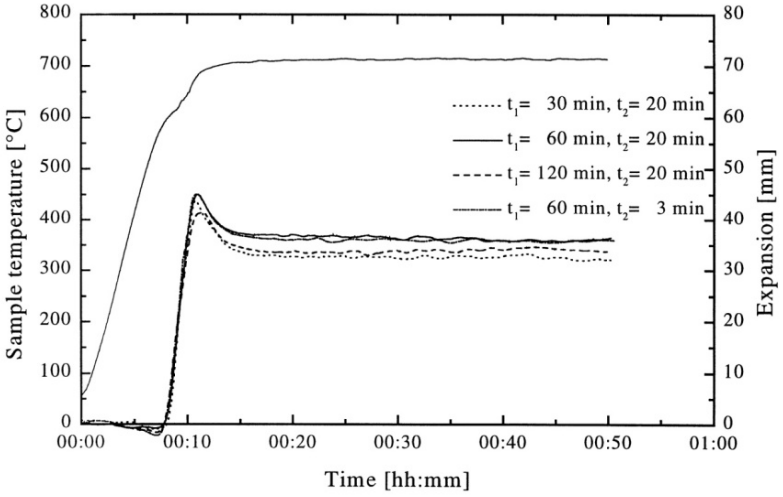

(b)

Figure 2.8. Effects of compaction temperature and time: (a) expansion of Al compact with 0.6 per cent TiH_2, (b) expansion curves of AlSi7 samples prepared with different pre-heating (t_1) and hot pressing (t_2) times [27]

2.3.4. The Expansion Behavior of PCM Aluminum Foams

Aluminum foams foamed by PCM technique shows characteristic expansion behavior shown in Figure 2.9 [27]. The figure shows expansion and temperature versus time curves of AlSi and 6061 alloys in which solidus and liquidus temperatures of the two are given as horizontal dotted lines.

Baumgartner *et al.* [28] compared the expansion behavior of aluminum and different aluminum alloys (Figure 2.10). Volume expansion takes place in four stages: first, before the melting temperature of the alloy is reached, the expansion is small, resembling the volume increase also found for metal foams without foaming agents. The actual expansion starts when the metal starts to melt and the released gas can inflate the pores. In stage two the volume increases to multiple times the initial volume. The expansion even accelerates as the liquidus temperature is exceeded, and after maximum expansion has been achieved the foam collapses (stage three) due to the now decreasing pressure in the cells as the foaming agent is exhausting. Finally, the foaming stays constant in the stage four. Figure 2.11 shows the cross sections of aluminum foams held for different foaming times in furnace. The foam with a well-formed uniform pore size and because of long foaming time collapsed and coalesced foam structure is observable. The volume of a metal sample as a function of time and images of four different expansion (including the unexpanded precursor which is 9 mm in height and 32 mm in diameter) are shown.

The density and density distribution of the growing foam can be controlled by several parameters. The blowing agent content in the precursor material is obviously important, but furnace temperatures and heating rates also have an influence. The mold material, mold shape, and type of furnace naturally influence the heating rate and, therefore, must also be considered. The difficulty is that the liquid foam is thermodynamically unstable, and conditions change constantly during foaming. There are various intermediate stages: at first, only the mold is heated directly, whereas the foamable material receives heat indirectly via heat conduction through the mold. Initially, there are merely some point contacts between the piece of foamable material in the mold and the mold walls. However, as the temperature increases, the precursor softens and assumes the contour of the mold, thus increasing the transfer of heat. Moreover, heat transfer via

radiation gains importance with rising temperatures. The reflectivity of the mold and precursor surfaces may change during the process and add a further variable. Finally, after foaming begins, the thermal conductivity of the precursor rapidly decreases, thus reducing the heat flow. The phenomena during cooling are also quite complex and difficult to describe for reasons similar to those mentioned for the heating phase [28].

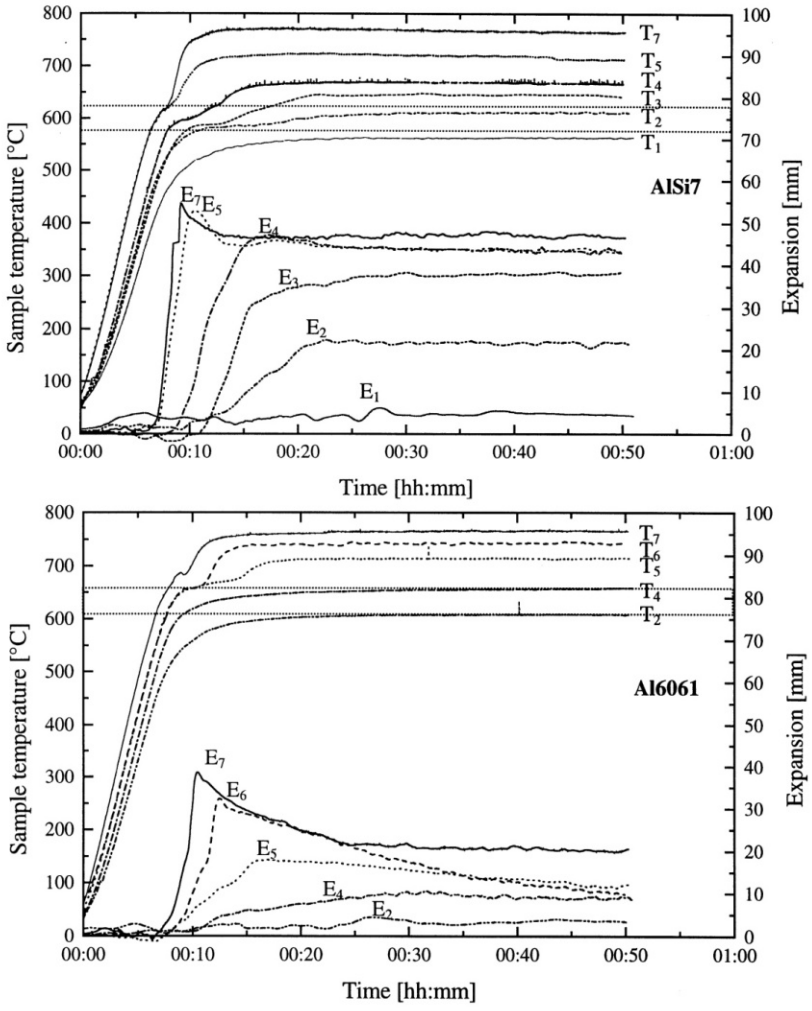

Legend:

$T_{furnace}$ [°C]	600	650	675	700	750	775	800
E curve	E_1	E_2	E_3	E_4	E_5	E_6	E_7
T curve	T_1	T_2	T_3	T_4	T_5	T_6	T_7

Figure 2.9. Expansion (E) and temperature (T) curves of AlSi7 and 6061 alloys foamed at different nominal furnace temperatures (600-800 °C) [27]

2.3.5. Effects of Ambient Pressure and Heating Rate on Foaming

In addition to foaming at atmospheric pressure, foaming at various pressures were investigated by several researchers [30, 51]. Moreno *et al.* [51] carried out foaming experiments under pressures between 0.01 and eight bar and found a great influence of the gas pressure on the foaming behavior. Under low pressures high coalescence, instabilities and rising bubbles characterize the foams. Under high pressures, beside a reduced expansion, a small average cell size and high homogeneity was observed. Release from high pressure to normal pressure leaded to an increased expansion.

Different furnace temperatures lead to different heating rates and influence the foaming process. Clearly, higher heating rates lead to an earlier expansion of the foamable precursor material because the melting temperature is reached at an earlier time. The effect of heating rate on foam expansion can be seen in Figure 2.12.

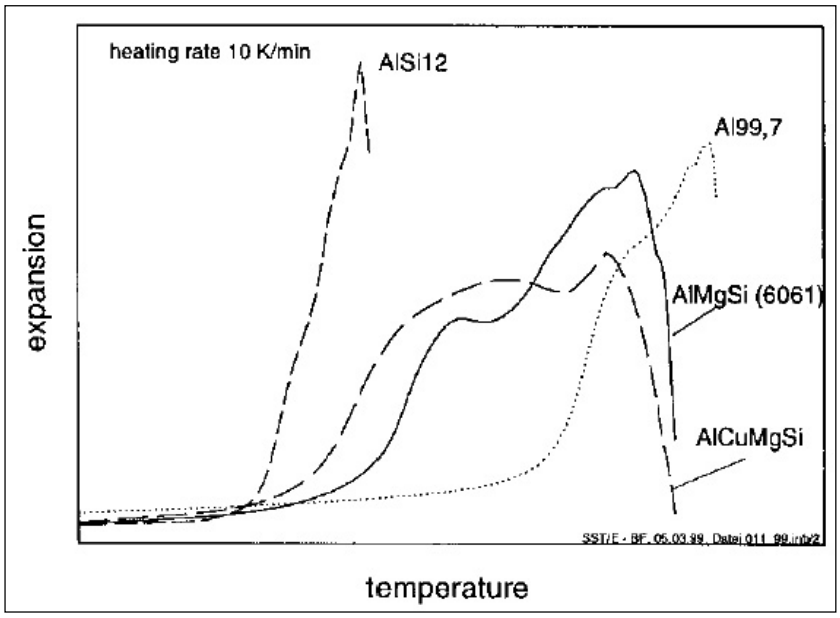

Figure 2.10. Analysis of foam growth of Al and some typical alloys [28]

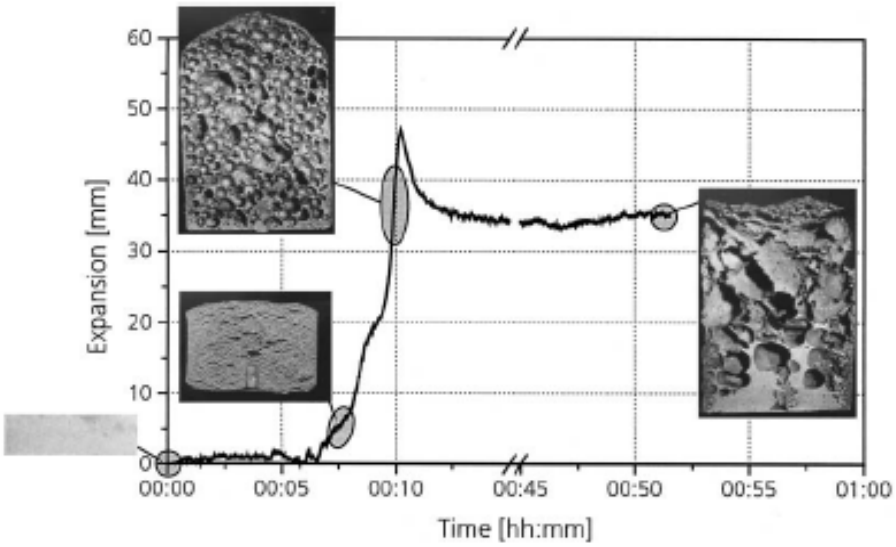

Figure 2.11. Expansion behaviour of Al-TiH_2 compacts when foamed at 750 °C [5]

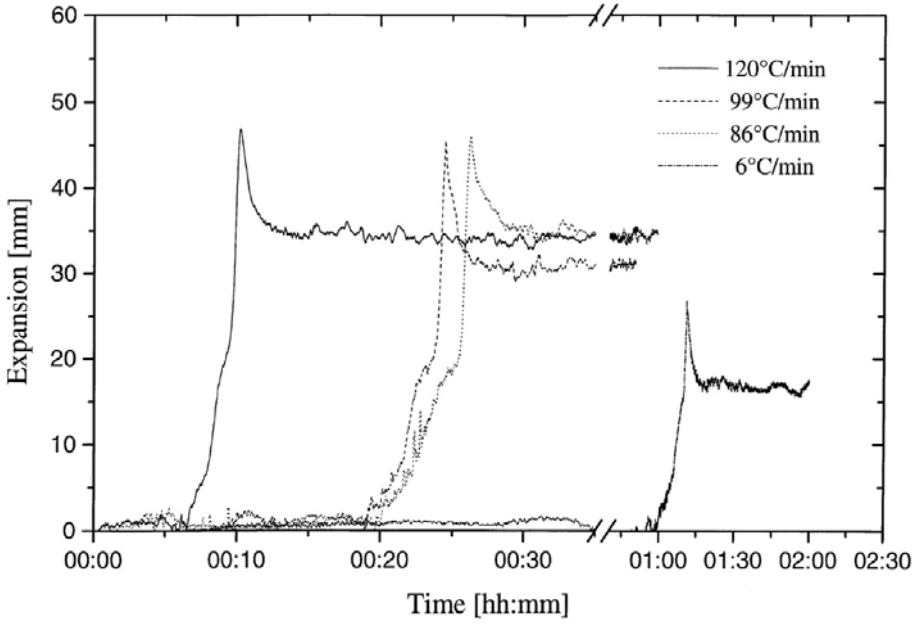

Figure 2.12. Foam expansion curves of 6061 alloys for different heating rates at 800 °C nominal furnace temperature [27]

2.4. Metal Foam Stabilization

Liquid metallic foams are systems which go through a series of transient states and change their morphology constantly throughout their lifetime. They are hardly ever stable, at the best metastable. While some of the rapid changes in a foam are an essential part of the process, others are deleterious and limit the applicability of metal foam technology. A foam can be called (kinetically) stable, if it does not change considerably in the time span between completion of the blowing process and solidification. The forces acting on a foam are; gravity, external atmospheric and internal gas pressure, mechanical forces and forces within the metallic phase (surface tension, capillary forces etc.) [41]. Any imbalance of these forces will lead to the movement of the foam. The difficulty in understanding the stability of the foams is that the effects are intertwined and it is not possible to study them separately. Figure 2.13 shows the interdependence of various effects and shows how they depend on each other.

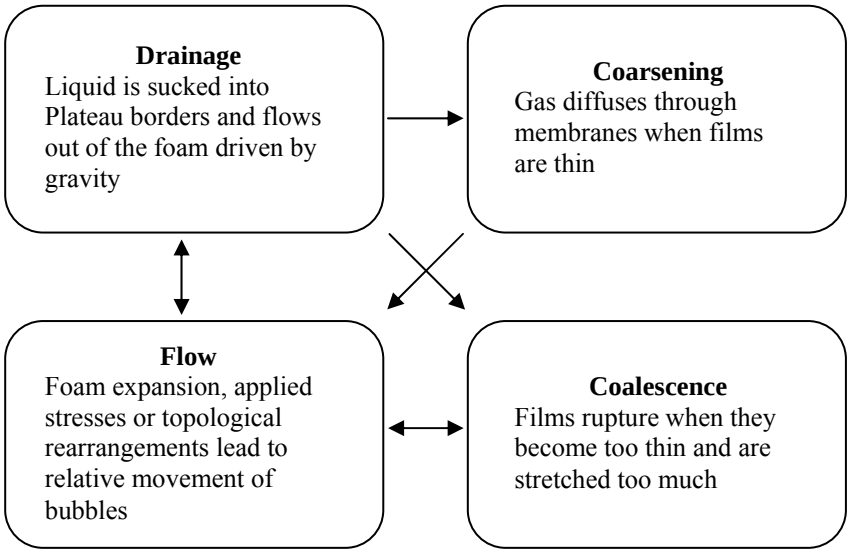

Figure 2.13. Interdependence of four principal mechanisms in foams [41]

During growth and after maximum expansion metal foams evolve rapidly. The presence of drainage and coalescence is obvious from Figure 2.11. It is a result of bursting liquid metal films and an accumulation at the bottom. The extent to which drainage takes place can vary very much. Coalescence, in contrast, is happening continuously in metal foams during expansion. Whenever a liquid film is stretched to such an extent that the film becomes thinner or drainage leads to a loss of liquid that the film becomes too thin, it ruptures. The existence of this critical thickness can be derived from sections of foams by ex-situ analysis or in situ analysis by X-ray radiography. Banhart [41] compiled some data obtained either by conventional metallography or by computed tomography on solidified samples, or from in-situ image and the result is shown in Figure 2.14. Despite the considerable scatter, one can conclude that pure aluminum foams have the thickest films and that alloying with silicon and copper lowers this limit notably. The presence of non-metallic particles in metallic foams makes them stable and prevents films from rupturing and liquid from draining out too quickly. The mechanism of stabilization has been discussed in different ways in the literature. Some authors explain stability by the reduction of drainage in liquid foams caused by the presence of particles, others stress that particles primarily prevent films from rupturing. The structure of the non-metallic constituent is very different for various metal foam types however they show many similarities: thick cell walls, wavy walls, energetically unfavorable cell structures, and stability. It is nearby to suppose that the origins of these similarities are lying in their stabilization mechanisms. Kennedy and Asavavisithchai [34] claimed that the mechanism for improving foam stability could be by the particles attaching to the gas/liquid interface and modifying its curvature, reducing the pressure difference between the Plateau border and the cell walls. This would also reduce the rate of drainage. Ceramic particles were generally concentrated at cell wall edges, which was an evidence of the stabilization effect. They added SiC, TiB_2 and Al_2O_3 to PCM Al foams to understand the effects of the ceramics in the foam structure. Addition of ceramics generally resulted in a significant improvement in foam expansion (≈ 500 per cent). The function of the particles was to reduce the critical cell wall thickness before rupture, resulting in increased foam expansion. Ceramic particles with their size, volume fraction and type were believed to be affecting the degree of foam expansion and stabilization positively. In direct foaming methods, the stabilization of the foam could be achieved when solid particles formed a certain structure, situated partly at the neighboring liquid–gas interfaces, and partly in the liquid gap between the interfaces.

The particles created an interfacial force (pressure), separating the two liquid–gas interfaces. As this force should be effective in a macroscopic scale, certain conditions to the structure of the solid particles should be fulfilled. Kaptay [52] gives a list of structures that will be able to separate efficiently the two liquid–gas interfaces (Figure 2.15):

- a closely packed single layer of particles (Figure 2.15a),
- a loosely packed single layer of particles (Figure 2.15b),
- a closely packed double layer of particles (Figure 2.15c),
- a loosely packed double layer of clustered particles (Figure 2.15d),
- a closely packed 'double+' layer of particles (Figure 2.15e),
- a loosely packed 'double+' layer of clustered particles (Figure 2.15f).

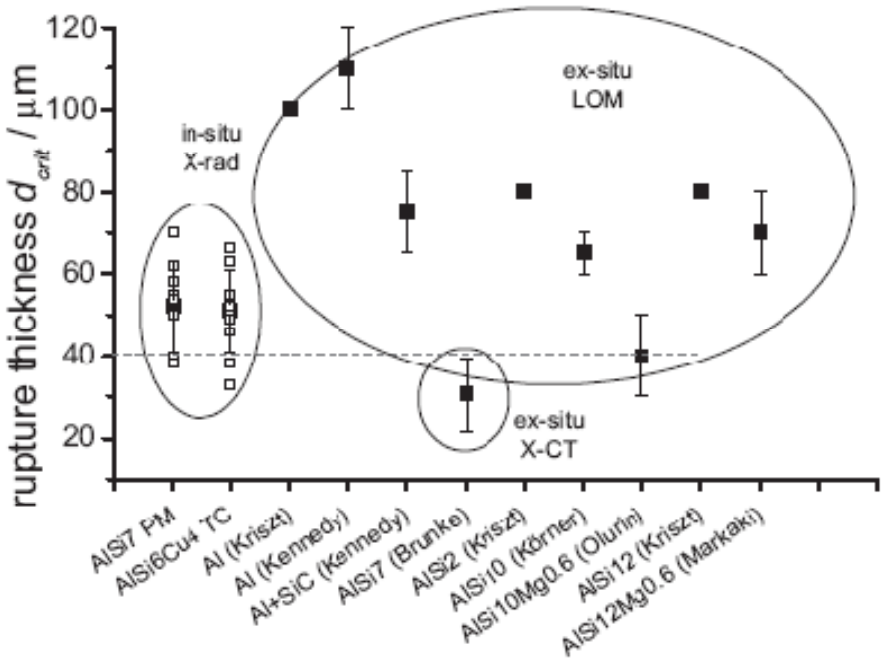

Figure 2.14. Critical thickness of cell features of various aluminum alloys foams made by PCM [41]

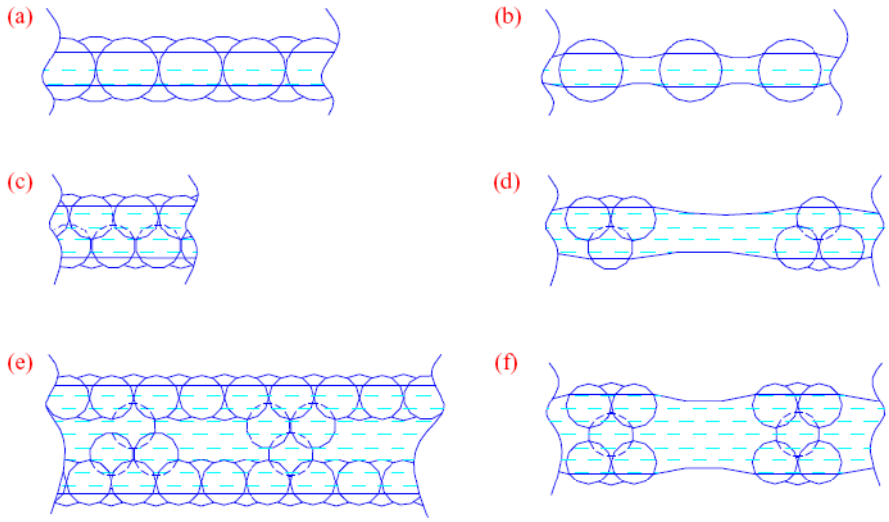

Figure 2.15. Solid particle stabilization mechanisms as proposed by Kaptay [52]

Other than solid ceramic particles, oxide content of the raw Al powder has an enhancing effect on foam structure. Oxides initially present in Al powders are dispersed in the melt during foaming. The oxides are believed to help stabilization of the metal foam film by adhering to the gas/metal interface and creating a direct mechanical bridge, which counteracts the forces trying to thin the film [39, 40]. Körner *et al.* [39] discussed the role of oxides in stabilizing aluminum foams by various experiments. First, they manufactured foams by using Al powders with different oxide contents. Low-oxide powders were found to lead to foams with a lower expansion and a higher degree of drainage. Second, they analyzed powder particles, precursor materials and foams by metallographic methods. As oxide films were very thin they could be made visible only after careful preparation. Körner *et al.* [39] observed irregular structures which were shown to be enriched with oxygen by energy dispersive X-ray analysis (EDX). The oxides seemed to form an interconnected network. In order to explain the mechanism of particle stabilization they developed a model based on the following assumptions:

- The original oxide network in the pressed powder is fractioned during foaming. Fragments cluster together and form network particles, which freely float in the melt. These network particles are infiltrated by liquid and can bear mechanical forces.

- The network particles are completely wetted by the melt and are therefore confined between the two interfaces of each film. The confinement together with the mechanical stability of the network particles creates a repulsive force, which prevents the films from thinning.

The model was supported by experimental observations in which it was found that in many cases in bulges of the cell wall oxide agglomerations were evident, whereas thin parts of films were oxide-free. Körner *et al.* [39] attributed the fundamental stabilization mechanism in PCM foams again on particle stabilization, but which were originated from the oxygen content of the underlying metal powder. The oxides were not present as compact particles but they formed crumpled structures and a tenuous network, the global oxide network. This network showed a kind of mechanical stability and could be fragmented by mechanical forces. Bubble nucleation and bubble growth led to a fragmentation of the network into smaller pieces which were referred to as oxide network particles. Oxide network particles were not stable particles but have dynamical nature since they could change their shape and size by coagulation and fragmentation. Network particles were not expelled from the liquid as the solid particles and formed ideal mechanical barriers against cell wall thinning. These barriers induced a long-range interfacial force, the disjoining pressure, which was the origin of foam stability. The internal network structure made aluminum oxide network particles behave as if they were completely wet by the liquid aluminum. This behavior was essential for stabilization. During foaming, network particles get captured within the foam structure (Figure 2.16).

Particle confinement between two opposing interfaces leads to an uneven, corrugated cell wall topography. The interface in-between two network particles becomes concave and the pressure within these particle free regions decreases due to the induced capillary pressure. As a whole, the network particles generate a counter pressure, the so-called disjoining pressure, which withstands the bubble pressure, stabilizes the cell walls and generates foam stability.

Due to electromagnetic screening of metals only mechanical forces are a possibility participating in the stabilization of thick cell walls. In a static situation, liquids cannot transfer mechanical forces. Prerequisite for the transfer of mechanical forces is the

presence of objects with solid state character, e.g., particles. These particles transfer forces from one interface to the other. As a result, a disjoining pressure is generated which balances the sucking effect of the Plateau borders and leads to stability.

As seen in Figure 2.17 [39], for solid particle stabilization (SPS) the particles are deliberately added to the melt. The origin of oxide network particles is oxidation during powder atomization. Oxide network particles have dynamical character, e.g., they can be fractured or also agglomerate. In contrast to solid particles, their size is not fixed and is strongly influenced by nucleation. In contrast to explained stabilization mechanisms endogenous particle stabilization (EPS) operates without any additional phase. EPS is based on the characteristics of endogenous solidification, where a huge number equal sized nuclei start growing within the melt during solidification. If foaming is on the same time scale as solidification, these particles can take the same role as the solid or network particles [39].

The existence of a universal stabilization mechanism claimed by Körner *et al.* [39] for all metal foams is still under dispute [41]. Most authors discuss the stabilization mechanisms of the type of the foam they investigate and the explanation is usually in terms of surface viscosity and cell surface alterations. There are stable foams in which no obvious mechanical forces exist. Without the gravity driven drainage, interface forces created by solid particles were shown to have a dominant influence on the resulting structure of the foams. The foaming experiments were done under microgravity or zero gravity e.g., in space [53, 54]. It seems more likely there is a complex and varying interplay between different effects in various types of metal foams and all the mechanisms proposed play an important role.

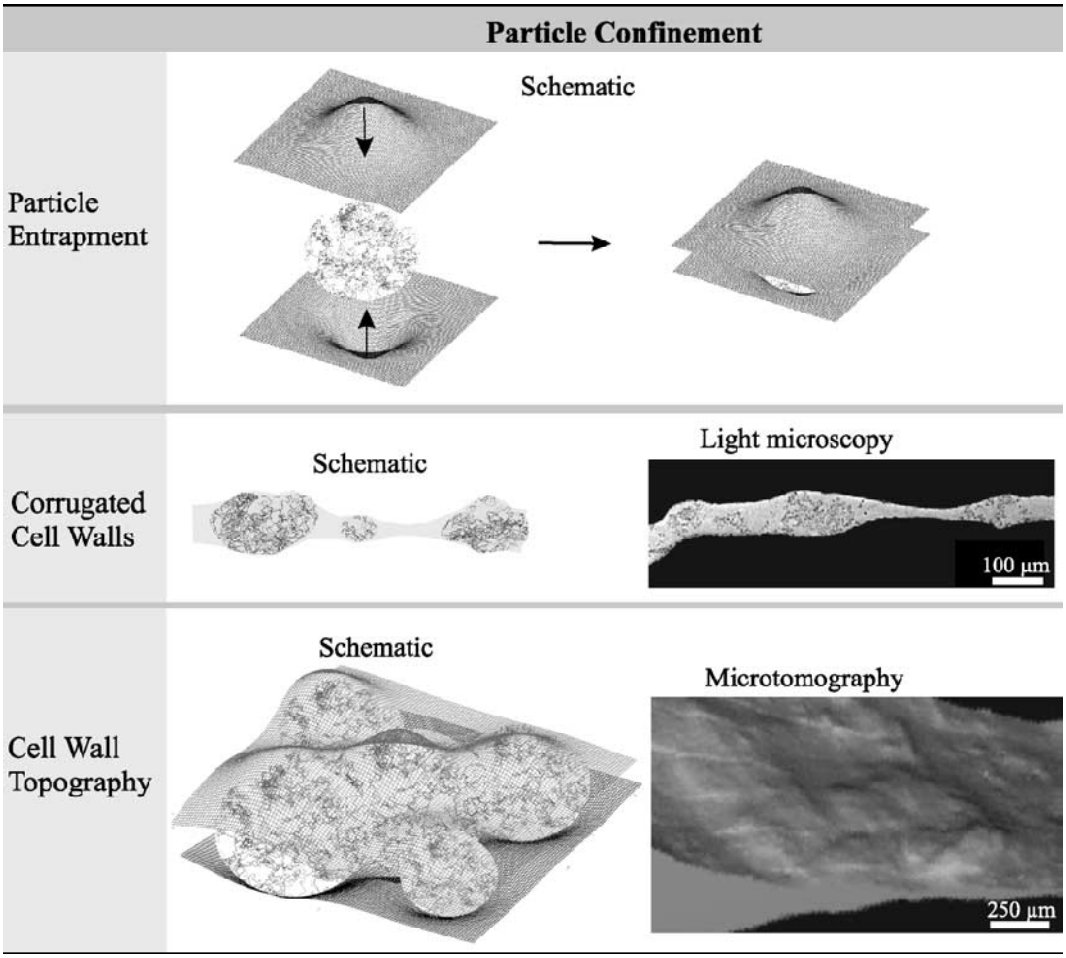

Figure 2.16. Particle confinement: The network particles get captured in between the interfaces during cell wall thinning and form lumps. As a result, cell walls show an uneven, corrugated topography [39]

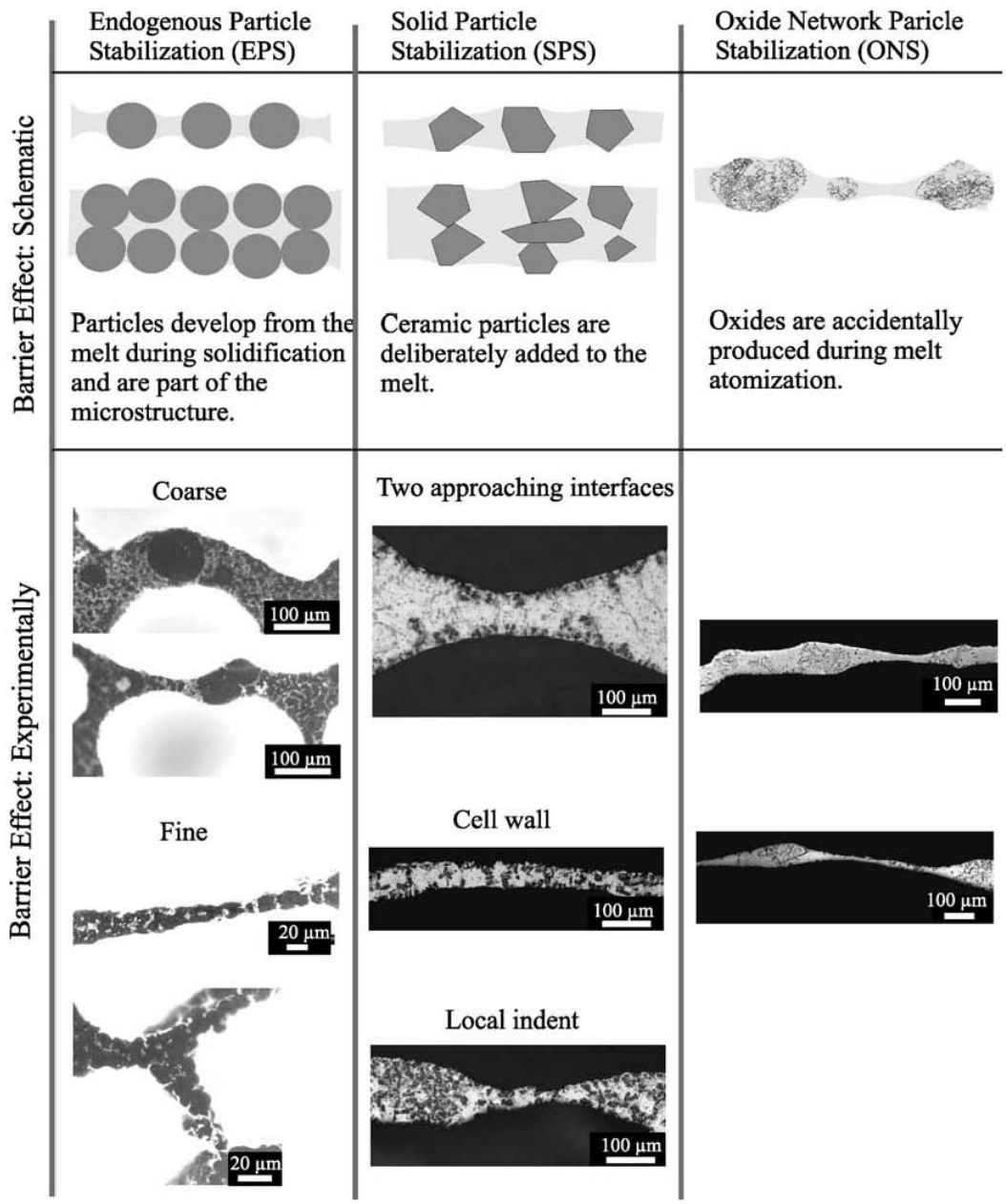

Figure 2.17. Particle stabilization: Top; schematic diagrams illustrating the effect of particles on stability as the wall thickness approaches the particle diameter. Bottom; optical micrographs illustrating the barrier effect. Left: AZ91, Middle: Al/SiC, Right: Al99.9. The particles are represented by the dark phase [39]

2.5. Mechanical Behavior of Aluminum Foams

Mechanical testing of cellular metals is a prerequisite for any structural and functional applications. The mechanical data are needed for evaluation of specific applications. The apparent moduli and strength of foam test samples depends on the ratio of the specimen size to the cell size, and can be influenced by the state of the surface. Ashby states that for a valid mechanical testing the specimens must be large (at least seven cell diameters of every dimension) and that surface preparation is necessary [3]. It must be noted that methods developed to make cellular metals give a wide range of different topologies. So each study must be considered with the specific foam manufactured by one of the methods explained before. Ideally it would be easier to work with metal foams that have uniform cell structures with known geometries like honeycombs, parallel or prismatic cells. The behavior of these structures under mechanical loading is well explained in literature. However these designed metal foams are very costly.

In order to use foamed metal in structural applications, it is important that their mechanical properties are properly characterized, and subsequently that reliable models of mechanical behavior be available to assist in the design process. A number of models have been proposed to study the mechanical properties of metallic foams. These include both mechanic and continuum models. The mechanic models generally start with a unit cell structure identification. Gibson and Ashby [1] did the early theoretical studies. They gave the relation between the basic mechanical properties and the relative density ρ_r ($\equiv \rho^*/\rho_s$) of metallic foams by using simple cubic models. When a closed cell foam is deformed the cell edges bend, and the cell faces carry membrane stresses. The contribution from cell face stretching to the overall stiffness and strength of the foam is by a term that is linear in the relative density ρ_r, while the contribution from cell edge bending is non-linear in the relative density. The result is that the yield strength in compression of a metallic foam σ_{cs} is related to the yield strength of the cell wall material σ_y by [1]:

$$\frac{\sigma_{cs}}{\sigma_y} \approx 0.3\,\Phi^{1.5}\left(\frac{\rho^*}{\rho_s}\right)^{1.5} + (1-\Phi)\left(\frac{\rho^*}{\rho_s}\right) \tag{2.1}$$

where Φ, the distribution constant, is the fraction of solid in the foam that is contained in cell edges. The remaining fraction (1- Φ) occupies the cell face. Similarly, the modulus E^* of the foam related to the elastic modulus of the cell wall material E_s according to:

$$\frac{E^*}{E_s} \approx \Phi^2 \left(\frac{\rho^*}{\rho_s}\right)^2 + (1-\Phi)\left(\frac{\rho^*}{\rho_s}\right) \tag{2.2}$$

The experimental studies on mechanical performance of metallic foams are generally compression testing for determining the strength and stiffness. Koze *et. al.* [55], testing aluminum foams made with PCM process, showed that compressive strength and elastic stiffness increases almost linearly with increasing density. Also for checking the size effects, they used long and short specimens for testing. The compressive strength and its scattering are lower for longer specimens due to the higher probability of the existence of a weak link. Krizst *et al.* [56] compared the deformation behavior of different types of closed cell aluminum foam (Alulight and Alporas) and found out that inhomogeneities in the density distribution might be the key factor in determining the mechanical behavior of foams. Andrews *et al.* [57] determined the uniaxial compressive and tensile modulus and strength of several aluminum foams including closed cell foams of Fraunhofer and Alulight manufactured by PCM method and discussed the effects of imperfections in the cellular structure, density variations, cell wall curvature and cell wall corrugations on the measured values of Young's modulus and plastic collapse stress. Bart-Smith *et al.* [58] established the mechanisms of compressive deformation that occur in closed cell Al alloys. By using X-ray computed tomography and surface strain mapping they determined the deformation modes and the cell morphologies that control the onset of yielding. Banhart and Baumeister [59] investigated the deformation behavior of Al6Si4Cu alloy by uniaxial compression testing. They discussed the effects of closed outer skin and anisotropy owing to the foaming direction in the PCM method. The results show that further refinements in manufacturing methodologies are necessary in order to improve the reliability of foams, which is a must in high performance applications that demand low failure probability and high reproducibility. For generating mechanical test data on a given foam it is necessary to conduct large number of experiments before ascertaining any property. A summary of the mechanical and physical properties of the commercially available Al foams is given in Table 2.2 [3].

Table 2.2. Range for mechanical properties of commercial aluminum foams: The data show the range of properties associated with the range of relative density, lower values are associated with lower densities except for densification strain, where the reverse is true [3]

Properties, (units), symbol	**Cymat**	**Alulight**	**Alporas**	**ERG**
Material	Al-SiC	Al	Al	Al
Relative density (-), $\rho_r=\rho^*/\rho_s$	0.02-0.2	0.1-0.35	0.08-0.1	0.05-0.1
Structure (-)	Closed cell	Closed cell	Closed cell	Open cell
Density (gr/cm^3)	0.07-0.56	0.3-1.0	0.2-0.25	0.16-0.25
Young's Modulus (GPa), E	0.02-2.0	1.7-12	0.4-1.0	0.06-0.3
Shear Modulus (GPa), G	0.001-1.0	0.6-5.2	0.3-0.35	0.02-0.1
Bulk Modulus (GPa), K	0.02-3.2	1.8-13.0	0.9-1.2	0.06-0.3
Poisson's ratio (-), υ	0.31-0.34	0.31-0.34	0.31-0.34	0.31-0.34
Compression strength (MPa), σ_{cs}	0.04-7.0	1.9-14.0	1.3-1.7	0.9-3.0
Tensile elastic limit (MPa), σ_{ys}	0.04-7.0	2.0-20	1.6-1.8	0.9-2.7
Tensile strength (MPa), σ_{ts}	0.05-8.5	2.2-30	1.6-1.9	1.9-3.5
Densification strain (-), ε_D	0.6-0.9	0.4-0.8	0.7-0.82	0.8-0.9
Hardness (MPa), H	0.05-10	2.4-35	2.0-2.2	2.0-3.5
Max. service temp. (K), T_{max}	500-530	400-430	400-420	380-420
Thermal cond. (W/m·K), λ	0.3-10	3.0-35	3.5-4.5	6.0-11

2.6. Manufacturing of Al_2O_3 Reinforced AlMgSi Foams and Effects of Al_2O_3 Addition on the Mechanical and Structural Properties

Al matrix containing dispersed ceramic particles is the common structure of the foams fabricated by direct foaming (Cymat, Metcomb) and by baking cast precursors (Formgrip). In the direct foaming ceramic particles are intentionally added into the aluminum or aluminum alloy melts to make them foamable. Subsequently, gas bubbles are created by blowing air or inert gases and the melt is foamed [5]. In the production of Formgrip foams, ceramic particle reinforced metal matrix composites (MMCp) are recycled as cast precursors by melting and stirring blowing agent into the melt before solidification. The precursor is heated to the liquid state and gas released from the blowing agent creates the foam [60]. Both methods make use of ceramic particles as stabilizers.

Precursors can also be manufactured by compacting mixtures of aluminum powder and blowing agent by the powder metallurgy techniques e.g., by hot pressing, extrusion or rolling [14]. Generally, TiH_2 powder is used as the blowing agent. Foams are made by baking of powder compact precursors in the liquid state (powder compact melting method, PCM) which contains solid particles originating from the oxide skins of the individual metal powders. These solid particles are believed to stabilize the foam [39, 41].

In the powder compact melting (PCM) method the precursor is prepared in the solid state. Segregation effects and brittle reaction product formation are lower compared to liquid state processes. It is easier to mix different metal powders with aluminum to obtain aluminum alloys and mix ceramic particles to obtain MMCp.

Blending aluminum powders with alloying powders or using alloy powders with low melting temperatures e.g., AlSi7, AlSi10, AlSi12, AlMgSiCu and AlSiCu are preferable because TiH_2 releases hydrogen gas at temperatures much below the melting temperature of pure Al [61]. Additionally, TiH_2 can be heat treated to retard the hydrogen gas release [29, 46, 47, 49, 50].

The idea of ceramic addition for stabilization in the melt-based methods is also applicable to powder compact melting method. Foaming takes place above the liquidus

temperature of the compacted alloy and an enhancement in stabilization, foam structure and mechanical properties is anticipated by ceramic particle addition.

Kennedy and Asavavisitchai [34] added up to three vol. per cent of ceramic particles to PCM Al foams and reported an increase in linear expansion of the composite foams. They used Al_2O_3, SiC and TiB_2 particles with a particle size of 10 μm. Only SiC addition was reported to decrease gravitational drainage and increase stability.

Elbir *et al.* [32] showed that SiC addition increases the compressive strength of the PCM Al foams. Kennedy and Asavavisitchai [33] found a similar result with six vol. per cent TiB_2 addition. In these studies, the matrix was pure Al and the main motivation was to improve structural quality of the foam.

Excluding the density, the main variables contributing to the mechanical properties of metallic foams are the alloy composition and the metallurgical state of the matrix metal [3, 62, 63]. Lehmhus and Banhart [62] fabricated PCM AlMg1SiCu (AA6061) alloy foams and altered the metallurgical state of the matrix alloy by heat treatment. The average hardness of the metal matrix and compression strength of the foams increased up to 100 per cent.

The studies on the effects of ceramic particle addition on the mechanical behavior and cell structure of PCM aluminum alloy foams are limited. Esmaeelzadeh *et al.* [36] added up to 10 vol. per cent of SiC with different particle size to PCM AlSi7 alloy foams. They reported that the linear expansion and the stability of the foams depended on the size and amount of SiC particles. Increasing the amount and/or decreasing the particle size decreased the drainage but the cell structure became non-uniform. Compression strength of AlSi7+SiC foams was lower than AlSi7 foams because of the heterogeneity of the cell structure.

Asavavisithchai and Kennedy [35] added Mg and Al_2O_3 to PCM Al foams and showed that Mg presence with the ceramic increased the stability of the composite foam. Improved wetting of Al_2O_3 by the alloy matrix also decreased the drainage. No results regarding the mechanical properties were given. The results of the studies mentioned

above show that the influence of the ceramic particles on PCM foams, whether positive or negative, depends on the particle size, amount and the type of the ceramic and also to the composition of the metal matrix.

To investigate the effects of ceramic addition and heat treatment on the structure and mechanical behavior AlMgSi foams were fabricated in the laboratory by PCM method. Al_2O_3 was used as the ceramic reinforcement considering the Mg content of the alloy. AlMgSi and AlMgSi + Al_2O_3 foams in as foamed and heat treated conditions were characterized by metallography, microhardness measurements and compression tests.

2.7. Manufacturing of MMCp Foams from Extruded Powder Compacts

Manufacturing of Al foams with closed porosity can be divided into two fundamental methods; foaming from melts and from solid precursors. In direct foaming from melts, Al foams can be made by blowing air or gas below the surface of the melt containing uniformly dispersed ceramic particles [12] or adding and stirring a bubble generator blowing agent to the melt after the viscosity adjustment by creating solid components in situ [11].

In foaming from solid precursors, first the precursor is prepared by compacting powder mixtures of matrix material and blowing agent [14] or solidifying ceramic particle reinforced metal matrix composite (MMC_p) melts after dispersion of the blowing agent [64]. Then the precursor is heated to the melting temperature of the alloy and foaming takes place as the blowing agent decomposes and releases gas. Foam stabilization achieved in most of these methods is usually attributed to the ceramic particles that are intentionally mixed into the Al melts or already available in MMC_p melts and to the solid particles generated in situ by addition of alloying elements. However, foaming from the powder compact precursors does not generally involve addition of solid particles other than elemental metal powders or powders of Al alloys and the blowing agent. Currently, AlSi7, AlSi12, AlSi6Cu4, AlMg1SiCu and similar alloy powders are known to show good foamability, which is an expression used for describing how much porosity and kind of quality and also the degree of stability of the foam that can be achieved [61].

Production of foams from pure Al powder compacts is not common since it is not accepted as a good matrix material for foaming. To enhance foamability and physical properties of the Al foams ceramic particles were added [33-35] or Al powders with different oxide contents [39, 40] were used. Kennedy and Asavavisithchai [33, 34] reported that addition of up to six vol. per cent of 10 μm average particle size TiB_2, Al_2O_3 or SiC particles resulted in a significant increase of foam expansion however, it did not affect stability of the foam except for SiC. Authors believe that the enhanced foaming behavior was because of the reduction in critical cell wall thickness before rupture. Stability was affected by the degree of wetting which was particularly good for SiC. Elbir *et al.* [32] found that linear expansion of the foams was increased and the drainage and cell coarsening rates were decreased by SiC addition.

In an effort to improve wetting of Al_2O_3, Mg was added and an increase in the stability of the foams was reported [35]. An increase in oxide content of Al powders was also shown to have a positive effect on the expansion and stability of foams [40]. Stabilization mechanism is based on solid particles originating from the oxygen content of metal powders [39]. However, since oxide content of Al powders are dependent on manufacturing conditions, and excessive oxide contents can have an adverse effect on compaction and also on mechanical properties of foam products, ceramic particle addition seems to be a better way of making improvements in Al foam manufacturing.

In the previous works, Kennedy and Asavavisitchai [33-35] used cold compaction for composite precursor manufacturing while Elbir *et al.* [32] used hot compaction. In order to analyze the effects of different ceramic particle additions on foaming of Al, powder compacts were prepared by hot extrusion of Al-Al_2O_3 and Al-B_4C mixtures. The quality of the composite precursors can be increased by hot extrusion. B_4C is an interesting reinforcement material in Al composite manufacturing. It is a hard ceramic material used in tank armor, bulletproof vests or as an absorbent for neutron radiation arising in nuclear power plants, although its use in metal foam industry is rare.

2.8. Mechanical Properties of Hypereutectic AlSi Foams Manufactured by Using PCM Method

The selection of the matrix alloys for foam production is important and one has to consider some technical and economical requirements. In PCM method examples of these considerations are compaction and foaming behavior of the powders and achievable mechanical properties of the foam. In addition, the alloy powders or powders that will be used in the blend must be available in the market. The blowing agent, TiH_2, in as received condition decomposes hydrogen at approximately 400 °C, which is well below the melting temperatures of the common Al alloys. This gap can be narrowed by heat treating and oxidizing the blowing agent [46, 47, 50]. Another possibility is using low temperature melting alloys [61].

The binary AlSi alloys like AlSi7 and AlSi12 are the first alloys to be foamed owing to their low melting temperatures. The silicon content in the commercially available foams is generally below the eutectic composition. To see the effects of higher Si content on the foaming behavior, microstructure and mechanical properties, hypereutectic AlSi alloy foam was manufactured and some of its mechanical properties were characterized. In casting of aluminum alloys, more silicon is added to increase the fluidity of the molten alloy as well as improving the wear resistance of the product. Wear resistance increases because of the primary Si particles that have been crystallized and grown before the eutectic temperatures. Aluminum and silicon constitute a simple binary eutectic system with the eutectic point at 12.2 wt. per cent and 577 ° C. This is shown in the binary phase diagram in Figure 2.18 [64]. The primary Si particles are larger and have an angular geometry. After cooling below the eutectic point Al and finer Si particles are formed. The eutectic Si particles are complex shaped. Powder metallurgy (PM) processing offers some significant advantages over casting, particularly in its ability to produce hypereutectic alloys with relatively fine Si particles, which can provide a wear-resistant and good machinable product. Although wear resistance of foam products are not of interest, primary Si generated in situ may act as a ceramic or a solid particle addition hence help with foam stabilization and expansion. Fine eutectic Si will increase the strength of the matrix. In addition, the strength and hardness levels of the foams can be increased by further heat treatment.

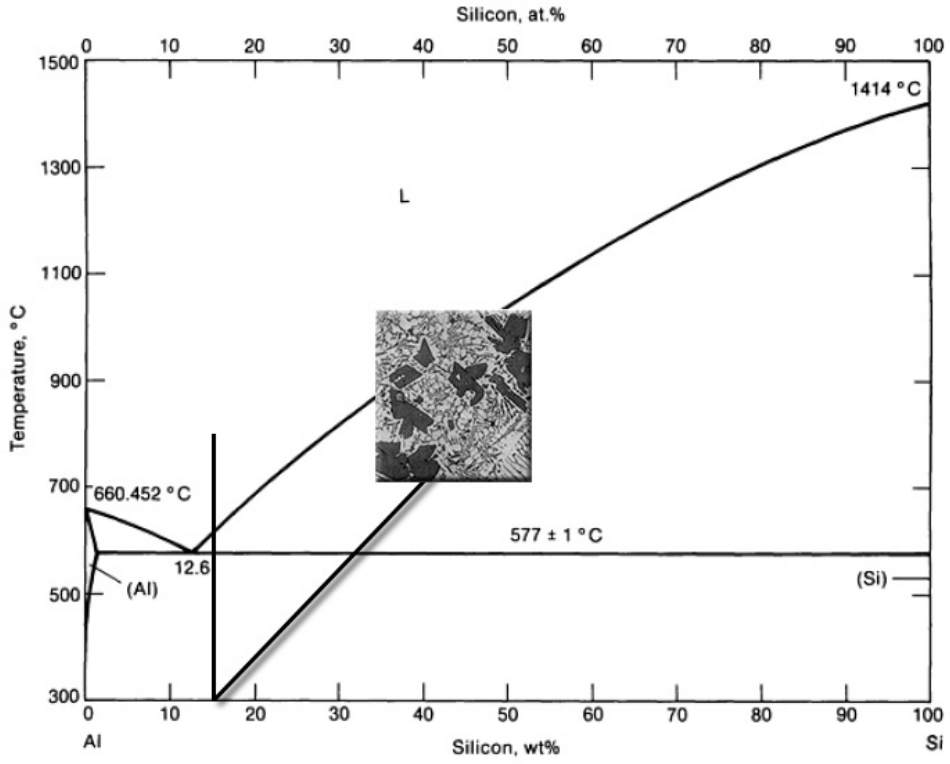

Figure 2.18. Al-Si phase diagram and typical microstructure at 16 per cent Si [64]

3. MATERIALS AND METHODS

3.1. Manufacturing of Al_2O_3 Reinforced AlMgSi Foams and Effects of Al_2O_3 Addition on the Mechanical and Structural Properties

3.1.1. Materials

AlMgSi powder was obtained by degassing and removing the wax from the premix powder of ECKA, Austria (Trade name Alumix 321). This mixture contains elemental powders of Al, Mg, Si and Cu. The characteristics and amounts of the materials used including Al_2O_3 and TiH_2 (Sigma Aldrich) are summarized in Table 3.1. Figure 3.1 shows the SEM micrographs of the powders. The shape of particles in the AlMgSi blend is irregular. Other powders have an angular shape. TiH_2 powders were heat treated at 480 °C for three hours before addition to the mixture. To obtain the desired mixtures, powders were weighed and poured in a plastic bottle which was subsequently put inside a ceramic bowl rotating at 200 rpm on a tumbler mixer. For disturbing the mixture alumina balls were also added to the bottle. The plastic bottle was positioned so that during rotation the content followed a path like eight as shown in Figure 3.2. Mixing time was approximately one hour. The plastic bottle was carefully emptied on aluminum foils and the alumina balls and powder mixture were separated.

Table 3.1. Characteristics and amounts of powders used as starting materials

Powder	**Size**	**Amount (wt.%)**				
		Al	Cu	Mg	Si	wax
A321	63-200 µm	balance	0.15-0.35	0.45-0.75	0.85-1.15	1.5
		Mixture				
		A0	A3	A5	A10	
		A321	A321	A321	A321	
TiH_2	<43 µm	0.6 wt.%	0.6 wt.%	0.6 wt.%	0.6 wt.%	
Al_2O_3	<20 µm	0 vol.%	3 vol.%	5 vol.%	10 vol.%	

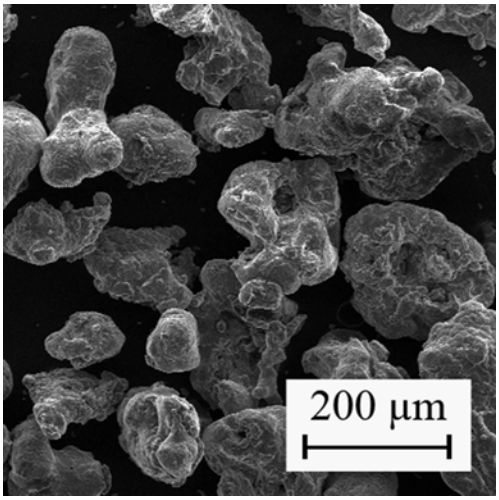

(a)

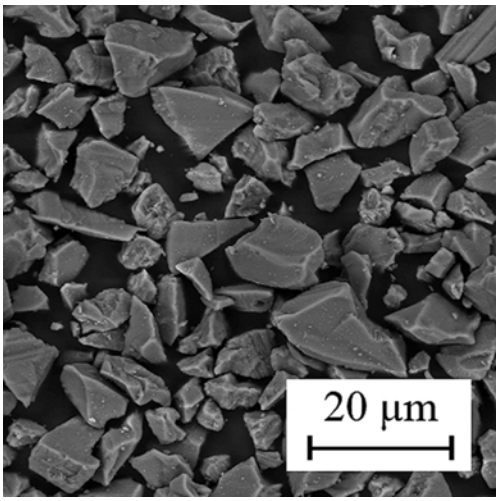

(b)

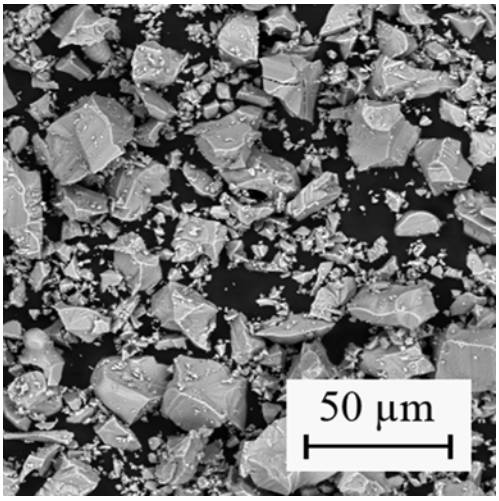

(c)

Figure 3.1. SEM micrographs: (a) A321 , (b) Al_2O_3 and (c) TiH_2 powders

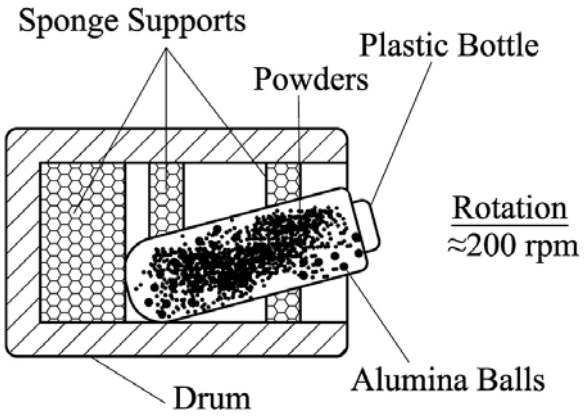

Figure 3.2. Schematic representation of mixing set-up used for blending metal powders and ceramics

3.1.2. Design and Implementation of Hot Compaction Press

The first step in foam manufacturing by using the PCM method is compaction of the powder mixtures to obtain precursors. The compaction of the precursors was done by 30 tones capacity hydraulic press. The trials on compaction of precursors showed that the hydraulic press available in the lab with its original hydraulic actuator unit and setup was not suitable. The schematic diagram of the hydraulic system before modification is shown in Figure 3.3a. The pump of the system was driven by an AC motor and fed the system with a flow of eight liters per minute. The pressure was set by the operator using the pressure control valve. Pressure was observed by the manometer connected to the hydraulic block. There was a two-way solenoid valve, actuated by a signal giving a flow of fluid to the top of the cylinder and then reversed the flow of fluid when the signal was off. The backflow was done by the spring system inside the valve. The solenoid valve was a two-way valve which drove the oil through point A or point B according to the 220 Volt AC signal. The signal was sent by the electronic controller. In this system compaction signal should be given to solenoid valve for continuous flow of fluid to the hydraulic cylinder. As a result, the hydraulic pump, the pressure valve and the solenoid valve worked continuously during compaction to maintain the pressure inside the cylinder. The continuous flow of the fluid in the hydraulic block created frictional heat within a short

time. This resulted in a pressure drop in the manometer readings after approximately 10 minutes. It was also not feasible to keep the pump working during the long compaction times. This could decrease the working life of the pump. A modification of the hydraulic press system to overcome these difficulties was necessary.

First consideration was the long holding time (min. 30 minutes) for hot compaction of powder mixtures. A check valve was placed between hydraulic cylinder and output of A of the solenoid valve (Figure 3.3b). By this way after desired pressure was reached, it was maintained inside the cylinder until a signal was sent for reversing the flow through B. However, with the old solenoid valve this reversing operation was made automatically when the signal was turned off by the spring system. This simple solenoid valve was not suitable because as soon as the signal was off, return spring reversed the flow back and locked pressure by the check valve was released. Therefore, a 4-way 3-position directional valve, with two solenoids was placed into the system. A signal started the flow from “P” to “A” to the cylinder and when the maximum load was reached signal was turned off and positioning of spool at rest was obtained with centering springs. At this position flow was not reversed through the cylinder, it was sent back to the tank inside the solenoid valve. During this stage there was no load on the pump. The pressure was constant inside the cylinder provided by the check valve not by the pump and the solenoid valve. It was even possible to turn off the pump. The modification of hydraulic cylinder let the user to hold the compaction die longer times for hot compaction without any heating inside the hydraulic system. It also made the process economical because pump was working for only one or two minutes maximum. When the hot compaction was finished the pump was turned on again and a signal was sent to the second solenoid which let the oil flow through “B” to “T”. By a t-connection oil was also sent to check valve through “X” which released the valve hence pressure inside the cylinder.

The second problem was minimizing the heat flow from the compaction dies through the punch and support of the hydraulic press. This was achieved by minimizing the surface contact of the compaction dies and the hydraulic press by machining channels at the bottom of the dies. Also, a refractory material was placed between the bottom part of the die and hydraulic press support. The refractory material was fixed on a stainless steel grid which further decreased the contact surface of the compaction setup.

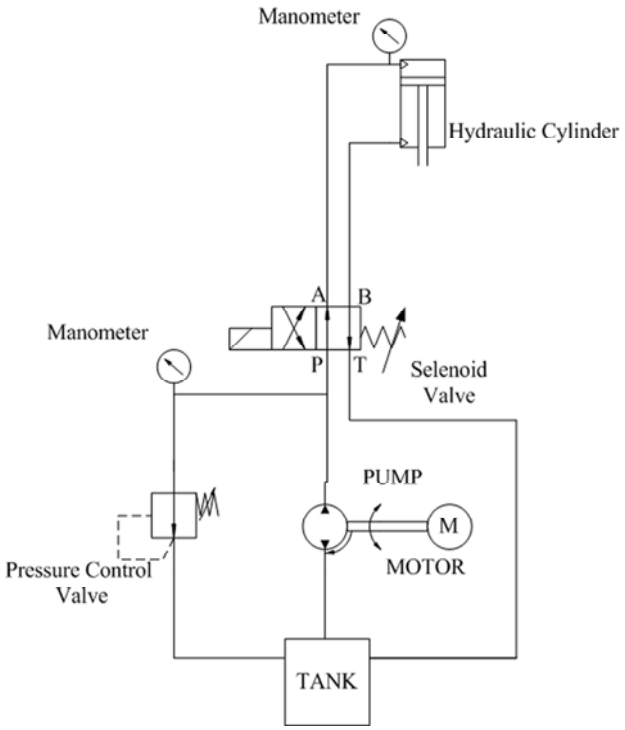

(a)

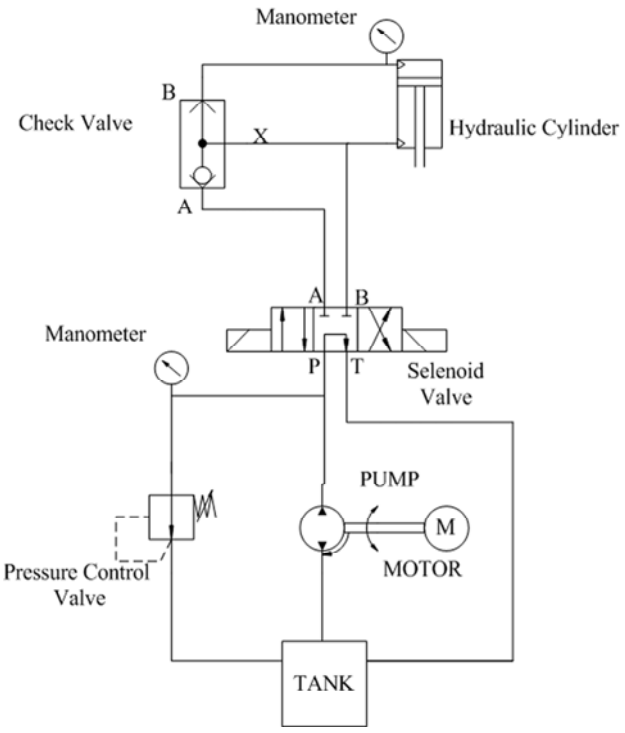

(b)

Figure 3.3. Schematic diagram of the hydraulic actuator circuit:
(a) before modification [66], (b) after modification

3.1.3. Manufacturing of the Foams

AlMgSi and composite foams were produced by PCM method. Compaction procedure started with cold pressing the powder mixture at 300 MPa, for easier handling, followed by hot pressing at 430 °C and 300 MPa for 30 minutes. After the modification of hydraulic press, it was possible to heat and press the powder mix for as long as one hour. Compaction dies and punches were manufactured from DIN 1.2344 (AISI H13) hot work tool steel and hardened to 54 HRC. The inside of the die and punch surfaces were grinded to achieve close tolerances. Only 10 to 20 mm of the punch height was kept close to the inside diameter of the punch considering the small gaps between the punch and die could be filled with fine aluminum powders especially at high temperatures and pressures. A channel, five mm in length with a small diameter was left close to the punch front. This collected the powder leakage from the punch-die gap and reduced sticking to the surfaces. To avoid sticking further, a high temperature resistant lubricant was used. Heating of the dies during compaction was done by cylindrical ceramic heaters. The compaction dies, punches and heaters used are shown in Figure 3.4. The temperature of the molds were adjusted by an on/off controller using a K-type thermocouple placed inside the die wall. After compaction cylindrical precursors with dimensions of Φ = 27 mm and h=13-15 mm were obtained. The height changed with the amount of powder mixture.

Figure 3.4. The equipment used for PCM foam manufacturing: from left to right; foaming molds, mold heaters, compaction molds, extrusion die and die holder

An example microstructure of the composite precursors is shown in Figure 3.5. It can be seen that the size of the ceramic particles plays an important role in the blending and hot compaction stage. When large Al alloy particles are mixed with fine Al_2O_3 particles the distribution of the ceramics is not homogeneous and ceramic particles tend to agglomerate. The agglomerates cannot be broken during cold and hot compaction and they remain between the opposing interfaces of large Al powders (Figure 3.5b). The hard and agglomerated ceramic particles affect the compaction density negatively. The powder compact with open porosity cannot be foamed successfully because hydrogen gas released escapes before it contributes to foam expansion.

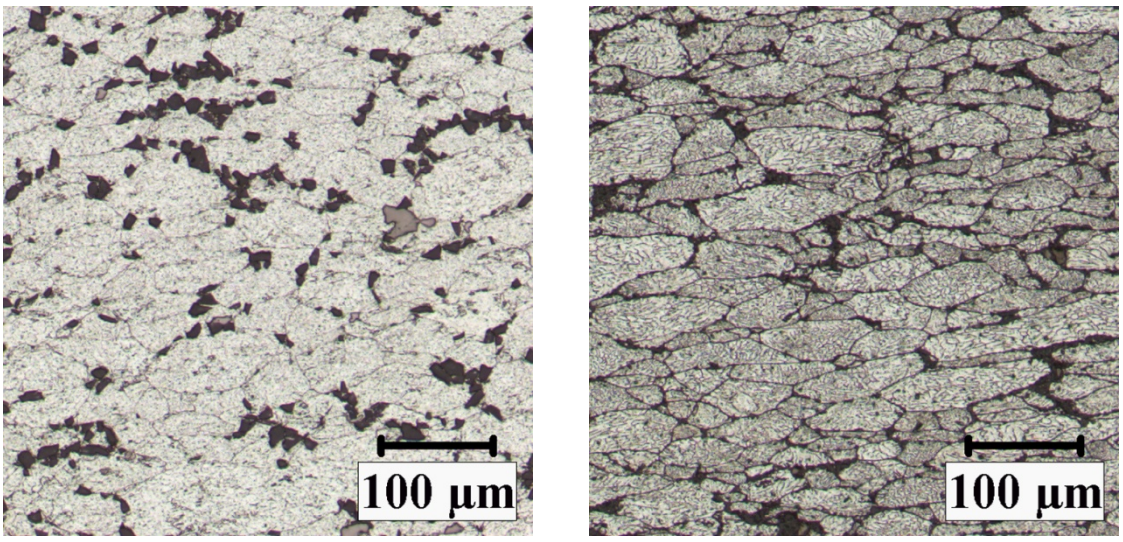

(a) (b)

Figure 3.5. Microstructure of the hot compacted precursor: (a) Al_2O_3 (<20 µm) particles are embedded in Al powders, the dark gray particle on the right hand side is TiH_2 (b) Al_2O_3 (<12 µm) particles agglomerated between large Al particles

Hot compacted precursors were foamed in a preheated standard chamber furnace at 750-800 °C in thin walled AISI 310 stainless steel cylindrical tubes. The inside diameter of the steel tubes was approximately 30 mm. Different heights of tubes were used for adjusting the expansion and the density of the foams for macrostructure analysis, namely 30, 48 and 60 mm. All of the foams that were used in compression testing were foamed

inside 60 mm height tubes. Top and bottom of the tubes were closed with AISI 310 plates and plates were fastened by AISI 304 stainless steel bolts (see Figure 3.4). The expansion of the powder compact after melting was observed through a quartz window on the furnace lid. When maximum expansion was reached, tubes were carefully taken out of the furnace, placed on a rotating platform and cooled by pressurized air. After cooling, the cylindrical foam specimens were obtained easily by removal from the mold (Figure 3.6).

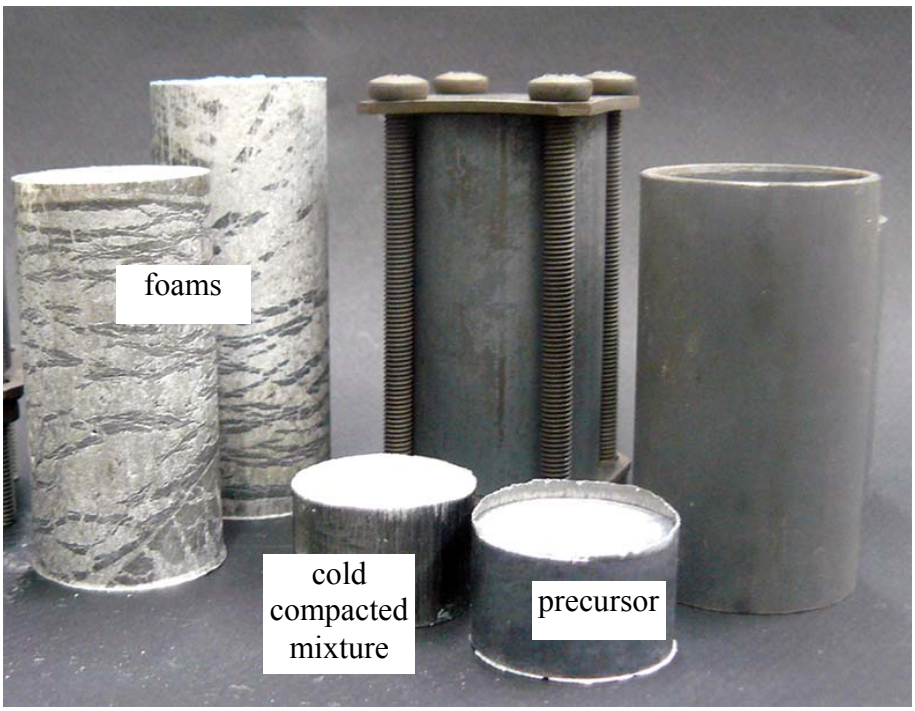

Figure 3.6. Precursor, foam, stainless steel tube and foaming mold assembly

3.1.4. Heat Treatment of AlMgSi and Composite Foams

In AlMgSi alloys maximum strength is achieved by the precipitation of Mg_2Si after solution heat treatment (SHT) and age hardening. During the preparation of the precursor and foaming of the powder compact Al_2O_3 may react with Mg to form spinel ($MgAl_2O_4$). This reaction may also occur during SHT. While the wetting of the ceramic by the matrix

alloy can be improved with the Mg present, the reaction with Al_2O_3 may inhibit the hardenability of the foam.

To analyze the effect of heat treatment on the AlMgSi matrix of the foams and identify the peak hardness after age hardening foam specimens with different heat treatment conditions, namely; as foamed, annealed, SHT, and SHT followed by aging for 2, 8 and 16 hours were prepared for microhardness testing. SHT and aging temperatures were similar to conventional 6061 alloy. Samples were heated to 530 °C inside the foaming furnace and held for 100 minutes. Subsequently, they were water quenched and dried. One of the samples was annealed at 420 °C for three hours, slowly cooled to 260 °C, held for one hour and finally slowly cooled to room temperature. Age hardening of the remaining samples was done inside a drying furnace at 175 °C. During heat treatment the solid skin of the foams seen in Figure 3.6 were not removed since this prevented water intrusion during the quenching stage of SHT.

3.1.5. Macro and Microstructure of the Foams and Microhardness Testing

Precursors with the same weight were foamed in steel tubes 30, 48 and 60 mm in height for observing the foam structure at different expansions. Apparent density of the foams were calculated by measuring total weight and dividing to the volume after measuring the necessary dimensions with a digital caliper. Foams were sectioned in longitudinal direction from the center by electro discharge machining (EDM). Sample foam sections were photographed for visual observation of the structure. Digital image analysis was used to measure the porosity from the cross section.

Microstructure of the cell walls for various specimens were characterized by cutting off 5 to 10 mm thick slices from the foams with a slow speed diamond saw, embedding in an epoxy resin and polishing. Analyses were done both under optical and electron microscope. Same metallographic samples were used for microhardness testing. At least 10 Vickers hardness measurements with a load of 25 gf for thin and 50 gf for thick cell walls were done at various locations for each specimen. Loading time was 10 s. The measurements were done after slight etching of the specimens with the Keller's agent. Etching was done to distinguish clean surfaces from grain boundaries, voids, ceramic or

dense oxide containing surfaces. Surfaces of foam cell faces were observed with SEM to identify the wetting of ceramic particles and their distribution in the matrix alloy. Slices were cut off the foams with diamond saw, washed in ultrasonic bath with ethanol and acetone, dried and moderately etched before the analyses.

3.1.6. Compression Tests

Compression tests were carried out at room temperature using a Zwick/Roell 100 kN capacity universal testing machine with a crosshead speed of 1 mm/min. Machine was programmed for unloading and reloading at selected deformations for determination of the elastic stiffness. The stiffness of the machine was much higher than foam samples. The displacement of the crosshead could be used to determine overall compressive strain. Compression was stopped at 80 per cent strain. The solid skin of all the samples was removed by machining in a conventional lathe (Figure 3.7). For compression testing minimum h/d ratio of specimens was kept at a minimum value of two. The solid layer at the top and bottom of the foams were cut off. The surfaces of the compression plates were cleaned and greased before all compression tests.

Figure 3.7. Removal of the outer solid skin of foams by machining

3.2. Manufacturing of MMC_p Foams from Extruded Powder Compacts

3.2.1. Materials

The metal powder was commercial purity aluminum obtained from Gürel Makina A.Ş., Istanbul (99 wt. per cent Al, see Table 3.2 for chemical analysis). Ceramic powders were commercial purity Al_2O_3 and B_4C. The blowing agent was titanium hydride (TiH_2, Sigma Aldrich). Ceramic powders were added to the Al-TiH_2 mixture up to 10 vol. per cent and blended dry in a tumbling mixer for 30 to 60 minutes (see Figure 3.2). Before preparation of the mixtures, TiH_2 powders were subjected to heat treatment at 480 ºC for three hours. Powder mixtures prepared for precursor and foam manufacturing are summarized in Table 3.3. Figure 3.8 shows the SEM micrographs of some of the powders and powder mixtures. Al powders have irregular shape with rounded edges, while the others have irregular and angular shape with sharp edges. An agglomeration in small Al_2O_3 powders is observable.

Table 3.2. Chemical composition of Al powder compact with 0.6 wt. per cent TiH_2

Element – Amount (wt.%)						
Silicon	**Iron**	**Copper**	**Zinc**	**Titanium**	**Aluminum**	**Other**
0.308	0.265	0.098	0.014	0.533	98.68	0.102

3.2.2. Powder Compaction

Cold pressing and hot extrusion was used for precursor production. 60 grams of powder mixtures were cold pressed uniaxially to 30 mm diameter cylinders at 300 MPa. Subsequently green compacts were hot extruded through a standard 0° die to a thin rectangular shape 20×2.5 mm^2 in cross section. Extrusion ratio with respect to the inside diameter of the die container and cross section of the extrude is 16.

Extrusion is a commonly used secondary operation in composite fabrication process. When performed at elevated temperatures, it combines hot compaction and hot mechanical working, yielding a fully dense product. Solid matrix is deformed by plastic flow or creep and powders are welded to each other and reinforcement material [67]. Selected extrusion parameters were 380-420 ºC extrusion temperature; and 3 to 5 mm/min ram speed.

Figure 3.9 shows a schematic view of the extrusion setup used in this study. The extrusion setup consists of a horizontal hydraulic cylinder, container, container holding unit, hydraulic power generator, ram and horizontal press body frame. The hydraulic cylinder has a 200 mm inside diameter. The fluid can flow inside the cylinder with a pressure up to 300 bar by the hydraulic pump running with 5.5 kW electric motor. The maximum hydraulic force is approximately 90 tones. Movement of the hydraulic piston hence the ram is controlled manually by a hydraulic control lever. Ram speed is adjusted by a flow controller. Heating of the extrusion container and die to desired temperatures is done by an on-off controlled clamped around the container. The extrusion die holder, extrusion dies and ceramic resistance heater are shown in Figure 3.4.

Table 3.3. Powder mixtures prepared for precursor manufacturing

Powders	**Al_2O_3**	**Al_2O_3**	**B_4C**	**Al**	**TiH_2**
Size	<12 µm	<20 µm	<30 µm	44-160 µm	<43 µm
	Amount				
Mixture	(vol.%)				(wt.%)
A1	-	-	-	100	0.6
CA1	5	-	-	95	0.6
CA2	10	-	-	90	0.6
CA3	-	5	-	95	0.6
CA4	-	10	-	90	0.6
CB	-	-	5	95	0.6

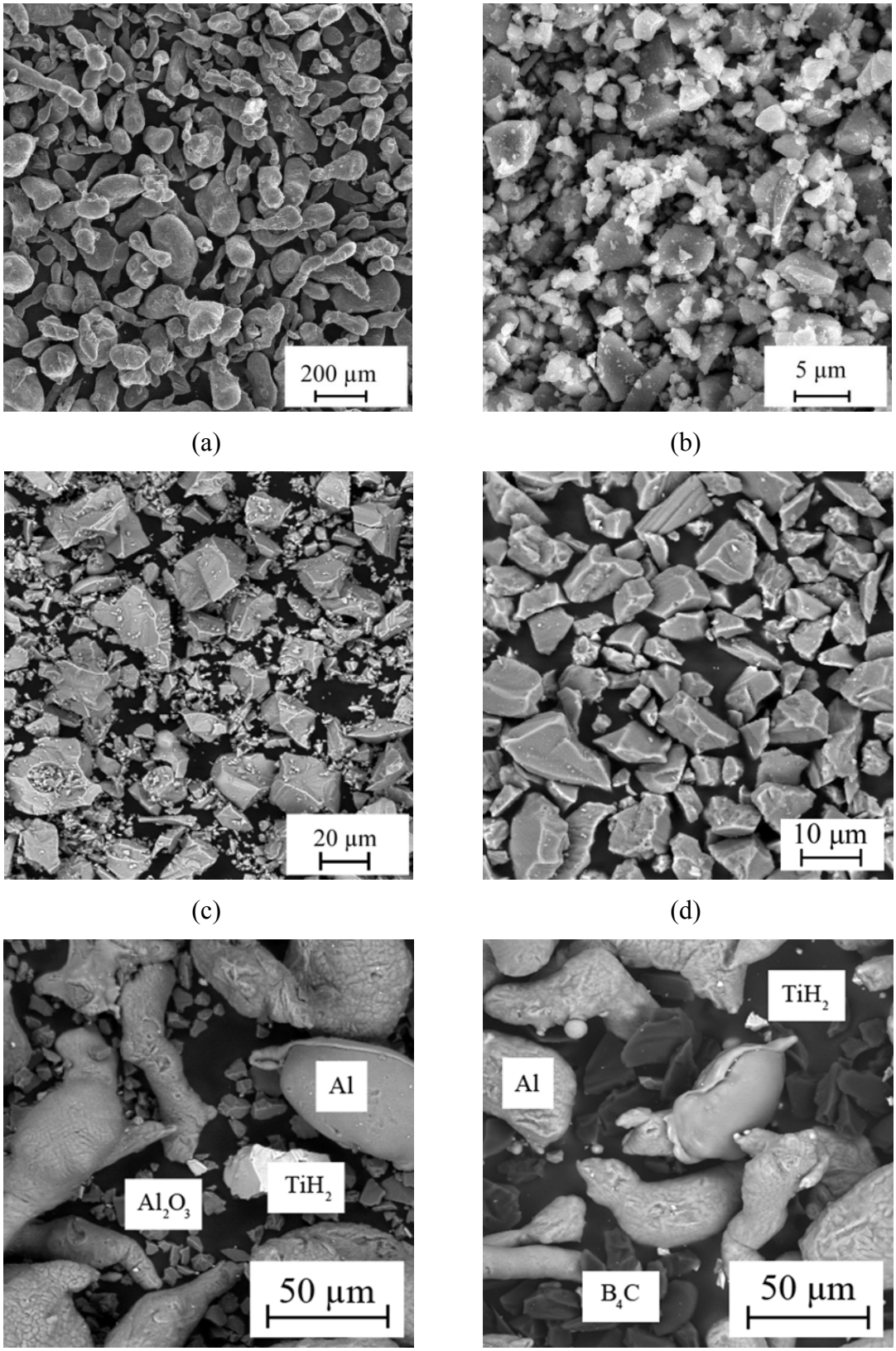

Figure 3.8. SEM micrographs showing the size and morphology of the powders:
(a) Al, (b) Al_2O_3 (<12 µm), (c) TiH_2, (d) Al_2O_3 (<20 µm), (e) CA3 mixture, (f) CB mixture

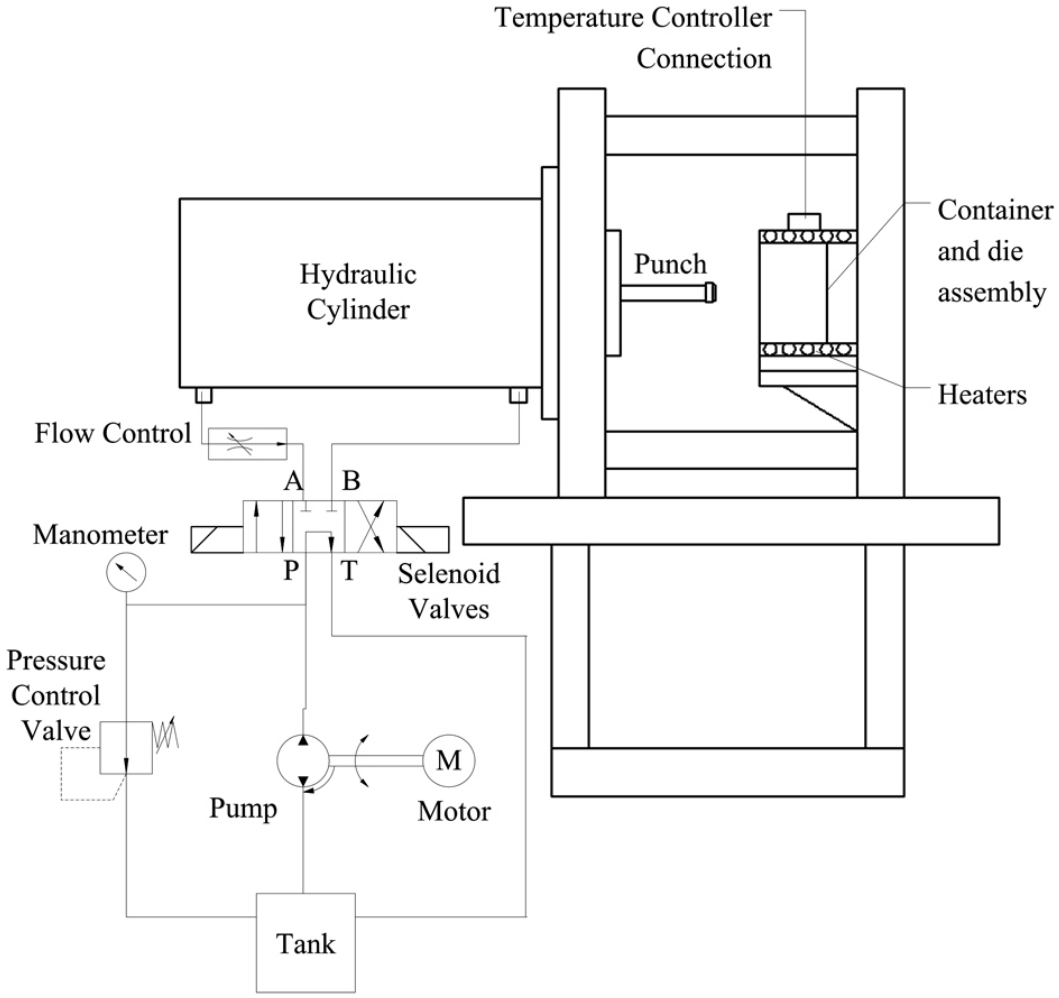

Figure 3.9. A schematic view of the extrusion setup used throughout this study [68]

3.2.3. Foaming

Foaming was done in a preheated furnace at different temperatures ranging from 800 to 850 ºC. Long extrusion products were cut into four centimeters long pieces and placed on a preheated stainless steel plate with a thin layer of ceramic refractory material above. Observation of free foaming experiments was done through a quartz window inside the furnace. For each mixture at least 10 precursors were foamed at selected temperatures. Times for initiation of foaming, maximum expansion, and collapse were also recorded. Some of the foams were taken out of the furnace after maximum expansion was reached and cooled with a ventilator for microstructure analyses.

3.3. Mechanical Properties of Hypereutectic AlSi Foams Manufactured by Using PCM Method

3.3.1. Materials and Manufacturing Method

Hypereutectic AlSi alloy powder was obtained by degassing and removing the wax from the premix powder of ECKA, Austria (Trade name, Alumix 231). This mixture contains elemental powders of Al, Si, Cu and Mg. Table 3.4 shows the approximate chemical composition of the powders provided by the manufacturer and optical spectroscopy analysis results of the precursor used for foam production.

The blowing agent, TiH_2, was supplied by Chemetall A.Ş., Turkey. Powders were heat treated at 480 °C for three hours before addition to the mixture. Figure 3.10 shows the SEM micrograph of the powders. The shape of particles in the blend is irregular and TiH_2 powders have an angular shape. Manufacturing was done with PCM method and the procedure is the same as the one described in Section 3.1. Foams had 30 mm diameter and 60 mm height after removal from the mold.

Table 3.4. Chemical composition of Alumix 231 and the results of chemical analysis of foamable precursor material (Alumix 231 + 0.5 wt. per cent TiH_2)

Element	Al	Si	Cu	Mg	Wax	Ti
Values provided by ECKA (wt. %)	Bal.	14-16	2.4-2.8	0.5-0.8	1.5	
Measured (wt. %)	Bal.	16.4	2.6	0.6		>0.3

3.3.2. Heat Treatment of Hypereutectic AlSi Foams

To analyze the effect of heat treatment on the matrix alloy of the foams and determine the hardness after age hardening 20 grams of metal powder mixture without the blowing agent was prepared with the addition of 0.5 wt. per cent pure Ti. Following the same procedure for foam production, solidified sample was cut into four by diamond saw.

The four pieces were separated as annealed, as foamed, solution heat treated (SHT) and SHT and aged. Details of the heat treatment were given in Section 3.1. Micro hardness testing and microstructural examinations were done on these samples. Without the blowing agent, the samples had low porosity and it was easier to embed into epoxy, polish for microstructure examination and measure hardness. AlSi foams manufactured were divided into three groups; as foamed, SHT and SHT + Aged.

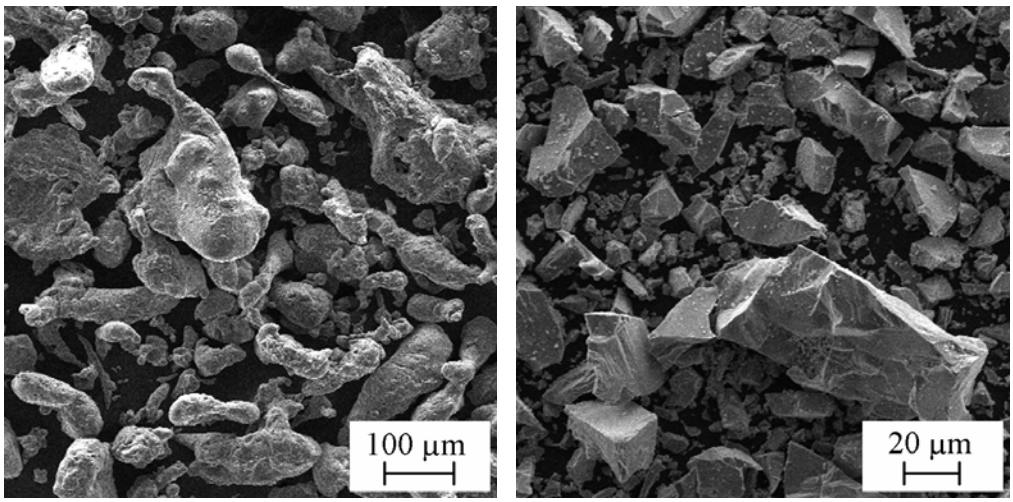

(a) (b)

Figure 3.10. SEM micrographs of A231 (a), and TiH_2 (b) powders

4. RESULTS AND DISCUSSION

4.1. Manufacturing of Al_2O_3 Reinforced AlMgSi Foams and Effects of Al_2O_3 Addition on the Mechanical and Structural Properties

4.1.1. Heat Treatment of TiH_2

Melting temperature of AlMgSi is approximately 580 °C. The alloy has a two-phase region, liquid and solid, until 650 °C. Above this temperature, the alloy is liquid. However, the blowing agent, TiH_2, starts to decompose at about 400 °C [46]. The mismatch between the melting point of the alloy and decomposition temperature of the blowing agent affects the quality of the foams [29]. TiH_2 is heat treated and oxidized at various temperatures between 400 and 520 °C to delay hydrogen gas releasing and shift decomposition temperature to higher values [47, 50]. To address this, TiH_2 powder were heat treated in air at 480 °C for three hours. Figure 4.1a shows XRD patterns of as received and heat-treated powders. It can be seen that after heat treatment, the peaks were shifted to higher angles and intensity values were decreased. This was an indication of formation of new layers with less crystalline phases on the TiH_2 powders. Some different peaks corresponding to titanium oxides were detected and are labeled on the pattern.

Matijesevic and Banhart [50] showed with transmission electron microscopy (TEM) analysis the oxide layer growth on TiH_2 particles during heat treatment. This layer was reported to inhibit hydrogen decomposition. Measurement of the mass change by thermo-gravimetric analysis (TGA) showed that the temperatures for hydrogen release and maximum hydrogen release rate increased approximately 100 °C and 60 °C after heat treatment of TiH_2 respectively. Exact temperature and time values found may vary when compared with the literature due to its strong dependence on purity of TiH_2, and due to the conditions of the measurement like the sample of the mass, heating rate and atmosphere.

Figure 4.1b shows TGA data of the two powders heated from room temperature up to 600 °C with a heating rate of 20 °C/min. The onset temperature of gas release was shifted approximately four minutes. The treatment showed the reduction of total gas release,

which was an indication of hydrogen loss during heat treatment. Although maximum rate of weight loss was higher for as received TiH_2, the average value of the curve was higher for heat treated TiH_2. During foaming heating rates are much higher (120 °C/min). However, the results showed that there would be more time for melting of the matrix alloy before the heat-treated TiH_2 releases hydrogen when compared with as received TiH_2.

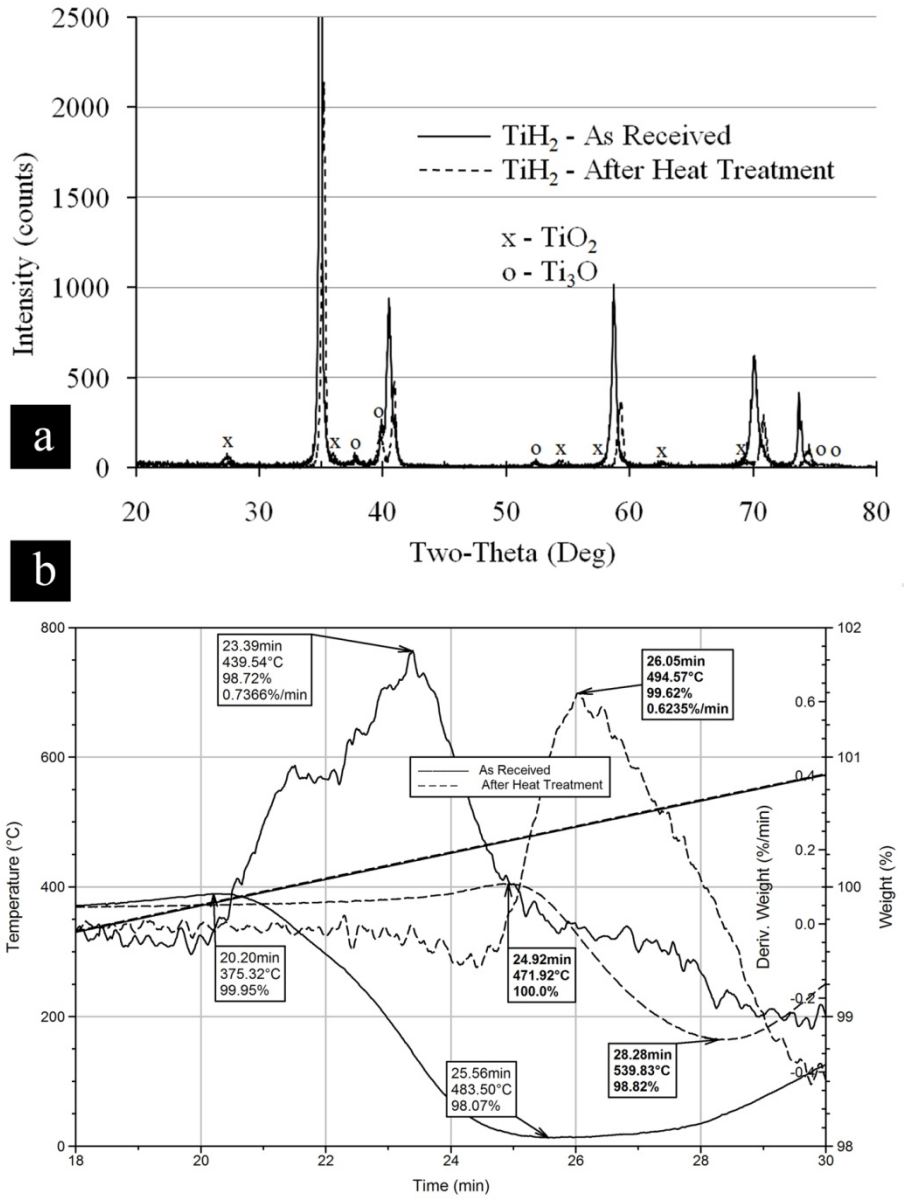

Figure 4.1. Effects of heat treatment on TiH_2: (a) XRD patterns of as received and heat treated powders showed formation of TiO_2 and Ti_3O oxides, (b) TGA data showed the retardation of hydrogen gas release after heat treatment

4.1.2. Macrostructure of the Foams

The most important property of the foams is its relative density (ρ_r). Relative density is found by dividing the foam density ρ^* to the density of matrix material ρ_s which was taken as 2.7 gr/cm^3 for AlMgSi alloy. Figure 4.2 shows the macrostructure of the AlMgSi foams with the same weight but with different expansions. At earlier stages of foaming the cells had grown in transversal direction perpendicular to the compaction direction and there was a heterogeneous distribution of cell sizes with different aspect ratios (ρ^*=1.13 gr/cm^3). Relative density was close to 0.42 and the structure was more like a solid containing isolated pores. As the expansion continued cell shapes became rounder and a relatively homogeneous distribution in size was observable (ρ^*=0.71 gr/cm^3). When the maximum expansion was reached general structure was more or less the same except the cells were larger in size and some cells were aligned in the upward foaming direction (ρ^*=0.57 gr/cm^3). The cells close to the mold wall were smaller and there was a thin solid skin at the mold-foam interface indicating the mold wall-melt interaction and solidification direction. There was no significant accumulation of the solid metal at the bottom although there was a density gradient from the bottom to the top.

The amount of Al_2O_3 changed the foam structure in composite foams. As seen in Figure 4.2 when three vol. per cent Al_2O_3 was added the cell shapes and sizes were not affected significantly. When the amount was increased to five per cent cells became larger but still there was a fine structure and other than a few number of cells cell size was homogeneous. Structure was significantly changed when Al_2O_3 content was increased to 10 vol. per cent. Number of the cells decreased and cell sizes became larger. The bottom of the foam was significantly denser. Cell walls were thinner and Plateau borders were small at the top of the foam, which was an indication of liquid drainage by gravitational forces. Here one most also consider the relative density of the composite foams. Using the rule of mixtures densities of the matrix materials of the composite foams was found as 2.74 gr/cm^3, 2.76 gr/cm^3 and 2.83 gr/cm^3 for 3, 5 and 10 vol. per cent of Al_2O_3 addition respectively. This means that the relative densities of the foams from left to right were 0.211, 0.208, 0.206 and 0.201. Foams were cut by EDM but some tearing of cell walls especially at the center of the foams could not be avoided. Porosity calculated from

binarized images shown in Figure 4.4, Figure 4.5 and Figure 4.6 are labelled on the figures. The results are close to relative densities calculated except A10 foam.

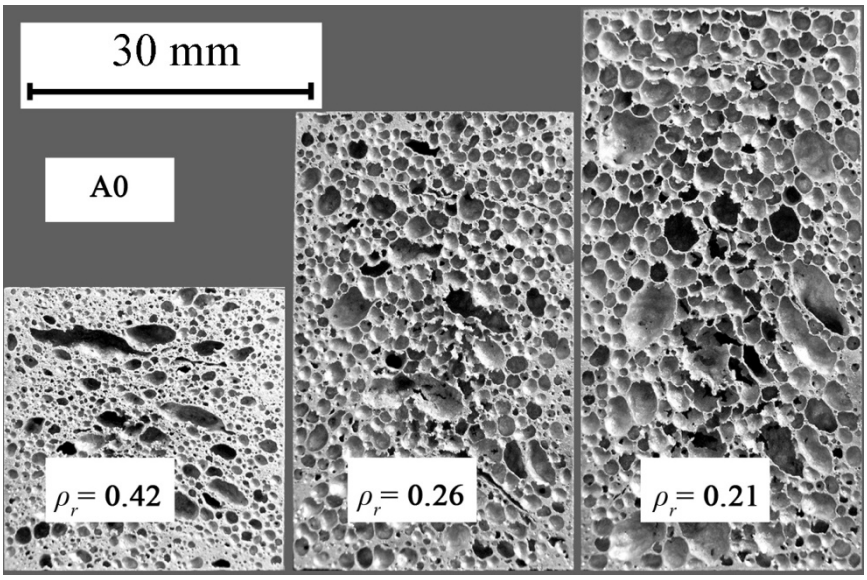

Figure 4.2. Cell morphology of AlMgSi foam at different linear expansion heights

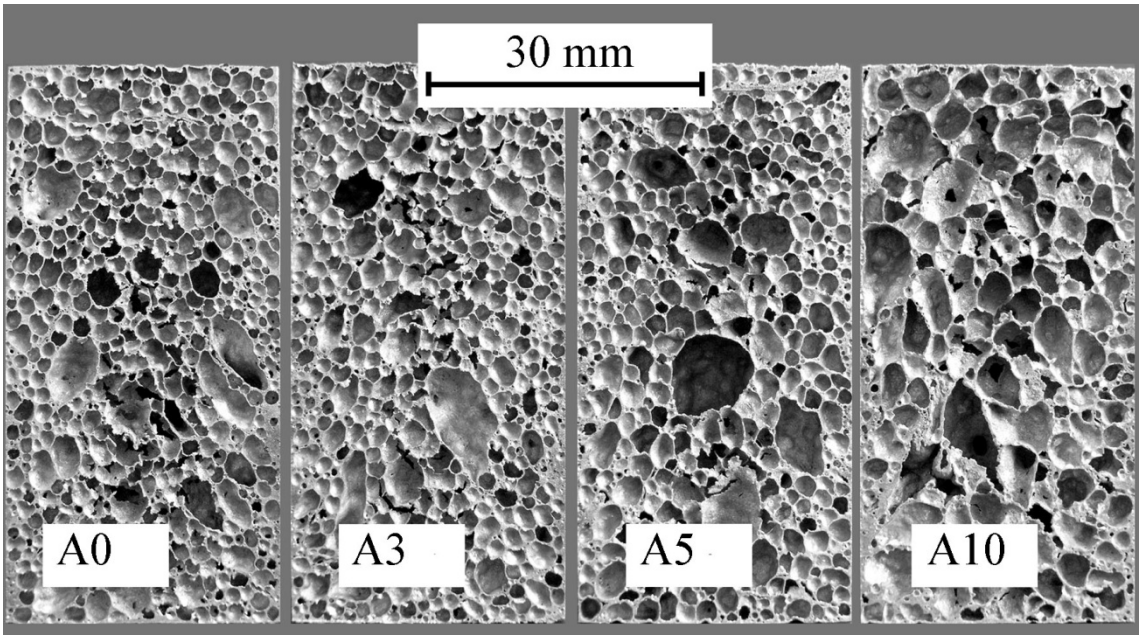

Figure 4.3. Cell morphology of AlMgSi and AlMgSi + Al_2O_3 foams with increasing amount of Al_2O_3

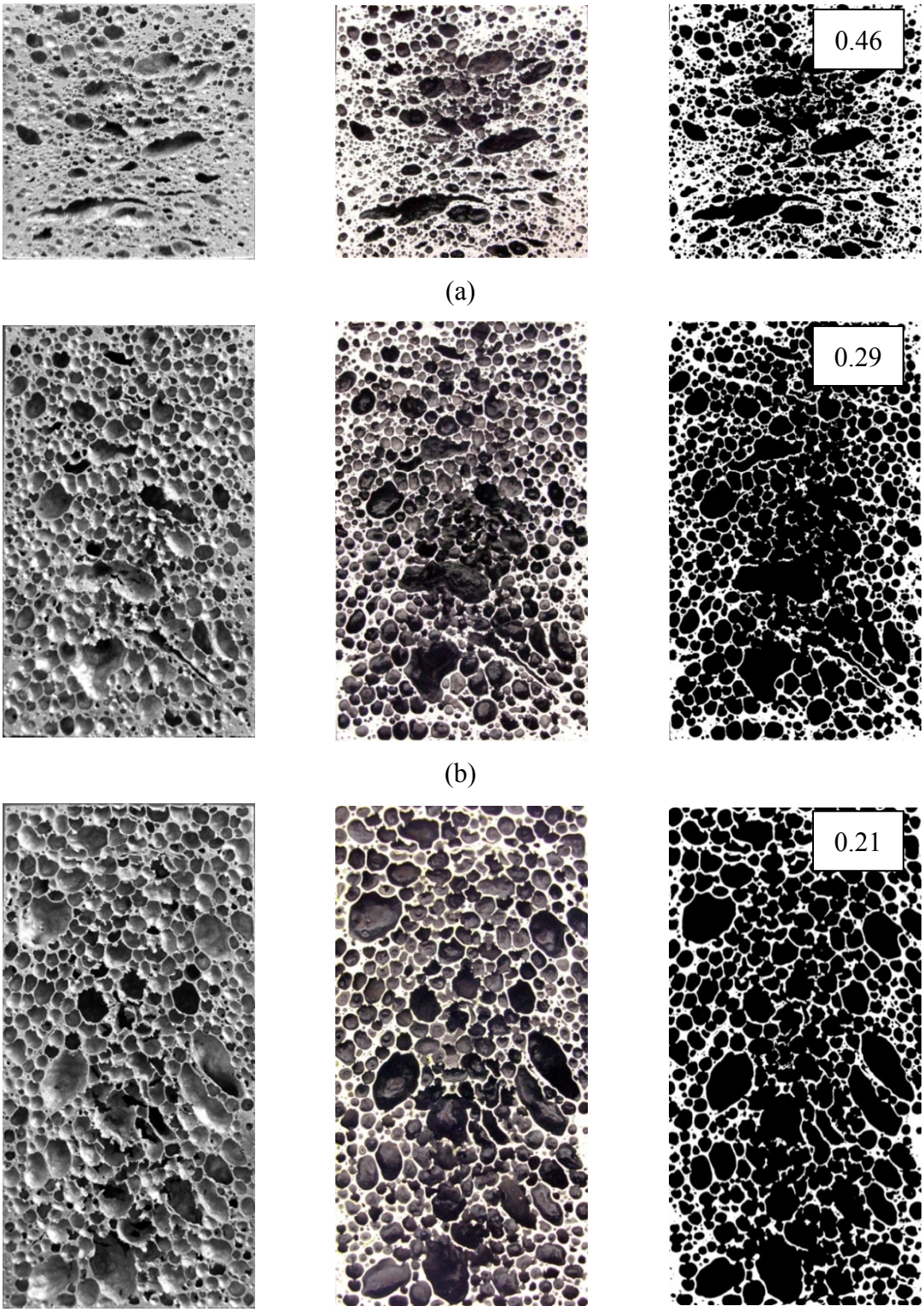

Figure 4.4. Digital image analysis of A0 foams, from left to right; original image, sprayed with black paint and ground, binarized by conventional thresholding:
(a) ρ_r=0.42, (b) ρ_r=0.26, (c) ρ_r=0.21

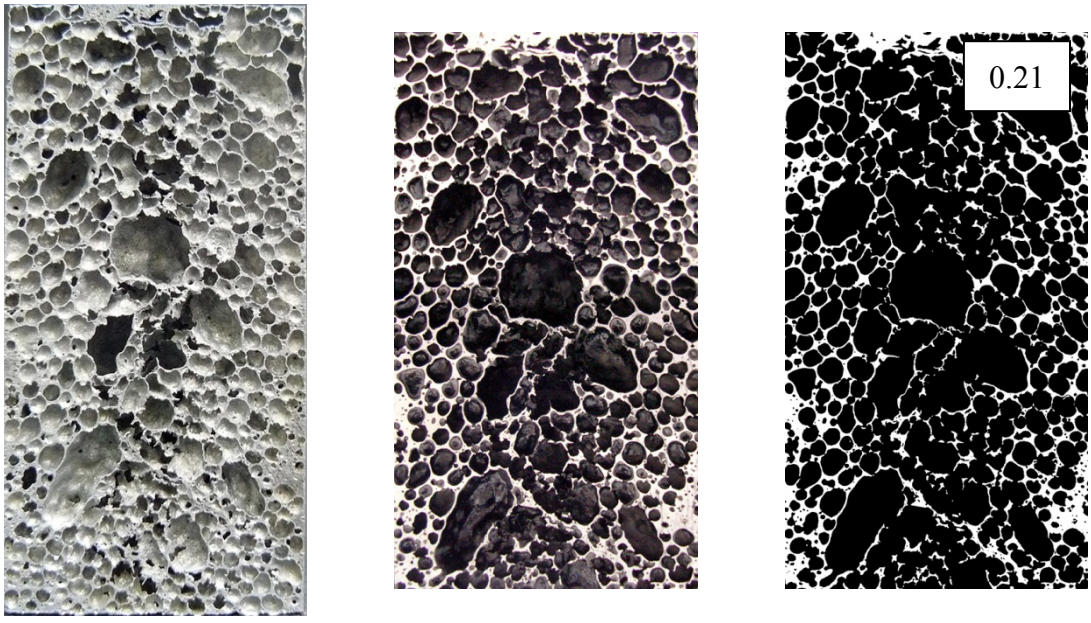

(a)

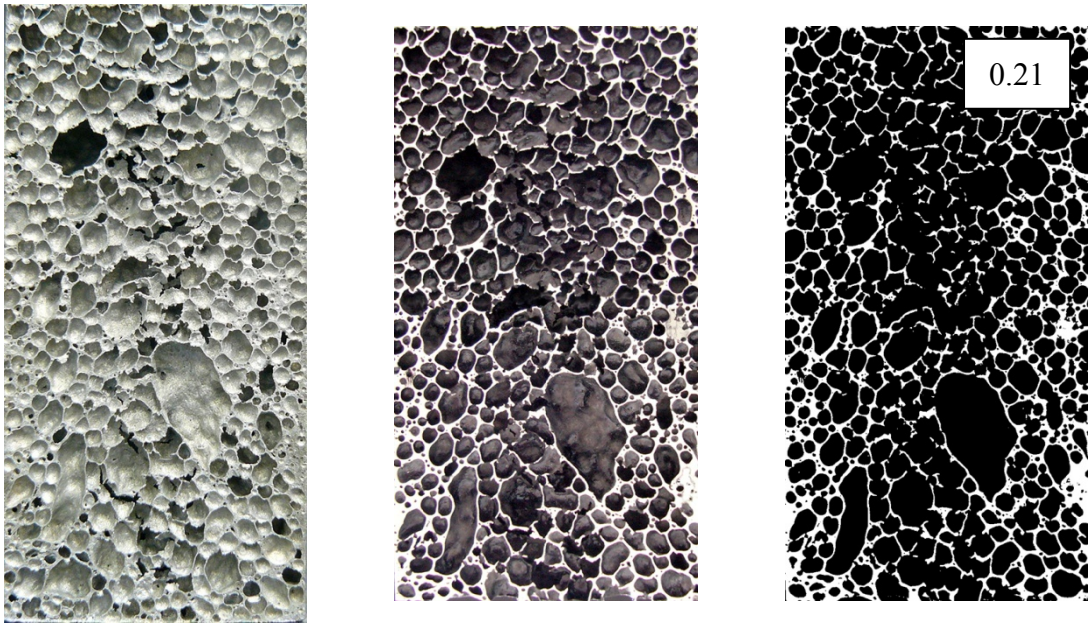

(b)

Figure 4.5. Digital image analysis of A0 and A3 foams, from left to right; original image, sprayed with black paint and ground, binarized by conventional thresholding: (a) ρ_r=0.211, (b) ρ_r=0.208

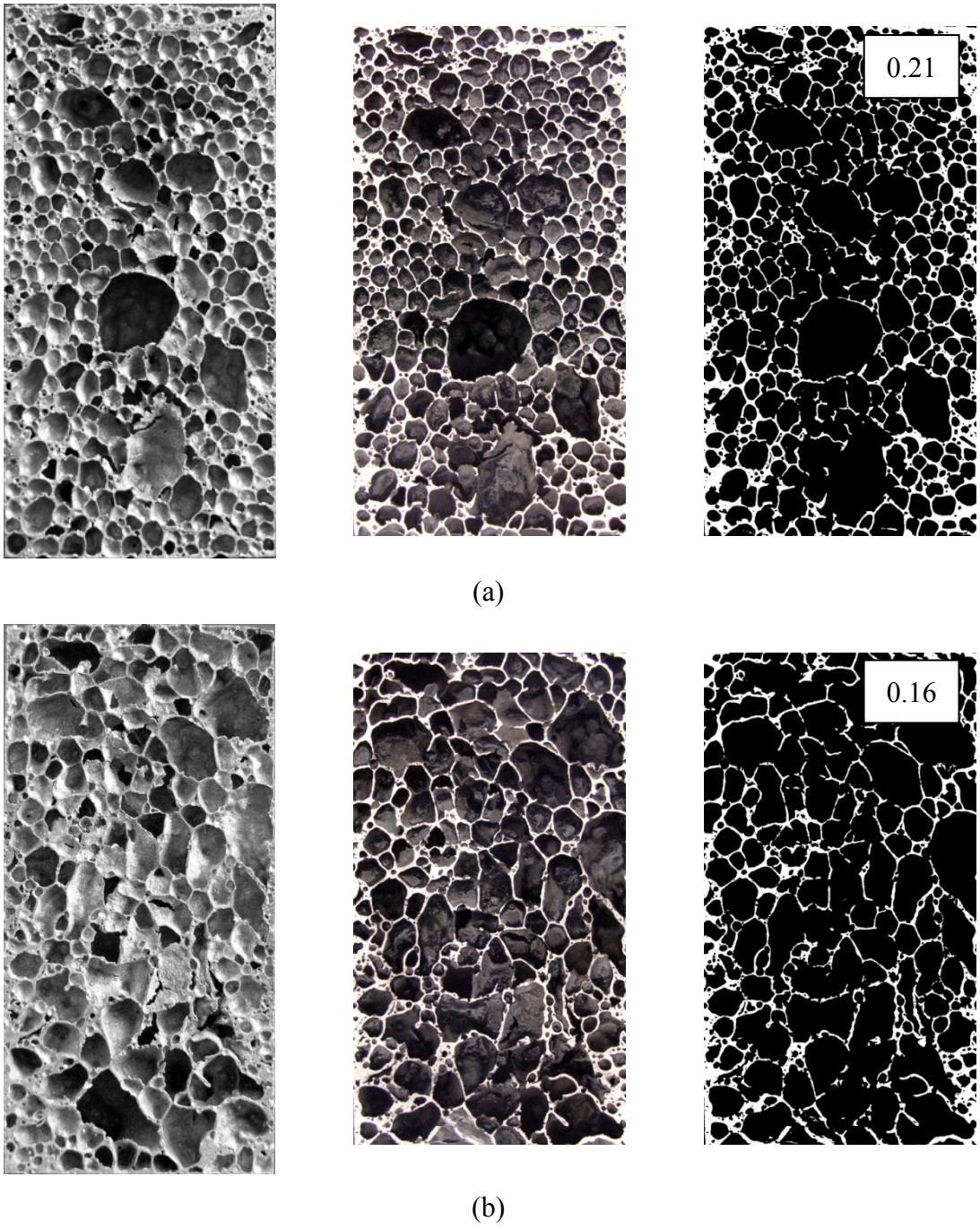

Figure 4.6. Digital image analysis of A5 and A10 foams, from left to right; original image, sprayed with black paint and ground, binarized by conventional thresholding: (a) ρ_r=0.206, (b) ρ_r=0.201

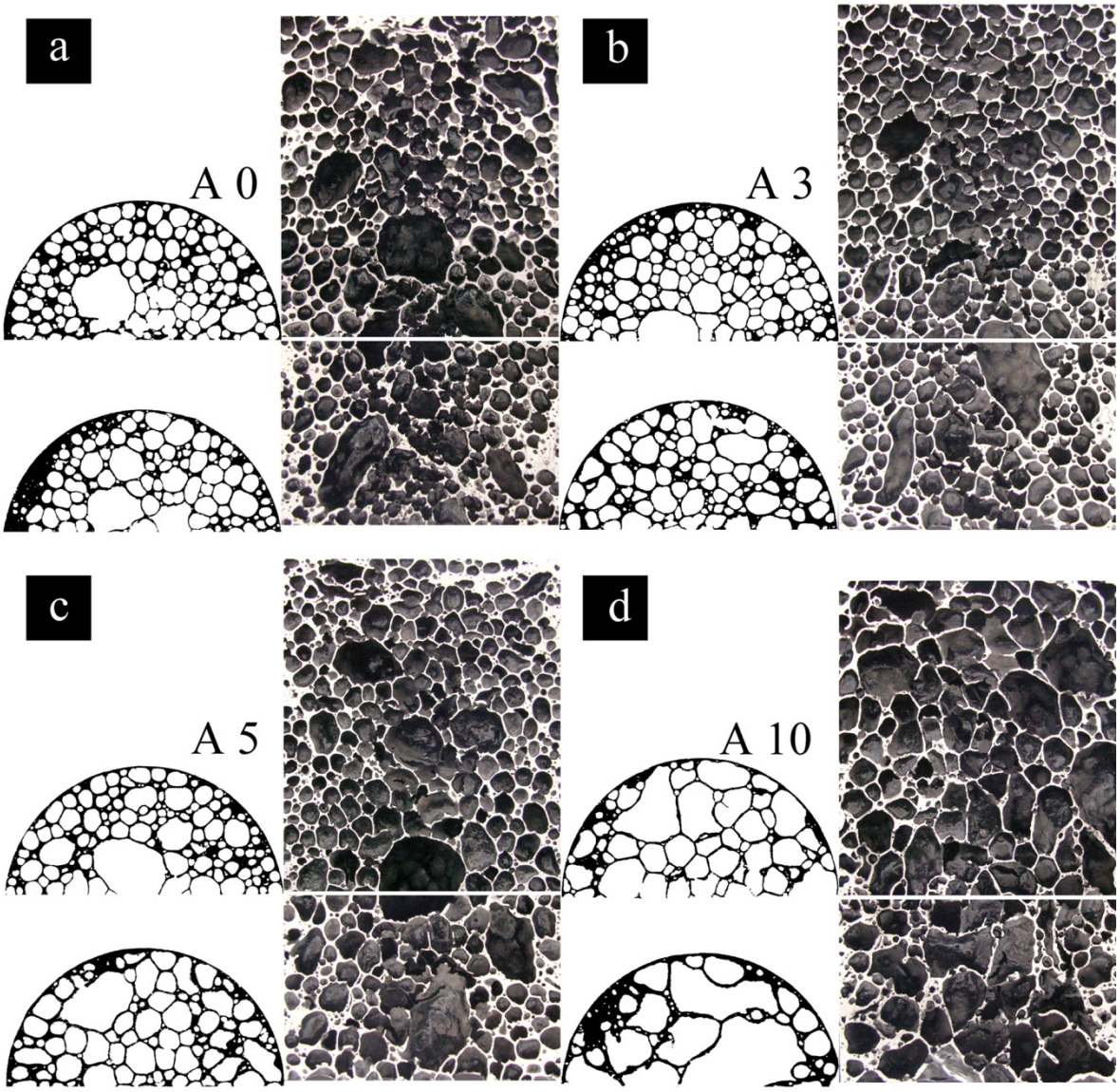

Figure 4.7. Cross-sections of AlMgSi and AlMgSi + Al_2O_3 foams showing the density difference and cell structure at the bottom and mid-portion

Figure 4.7 shows the cross-sections perpendicular to EDM cut surfaces at two different locations, close to the bottom and mid portions of the foams. The structure observed in A3 and A5 foams was more homogeneous in terms of cell size and number when compared to A0 and A10 foams. Density gradient was observed in all foams which was significantly high for A10 foams. Al_2O_3 addition seemed to decrease the gradients up to 5 per cent as seen in A3 and A5 foams.

4.1.3. Microstructure of the Foams

The microstructures of AlMgSi and composite foams are shown in Figure 4.8. All the samples shown were subjected to SHT and aging heat treatment. The important features observed were light gray oxide clusters and dark ceramic particle clusters. There were no clearly visible Mg_2Si precipitates even after etching meaning a complete solution in the matrix was achieved during SHT. After aging precipitates are generally too small to be identified by means of optical microscopy. EDX analysis of the oxide clusters showed that the oxide clusters were mainly Al and Mg oxides. These oxides were presumably covering the surface of the original powders in the blend and during foaming and cooling accumulated around the grain boundaries of solidified structure. Al_2O_3 particles followed a similar path as seen in the figure, they shared similar locations with the oxides. Al_2O_3 at the edges of the cell walls were embedded in the matrix, an indication of good wetting by the matrix. Agglomerated Al_2O_3 particles were observed in A5 and A10 foams.

While optical microscopy observations showed some portion of Al_2O_3 particles were embedded in the cell walls, SEM micrographs of the cell faces showed partially and poorly wetted Al_2O_3 particles (see Figure 4.9 to Figure 4.12). During foaming, stabilization is achieved by the balance of surface tension at the liquid-gas interface, the weight of the liquid cells and the air pressure inside the cells. Forces acting by surface tension cause the liquid-gas interface to be curved in an arc forming the Plateau border. Plateau borders separate edges of the cells and are the regions where three or more cell walls meet. At these regions, fluid pressure is lower than the cell walls. The pressure difference draws liquid from the cell walls into the cell edges. Then gravitational forces lead the liquid through the cell edges to the bottom of the foam causing the drainage. Drainage decreases the size of Plateau borders and thickness of the cell walls particularly at the top of the foams. After a critical thickness, cell walls burst and cells coalesce with adjacent cells resulting in formation of larger cells or they collapse because the new volume cannot withstand the forces that are acting. In order for a liquid foam to become more stable; the liquid gas interface in each cell must be altered by decreasing the surface tension, the drainage through Plateau borders must be slowed down by increasing the liquid viscosity, and the thinning of the cell walls must be obstructed by means of mechanical barriers. Oxides and Al_2O_3 particles observed in metallographic analyses of the foams are believed

to serve for this purpose. Partially wetted Al_2O_3 on the cell faces can decrease the effects of surface tension, oxides and ceramics can increase the viscosity of the melt and can act as mechanical barriers. The distorted and coarse structure of A10 foams suggests that the amount of ceramic must be kept low for PCM foams. Agglomeration of ceramic particles cannot be avoided when it is higher than three per cent, and has detrimental effects on the foam structure when added up to 10 per cent.

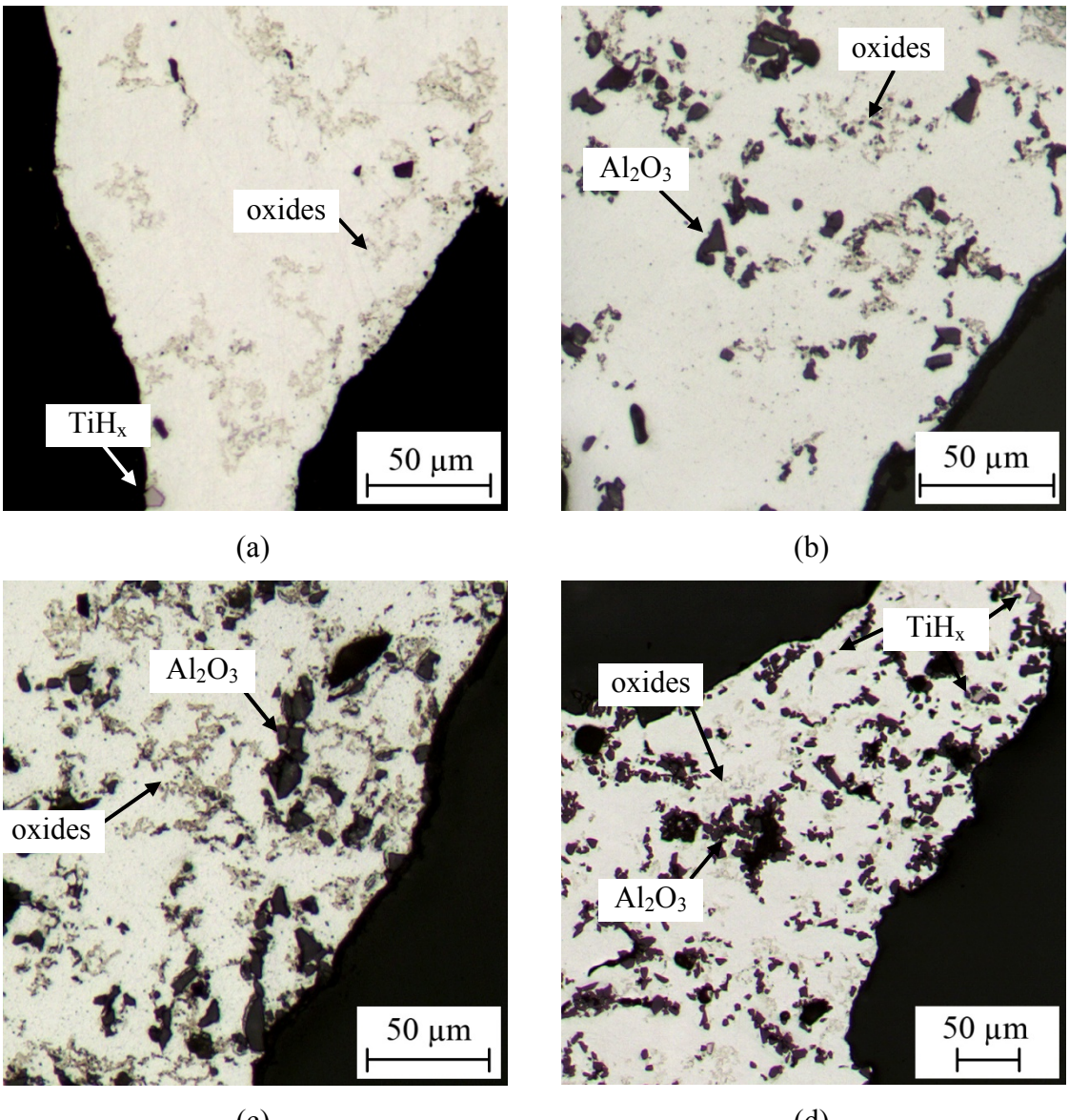

Figure 4.8. Optical micrographs showing the cell wall microstructure of the foams after SHT and warm aging: (a) A0, (b) A3, (c) A5 and (d) A10 foams

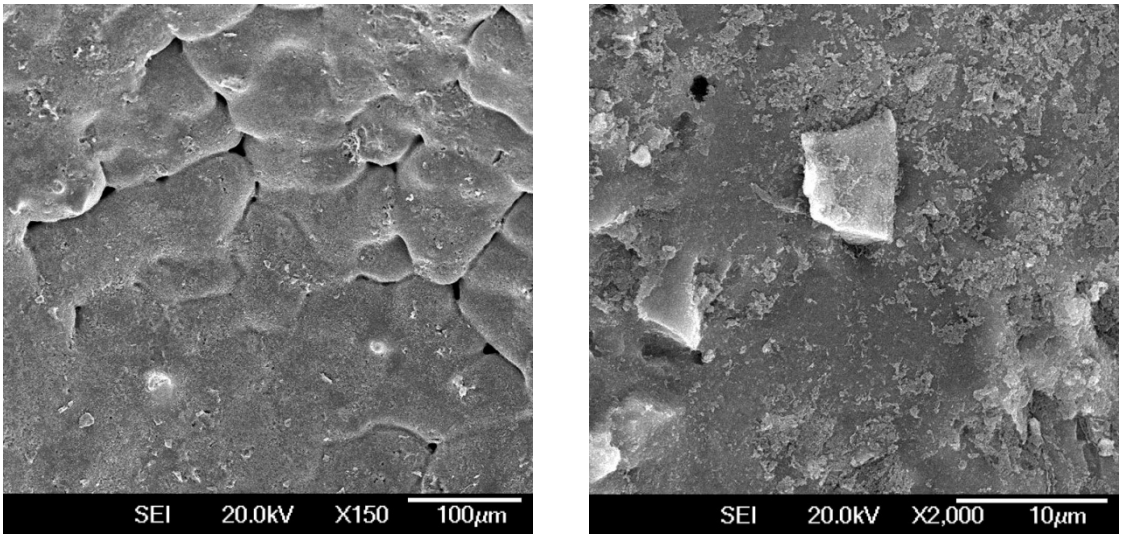

(a) (b)

Figure 4.9. SEM micrographs of cell faces of A0 foam: (a) boundaries of some of the particles are retained, (b) TiH_2 particle at the cell face partially wetted by Al alloy matrix

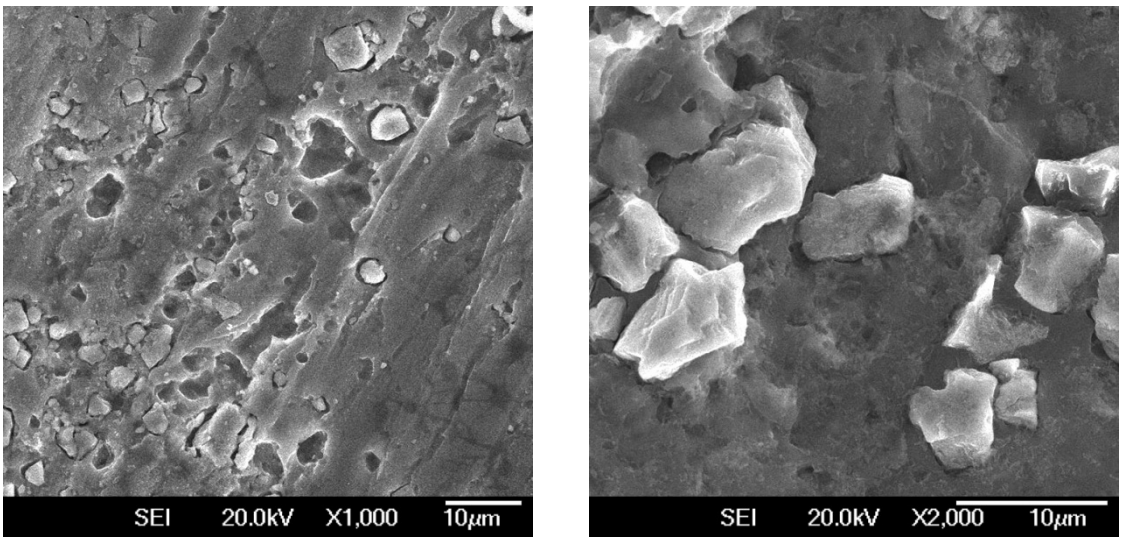

(a) (b)

Figure 4.10. SEM micrographs of A3 foam: (a) Al_2O_3 particles embedded on the cell wall (surface cut by diamond saw), (b) Al_2O_3 particles at the cell face partially wetted by Al alloy matrix

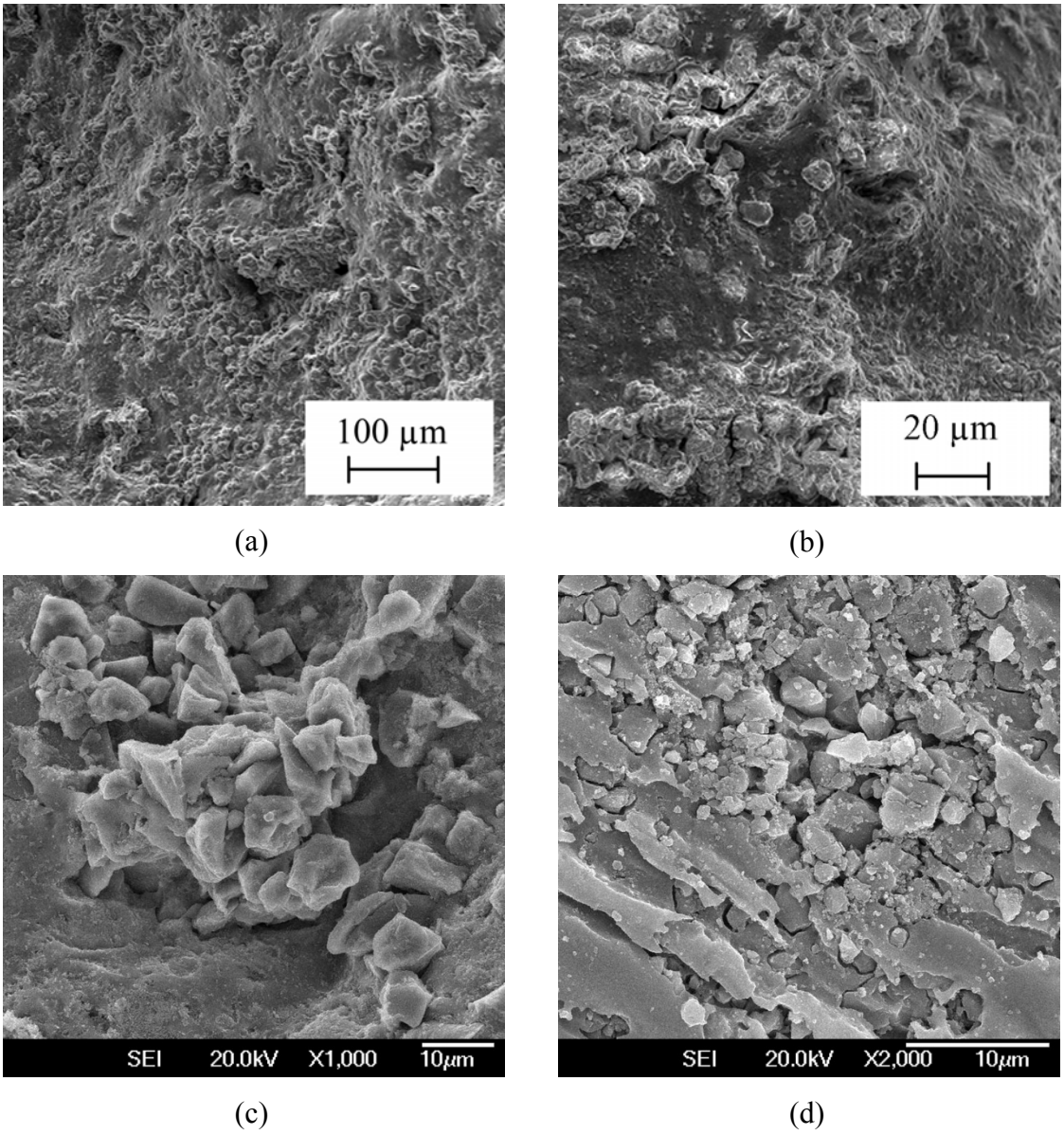

(a) (b)

(c) (d)

Figure 4.11. SEM micrographs of A5 foam: (a) Al_2O_3 partially wetted on the corrugated cell face, (b) Al_2O_3 particles free surfaces on the cell face, (c) agglomeration of Al_2O_3 particles is evident, (d) Al_2O_3 agglomerates on the cell wall (surface cut by diamond saw)

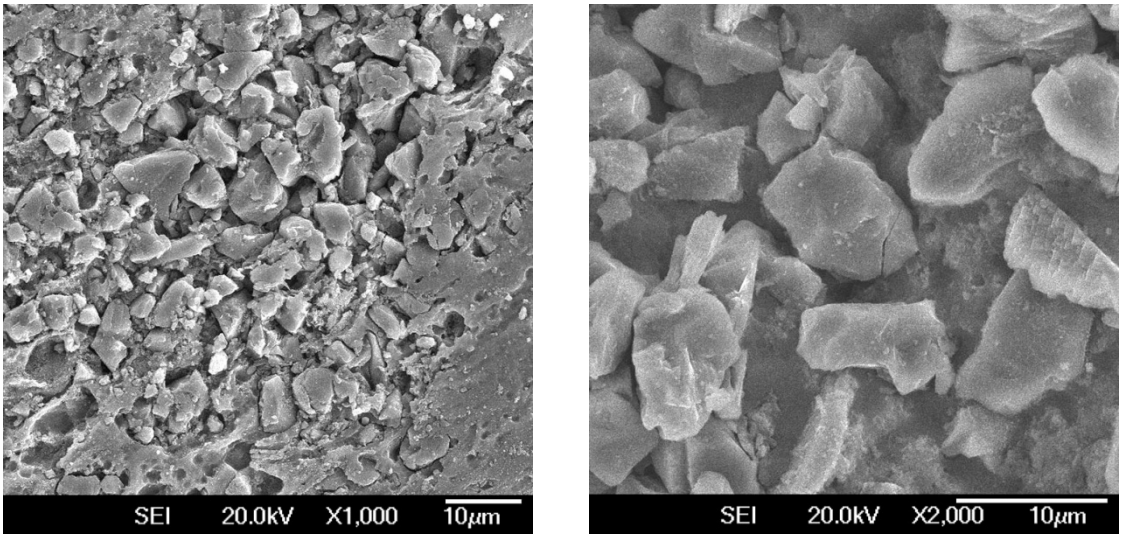

(a) (b)

Figure 4.12. SEM micrographs of A10 foam: (a) Al_2O_3 agglomerates embedded on the cell wall (surface cut by diamond saw), (b) Al_2O_3 particles at the cell face partially wetted by Al alloy matrix

The SEM micrographs of cell wall surfaces of A5 composite foam are shown in Figure 4.13. The surfaces were deeply etched after polishing. First picture covers the area where three cells meet (Figure 4.13a). A connected structure of ceramic particle clusters with oxide clusters covers the surface of the Plateau border. As mentioned before, the idea of balancing cell wall thinning by the sucking effect of Plateau borders of the foam can be theoretically done by building mechanical barriers between the approaching two liquid-gas interfaces. If the still foaming melt were purely liquid, this would not be possible since liquids cannot transfer mechanical forces. Körner *et al.* [39] explained how solid particles originating from oxygen content of the underlying metal powder used in PCM method can act as mechanical barriers against cell wall thinning. They induce a long-range interfacial force called the disjoining pressure, which stabilizes the foam. The oxide cluster observed in Figure 4.13c with the support of Al_2O_3 particles acting as a mechanical barrier and surface energy plus viscosity modifier can improve the foam stability even more. Figure 4.13d show oxides penetrating deeper into the cell wall supporting the idea of network structure of the oxides.

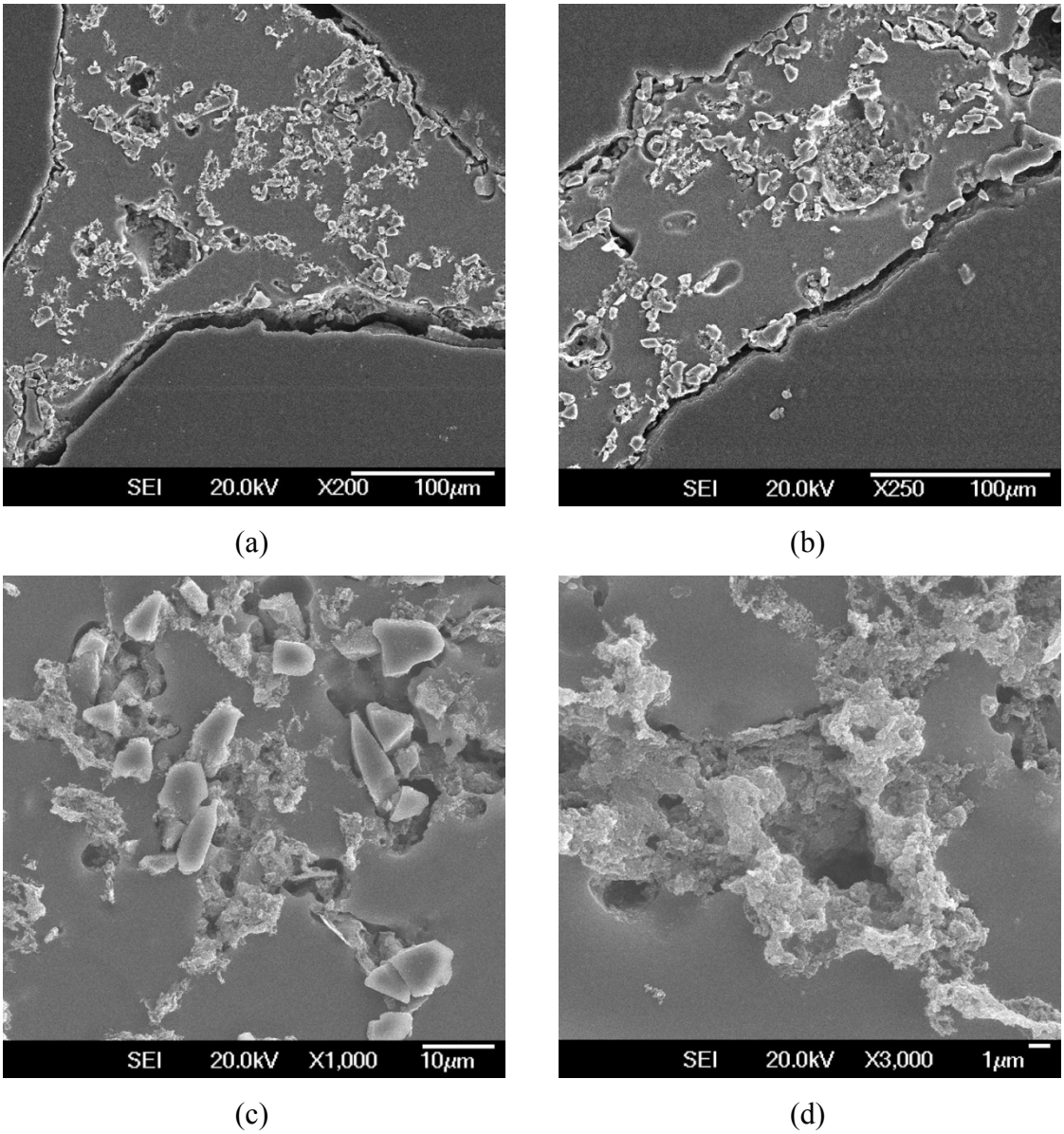

Figure 4.13. SEM micrographs showing the cell wall microstructure of A5 foam after grinding, polishing and moderately etching: (a) general view of the cell wall Plateau region, (b) Al_2O_3 particles and oxides on the cell wall along the cell edges, (c) Al_2O_3 particles and oxides sharing similar locations on the cell wall, (d) oxides penetrating to the depths of the cell wall

4.1.4. Microhardness Test

Microhardness tests were performed for specimens in different heat treatment states. Peak hardness of the AlMgSi foams was reached after SHT and 16 hours of aging at 175 °C. Same heat treatment temperature and time was applied to composite foams. Figure 4.14 shows the hardness values of AlMgSi and AlMgSi + Al_2O_3 foams. There was considerable variation of hardness values within the samples except for annealed sample, which was not solution heat treated and quenched. Hardness of AlMgSi samples in as foamed condition was very close to SHT and SHT plus aged samples when aging time was less than two hours. This showed that air-cooling after foaming might act as SHT and quenching heat treatments. The scatter in the hardness values suggested the low and non-uniform thermal conductivity of the foams affected the cooling rate of different sections of the foam in SHT quenching. The hardness of composite foams was very close to AlMgSi foams indicating the Mg content in the solution was not influenced by chemical reactions with Al_2O_3.

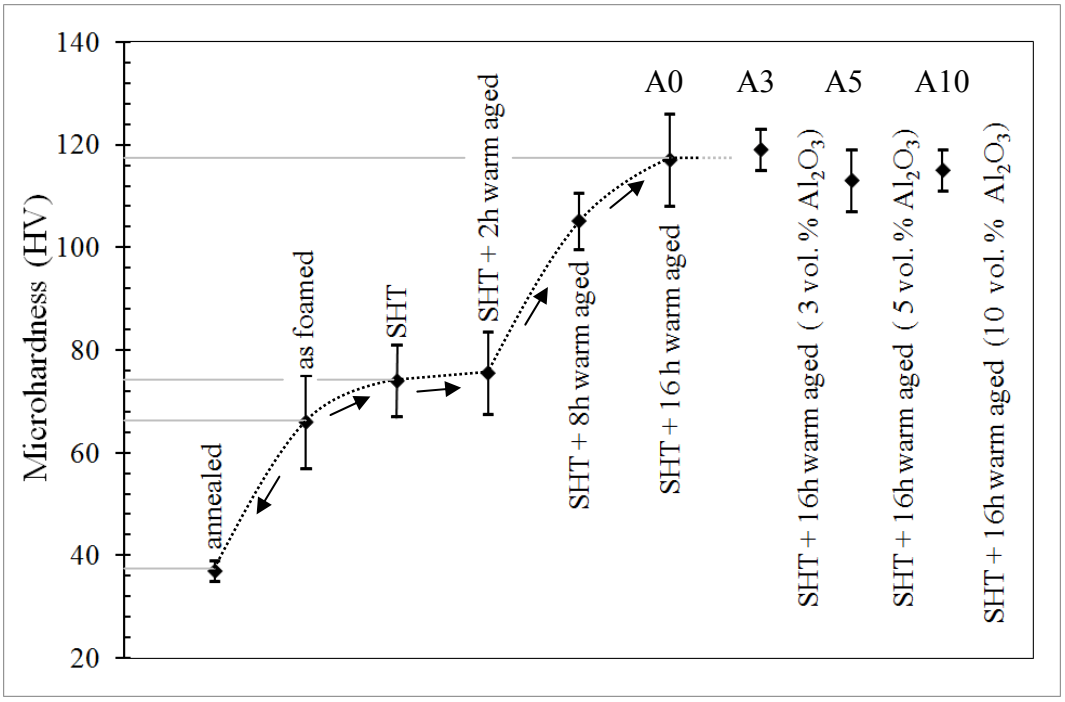

Figure 4.14. Microhardness testing results of the heat treatments for different amounts of Al_2O_3 addition

4.1.5. Compression Behavior of the Foams

The mechanical properties of the foams, which are significant for design and application purposes, are elastic modulus and strength. These properties can be found through compression testing. Precautions must be taken during the preparation of specimens for compression testing. First consideration is the solid skin that is present after removal from the mold. The solid skin can sometimes be as thick as one mm and forms a shell around the cellular structure. Second consideration is the foaming direction. Since it is from bottom to top and up to a height of 60 mm, it is inevitable to have a density gradient and anisotropic cell structure in the foam body. In general, bottom of the foams are denser because of drainage and cell dimensions are shorter in transverse direction. The solid skin, density gradient and direction of compression may affect the measured strength and compression stiffness of the foams. Solid skin also hides the macro defects (very large cells) in the structure of the foams and causes erroneous calculation of density and measurement of the strength. Therefore, in this study, the solid skin and the top and bottom parts of the foams were removed by machining and compression was done parallel to the foaming direction (see Figure 4.15).

Foams with similar relative densities were used for comparison of the behavior after full heat treatment. The compression curves of AlMgSi and composite foams are shown in Figure 4.16 and Figure 4.17. Compression curves for the foams in as foamed condition (solid lines) were relatively smooth. This is a typical behavior observed in ductile foams. An exception was for A10 foam, which had a wavy curve. This can be attributed to the density of the foam, which was significantly lower and to the higher amount of ceramic, which can affiliate brittleness to the metal matrix. A slight waviness observed in the compression curves of A3 and A5 foams suggested the latter was also effective. The curves of heat treated foams (dashed lines) were different. First, they showed a stress peak when strained up to 1-2 per cent. There was a drop in stress after the peak followed by a oscillating curve where the stress raised moderately with increasing strain. The difference observed in the two groups of curves was an indication of different failure modes of the cells. In compression, closed cell ductile foams collapse plastically generally by bending and/or stretching of the cell walls. Failure is localized in the beginning in a band transverse to the loading direction usually at the upper section of the foam where density is lower.

With the increasing strain the deformation band propagates throughout the foam and new bands may start to form at different sections at the same time. There is continuous rise of the stress with the strain since density of the foam is also increasing continuously with progressive compression. The measured deformations in as foamed samples were a result of these interactions. A similar behavior was observed in heat treated foams except this time some of the cell walls were broken and crumbled since the matrix had become relatively brittle. Fracture of the cell walls affected the deformation curve in two ways. At the beginning of the loading cell walls started to bend and a sudden fracture occurred since the cell walls could not deform plastically anymore. There was a drop in stress or softening until the fractured deformation band was densified and the foam continued to carry the load. This cycle continued progressively with increasing strain with a mixture of deformation modes in which cell walls bent plastically and crushed in a brittle manner. When some portion of the cell walls crumbled and fell off, they did not contribute to densification. Because of this, heat treated foams tended to start densification later than the foams with the same relative density in as foamed condition.

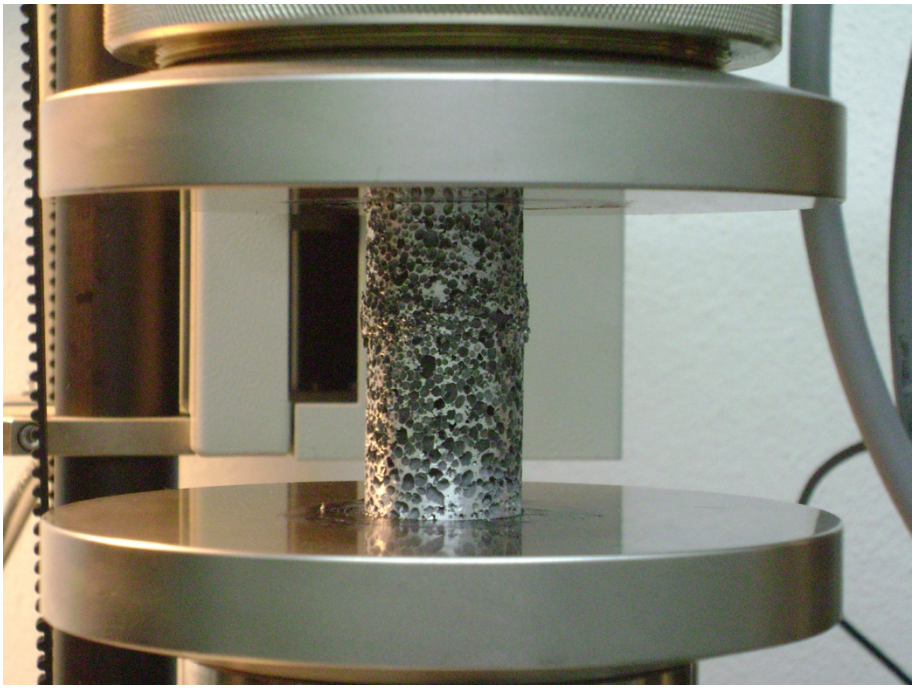

Figure 4.15. Compression testing of the foams

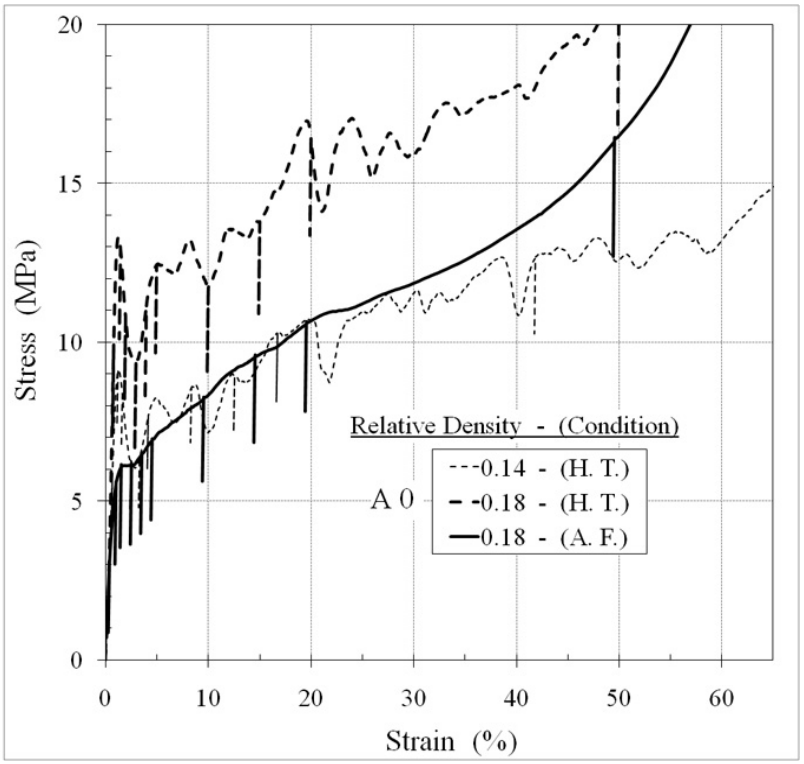

(a)

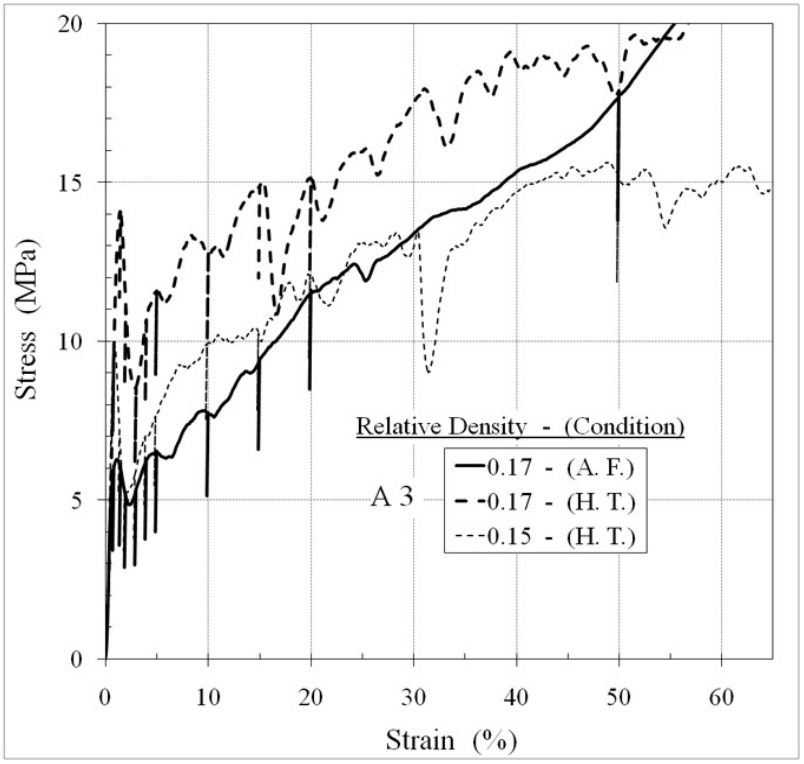

(b)

Figure 4.16. Compression stress-strain behavior of heat treated (H.T.) and as foamed (A.F.) AlMgSi and composite foams: (a) A0, (b) A3

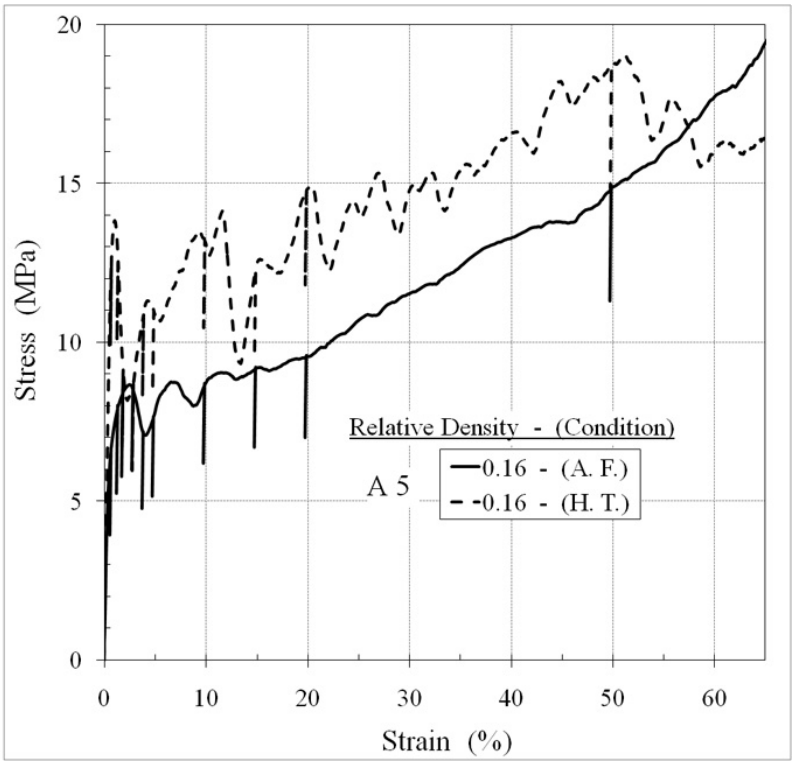

(a)

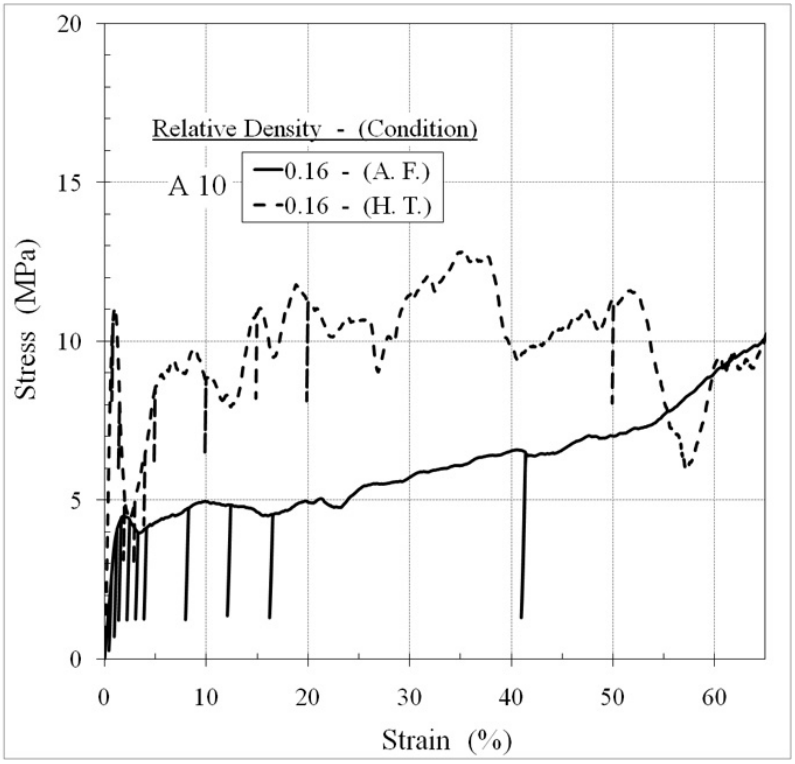

(b)

Figure 4.17. Compression stress-strain behavior of heat treated (H.T.) and as foamed (A.F.) composite foams: (a) A5, (b) A10

The elastic stiffness in compression, E^*, was determined from the slope of the unloading lines (see Figure 4.16 and Figure 4.17). Unloading lines at different strain rates starting from 0.85 per cent up to 50 per cent strain were measured. It was seen that there was negligible change at strains up to 15-20 per cent. At 20 per cent and 50 per cent strain these values were higher since the density of the deformed foam had increased significantly. For all the specimens elastic stiffness in compression were taken from the maximum value of the slope of unloading lines measured until 10 per cent strain.

Gibson and Ashby [1, 3] related some basic mechanical properties of the metallic foams to the relative density by the so-called "scaling laws". The unloading modulus E^* of a closed-cell foam is related to the elastic modulus of the cell wall material E_s and to the relative density of the foam according to:

$$\frac{E^*}{E_s} \approx \Phi^2 \left(\frac{\rho^*}{\rho_s}\right)^2 + (1-\Phi)\left(\frac{\rho^*}{\rho_s}\right) \tag{4.1}$$

where Φ is the fraction of solid in the foam which is contained in the cell edges of the foam. The remaining fraction of solid is contained in the cell faces. When written for different kind of foams this relation takes the form [3]:

$$\frac{E^*}{E_s} = C_1 \left[\Phi^2 \left(\frac{\rho^*}{\rho_s}\right)^2 + (1-\Phi)\left(\frac{\rho^*}{\rho_s}\right)\right] \tag{4.2}$$

where C_1 is a parameter that is related to the topology of the foam and varies from 0.1 to 1.0 for different kind of foams [3]. If the fraction of solids in the cell edges is taken as 100 per cent then the foam is open cell and the relation can be written as:

$$\frac{E^*}{E_s} = C_2 \left(\frac{\rho^*}{\rho_s}\right)^2 \tag{4.3}$$

where C_2 is again the parameter which is related to the topology of the foam and varies between 0.1 to 4 for different kind of foams [3]. To allow for comparison of the measured modulus with the results of this equation, the foam modulus measured was normalized by

the cell wall modulus, E_s = 70 GPa for AlMgSi foams. The cell wall modulus of the composite foams were calculated using the equation [69]:

$$E_l = \frac{E_m E_r}{f E_m + (1-f) E_r} \tag{4.4}$$

where E_l is lower bound elastic modulus of a composite material, E_m is the elastic modulus of the matrix material ($E_{Al\ alloy} \approx$ 70 GPa), E_r is the elastic modulus of the reinforcement material ($E_{Al_2O_3} \approx$ 400 GPa), and f is the volume fraction of the reinforcement. Using this equation E_s values for 3, 5 and 10 vol. per cent Al_2O_3 reinforced matrices were calculated as 71.8, 73.0 and 76.3 GPa respectively.

Figure 4.18 shows the normalized unloading modulus (E^*/E_s) –relative density (ρ^*/ρ_s) plots of AlMgSi foams. The lines on the plot belong to the correlations made according to Eqs. 4.2 and 4.3. For the relative density values ≤ 0.16 the scaling law for closed cell foams has a better fit to the experimental data. The correlations made are for Φ = 0.95 and 0.80, fraction of solids in the cell edges and remaining solid (1-Φ) in the cell faces. However, overall data fit better to the correlations made by Eq. 4.2 with solid fraction of 95 per cent for closed cell foams and Eq. 4.3 which is for open cell foams. C_1 and C_2 values for A0 foams are given below:

$$\frac{E^*}{E_s} = 0.872\left[0.95^2\left(\frac{\rho^*}{\rho_s}\right)^2 + (0.05)\left(\frac{\rho^*}{\rho_s}\right)\right]$$
$$\frac{E^*}{E_s} = 1.066\left(\frac{\rho^*}{\rho_s}\right)^2 \tag{4.5}$$

For low relative density values the second linear term in Eq. 4.2 dominates, implying that cell face presence is more significant in the mechanism of deformation in closed cell foams. In Figure 4.18 this behavior can be observed if the E/E_s values of the correlation lines below and above ρ_r = 0.16 are compared. When relative density is increased values obtained from the model for open cell foams are higher.

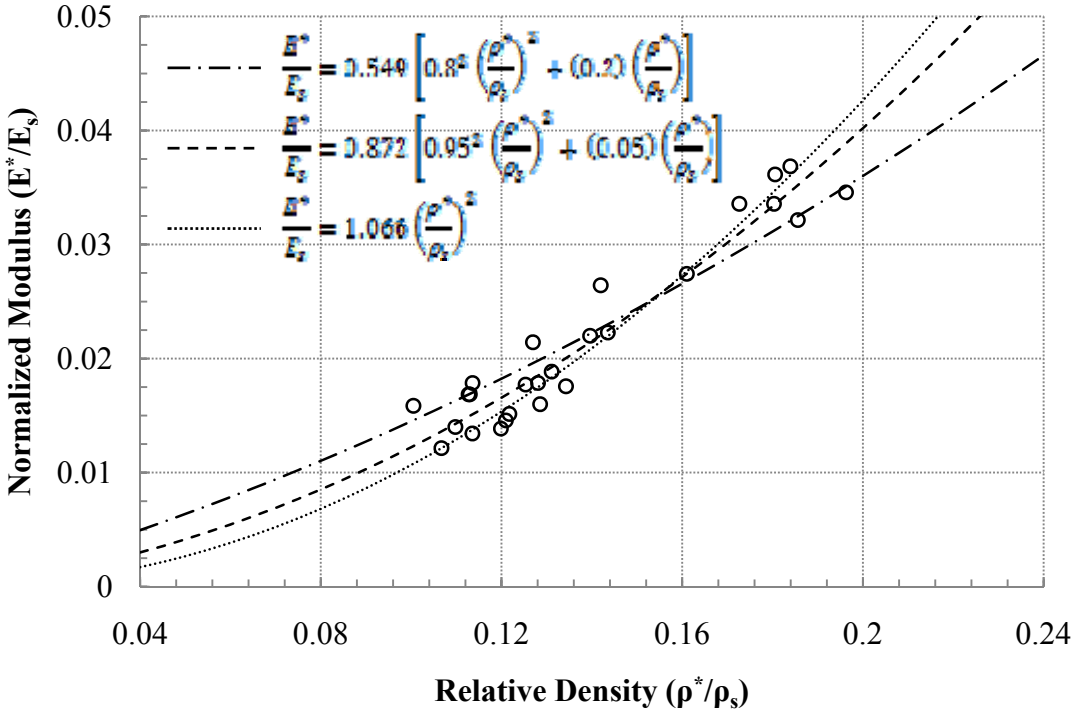

Figure 4.18. Normalized unloading modulus – relative density plots and data obtained using the correlations given in Eqs. 4.2 and 4.3 for AlMgSi foams with E_s=70.0 GPa

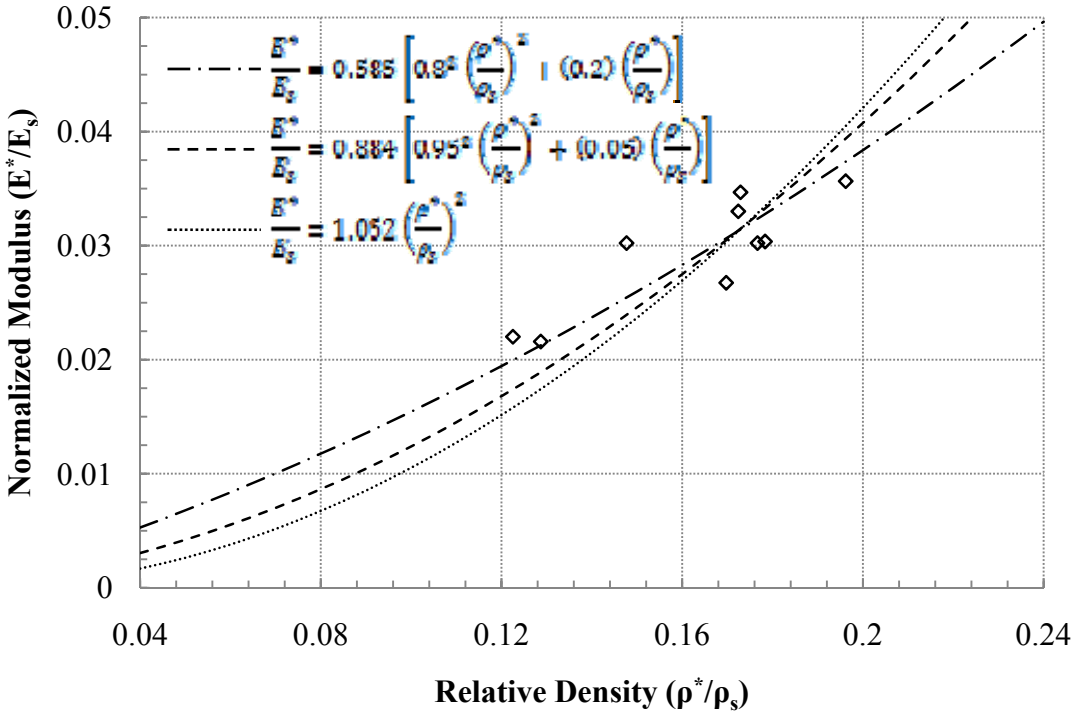

Figure 4.19. Normalized unloading modulus – relative density plots and data obtained using the correlations given in Eqs. 4.2 and 4.3 for A3 foams with E_s=71.8 GPa

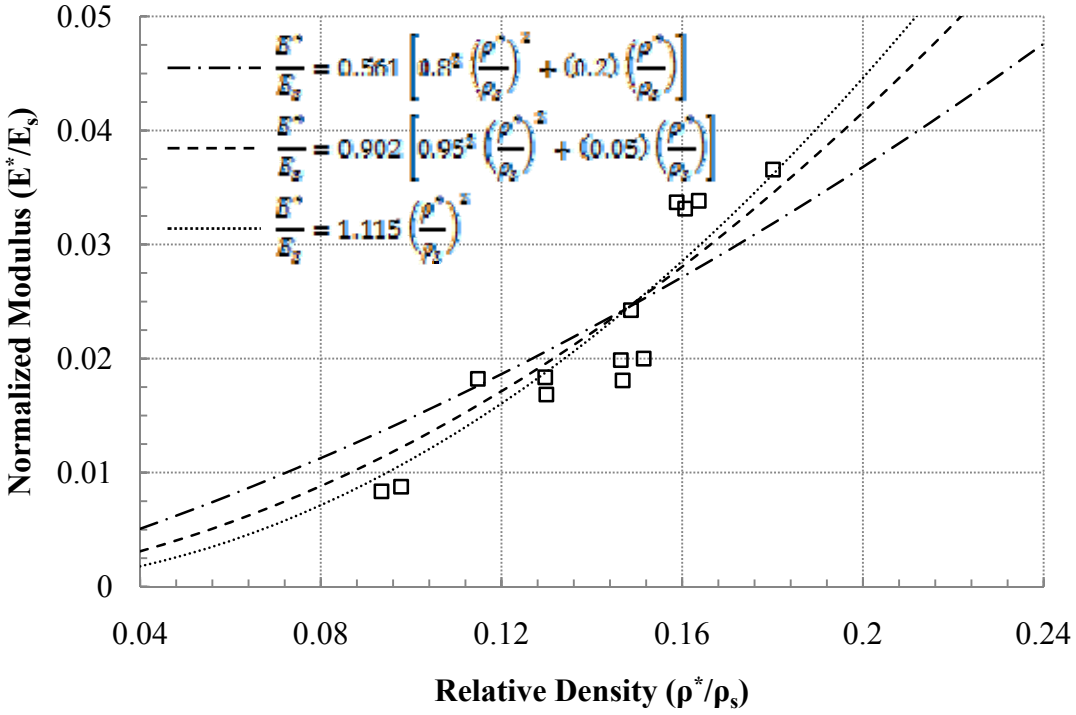

Figure 4.20. Normalized unloading modulus – relative density plots and data obtained using the correlations given in Eqs. 4.2 and 4.3 for A5 foams with E_s=73.0 GPa

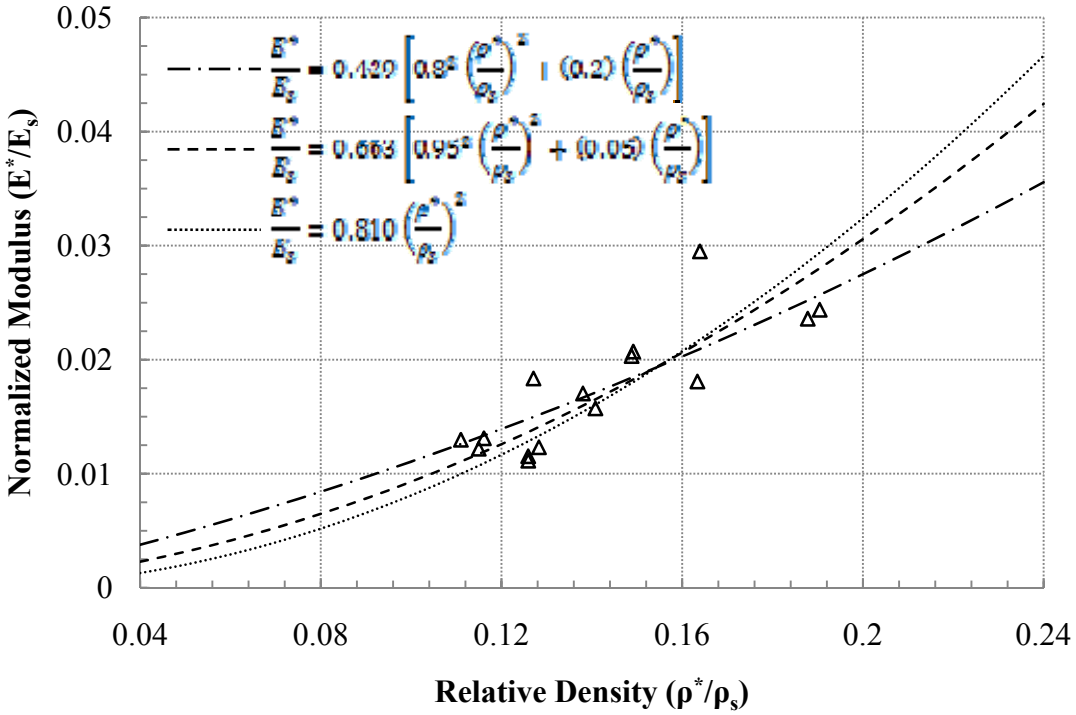

Figure 4.21. Normalized unloading modulus – relative density plots and data obtained using the correlations given in Eqs. 4.2 and 4.3 for A10 foams with E_s=76.3 GPa

The experimental data for composite foams were normalized by the E_s values calculated from Eq. 4.4. Figure 4.19, Figure 4.20 and Figure 4.21 show the normalized modulus relative density plots and the correlations made using Gibson and Ashby model [1, 3]. Experimental data fit better to the correlations made by Eq. 4.2 with solid fraction of 95 per cent for closed cell foams and Eq. 4.3, which is for open cell foams. The correlation equations with different C_1 and C_2 values found for A3, A5 and A10 foams are given in Eqs. 4.6 to 4.8 respectively:

$$\frac{E^*}{E_s} = 0.884\left[0.95^2\left(\frac{\rho^*}{\rho_s}\right)^2 + (0.05)\left(\frac{\rho^*}{\rho_s}\right)\right]$$

$$\frac{E^*}{E_s} = 1.052\left(\frac{\rho^*}{\rho_s}\right)^2 \tag{4.6}$$

$$\frac{E^*}{E_s} = 0.902\left[0.95^2\left(\frac{\rho^*}{\rho_s}\right)^2 + (0.05)\left(\frac{\rho^*}{\rho_s}\right)\right]$$

$$\frac{E^*}{E_s} = 1.115\left(\frac{\rho^*}{\rho_s}\right)^2 \tag{4.7}$$

$$\frac{E^*}{E_s} = 0.663\left[0.95^2\left(\frac{\rho^*}{\rho_s}\right)^2 + (0.05)\left(\frac{\rho^*}{\rho_s}\right)\right]$$

$$\frac{E^*}{E_s} = 0.810\left(\frac{\rho^*}{\rho_s}\right)^2 \tag{4.8}$$

Experimental data and the correlation equations between relative density and normalized modulus showed that compression properties of the foams were close to the values expected from open cell foams. C_2 values obtained for open cell foam model were also close to each other for A0, A3 and A5 foams. This value was considerably low for A10 foams. Figure 4.22 shows the experimental data of A0, A3 and A5 foams as if they were the same kind of foam and correlations were made according to Eqs. 4.2 and 4.3. The C_1 and C_2 values found are given in Eq. 4.9.

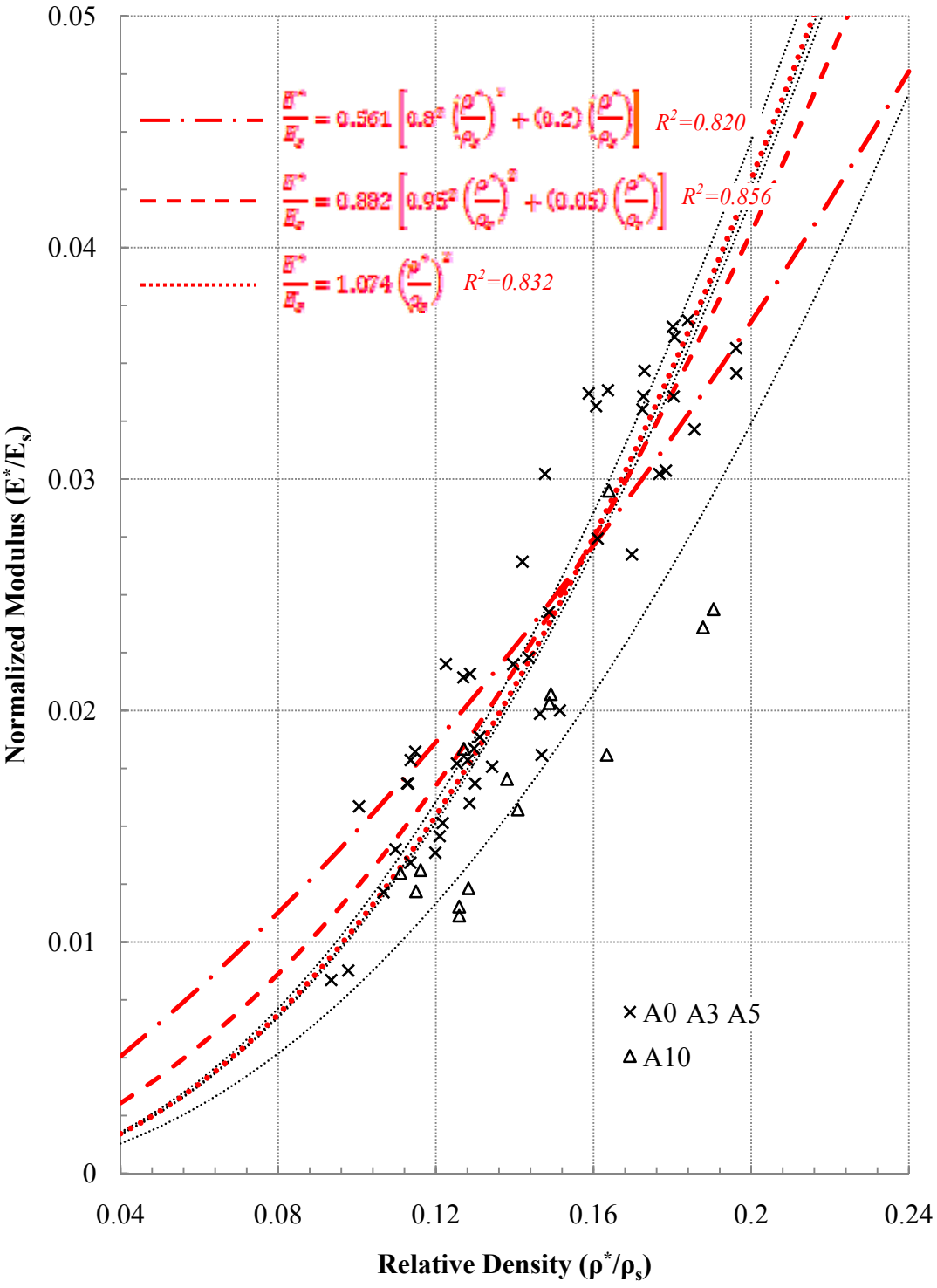

Figure 4.22. Normalized modulus - relative density plot of the AlMgSi and composite foams; the red lines are showing the values obtained from the correlations for all the data of A0, A3 and A5 foams for different solid fractions and the correlation obtained for open cell foams, lines with gray color show the correlations obtained for open cell foams given in Eqs. 4.5 to 4.8

$$\frac{E^*}{E_s} = 0.882\left[0.95^2\left(\frac{\rho^*}{\rho_s}\right)^2 + (0.05)\left(\frac{\rho^*}{\rho_s}\right)\right]$$

$$\frac{E^*}{E_s} = 1.074\left(\frac{\rho^*}{\rho_s}\right)^2 \tag{4.9}$$

McCullough *et al.* [70] also analyzed compressive stress-strain behavior of AlMgSi foams. The specimens they used for compression test were cut from flat plates of Alulight foam. Their solid skin was removed. When testing was done in the longitudinal direction (perpendicular to the foaming direction) the experimental data of unloading modulus for the relative density range ρ^*/ρ_s= 0.1 - 0.4 was approximated by [70]:

$$\frac{E^*}{E_s} = 1.286\left(\frac{\rho^*}{\rho_s}\right)^2 \tag{4.10}$$

which is close to the values obtained for A0, A3 and A5 foams. The test could not be performed in the foaming direction since the height of the panel was only 9 mm including the solid skin. Therefore, they used small cuboid foam specimens and dimensions were 15 x 10 x 7.5 mm. The reason for the difference in the correlations can be due to the geometry and lower height to thickness ratio of the specimens they used. In addition, it may be necessary to compare the results in the same relative density range, which was maximum 0.2 in this study.

According to Gibson and Ashby [1, 3] the compression strength of a closed cell metallic foam σ_{cs} is related to the yield strength of the cell wall material σ_y by [1]:

$$\frac{\sigma_{cs}}{\sigma_y} \approx \ 0.3\,\Phi^{1.5}\left(\frac{\rho^*}{\rho_s}\right)^{1.5} + (1-\Phi)\left(\frac{\rho^*}{\rho_s}\right) \tag{4.11}$$

where Φ is the fraction of solid in the foam which is contained in the cell edges of the foam. When written for different kind of foams this relation takes the form [3]:

$$\frac{\sigma_{cs}}{\sigma_y} = C_3\left[\ \Phi^{1.5}\left(\frac{\rho^*}{\rho_s}\right)^{1.5} + (1-\Phi)\left(\frac{\rho^*}{\rho_s}\right)\right] \tag{4.12}$$

where C_3 is a parameter that is related to the topology of the foam and varies from 0.1 to 1.0 for different kind of foams. For open cell foams the scaling law can be written as [3]:

$$\frac{\sigma_{cs}}{\sigma_y} = C_4 \left(\frac{\rho^*}{\rho_s}\right)^{1.5} \tag{4.13}$$

where C_4 is a parameter and varies from 0.1 to 1.0. The yield strength of the cell wall material, AlMgSi can be estimated by using the microhardness measurement results. As shown in Figure 4.14 hardness of as foamed samples were approximately 65 kgf/mm^2. After SHT and aging this value increased to 118 kgf/mm^2. Lehmus and Banhart [62] studied the effects of heat treatment on the aluminum foams with a similar chemical composition. The maximum hardness they found after SHT and aging were HV ≈ 100 ± 15 kgf/mm^2 which is consistent with the values obtained in this study. Assuming the yield strength of the cell wall material, σ_y, is equal to *HV/3* the yield strength of AlMgSi foams can be found as 215 MPa after foaming and 385 MPa after heat treatment.

In Table 4.1 typical mechanical properties of chemically similar wrought alloys, 6061 and 6063, are shown. Estimated values for the foams are very close to the tensile strength values of annealed and solution heat treated (T4 temper) 6061 alloys. Heat treated foams yield strength value estimation is significantly higher. Since Gibson and Ashby model [1, 3] suggests using the yield strength values of the solid material, normalization of compression strength of the foams was done by both using estimated yield strength values and the yield strength of 6061 alloy given in Table 4.1.

Compression strength (collapse strength) of the foams was determined from the initial peak of the deformation curves. When the peak was not significant, values were taken from maximum stress value of the flat portion of the curves at strains less than three per cent. Correlation curves together with the normalized experimental data of AlMgSi and composite foams are given in Figures 4.23 - 4.30. To allow for a comparison heat treated (HT) foams were normalized by 276 MPa, the yield strength of T6 temper 6061 alloy and 385 MPa, the result obtained from microhardness measurement. Foams in as foamed condition (AF) were normalized by 145 MPa, the yield strength of T4 temper 6061 alloy and 215 MPa, the result obtained from microhardness measurement. Hardness values of

the as foamed samples were very close to hardness of the SHT (≈ T4) samples so it is convenient to normalize compression strength of these foams by the yield strength of T4 temper 6061 alloys. Microhardness measurement also showed that ceramic addition did not change the strength of the matrix alloy significantly. Therefore same solid yield strength values were used for composite foams. Best fits to the correlation equations were achieved by assuming foams were open cell. Although scaling law specifies that normalized compression strength is proportional to $\rho_r^{1.5}$ some of the experimental data showed a better fit when it is proportional to ρ_r^2 (see Figure 4.27 and Figure 4.28).

Table 4.1. Typical mechanical properties of alloys 6061 and 6063 and estimated strength values of the AlMgSi foam cell wall material

Alloy	**Temper**	**Yield Strength (MPa)**	**Tensile Strength (MPa)**	**HV/3 (MPa)**
6061 [71]	O	55	**124**	-
	T4	145	**241**	-
	T6	276	**310**	-
6063 [71]	O	48	90	-
	T4	90	172	-
	T6	214	241	-
AlMgSi Foam	Annealed	-	-	**120**
	As Foamed	-	-	**215**
	SHT + Aging	-	-	**385**

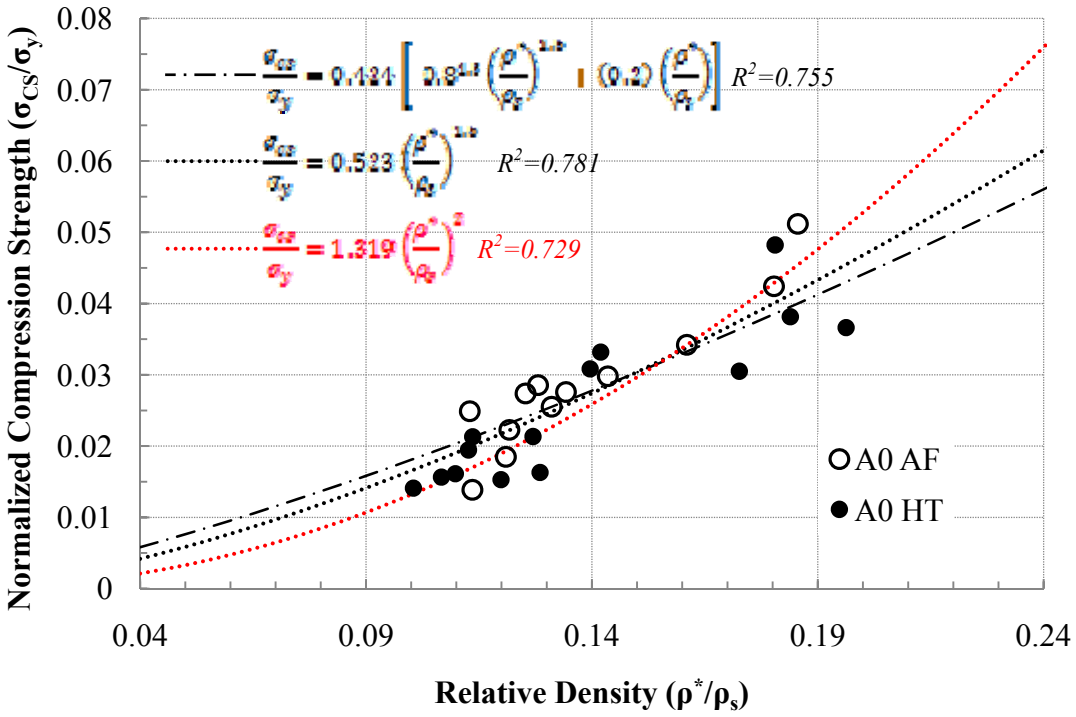

Figure 4.23. Normalized compression strength – relative density for A0 foams. The normalizing solid yield strengths are: 145 MPa (AF), 276 MPa (HT)

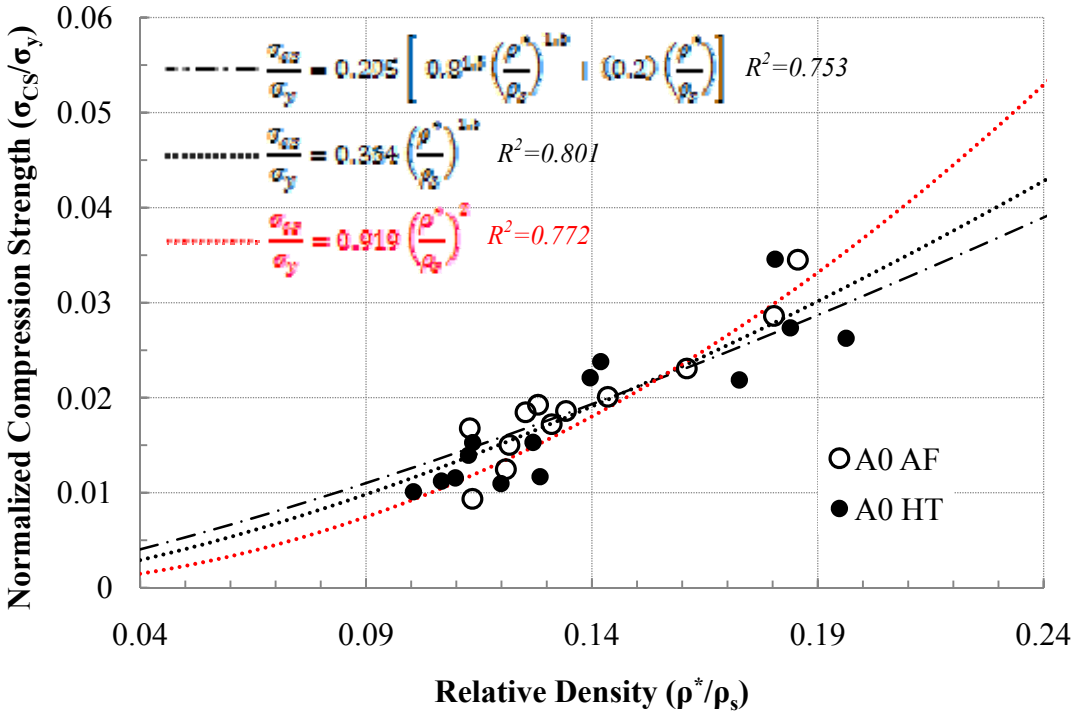

Figure 4.24. Normalized compression strength – relative density for A0 foams. The normalizing solid yield strengths are: 215 MPa (AF), 385 MPa (HT)

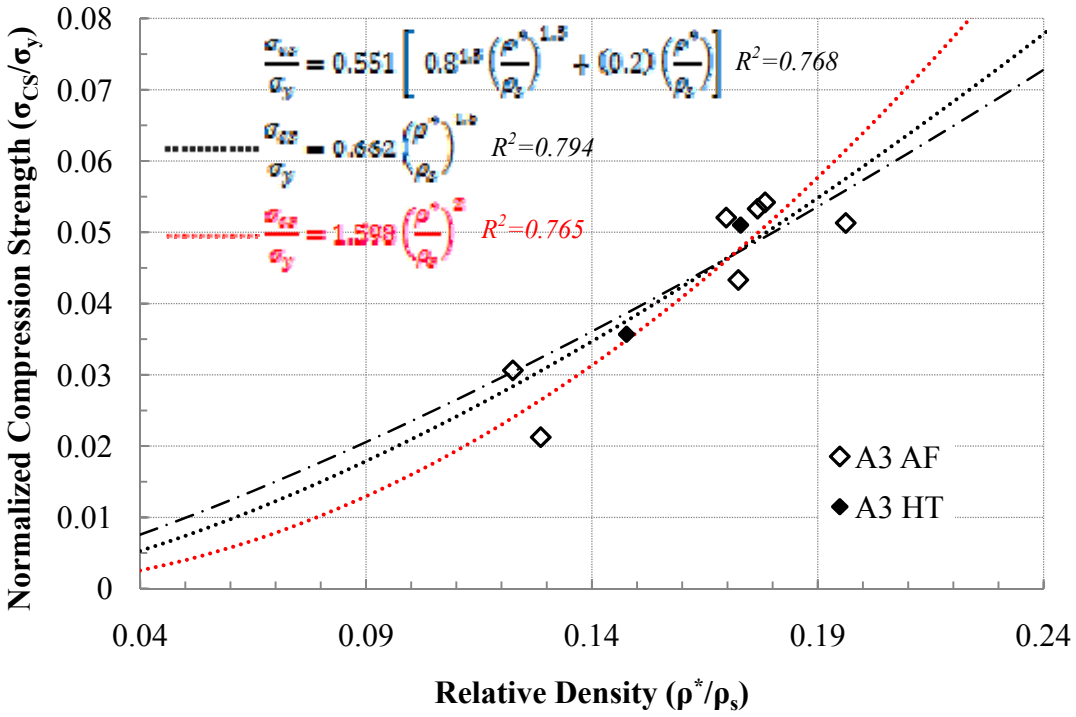

Figure 4.25. Normalized compression strength – relative density for A3 foams. The normalizing solid yield strengths are: 145 MPa (AF), 276 MPa (HT)

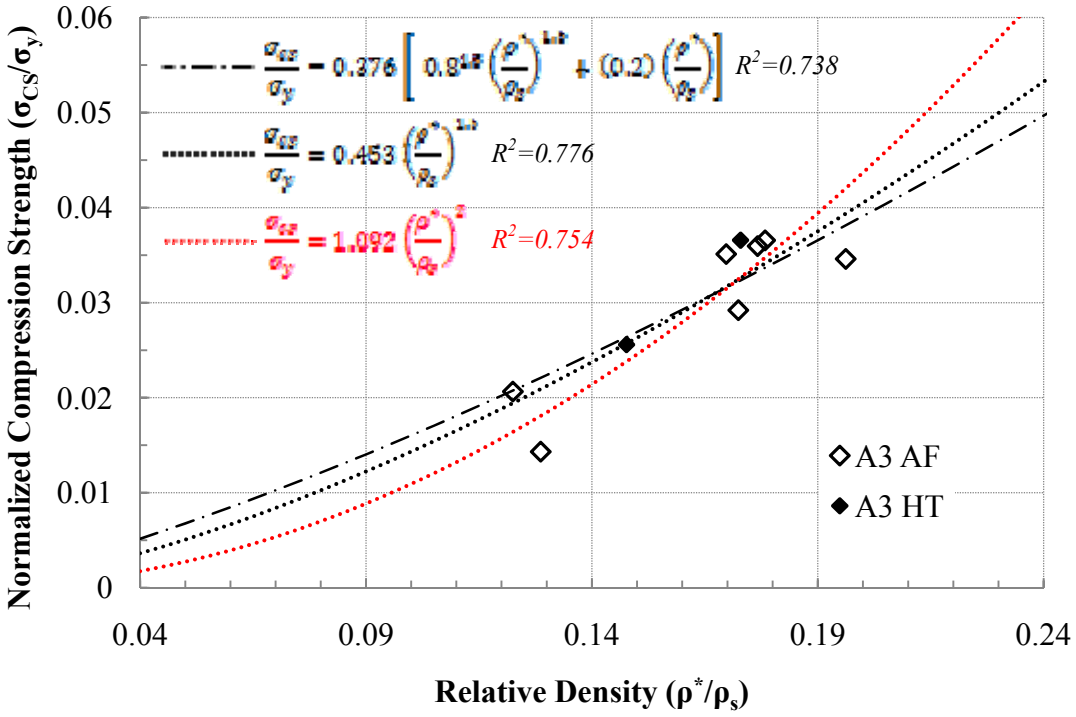

Figure 4.26. Normalized compression strength – relative density for A3 foams. The normalizing solid yield strengths are: 215 MPa (AF), 385 MPa (HT)

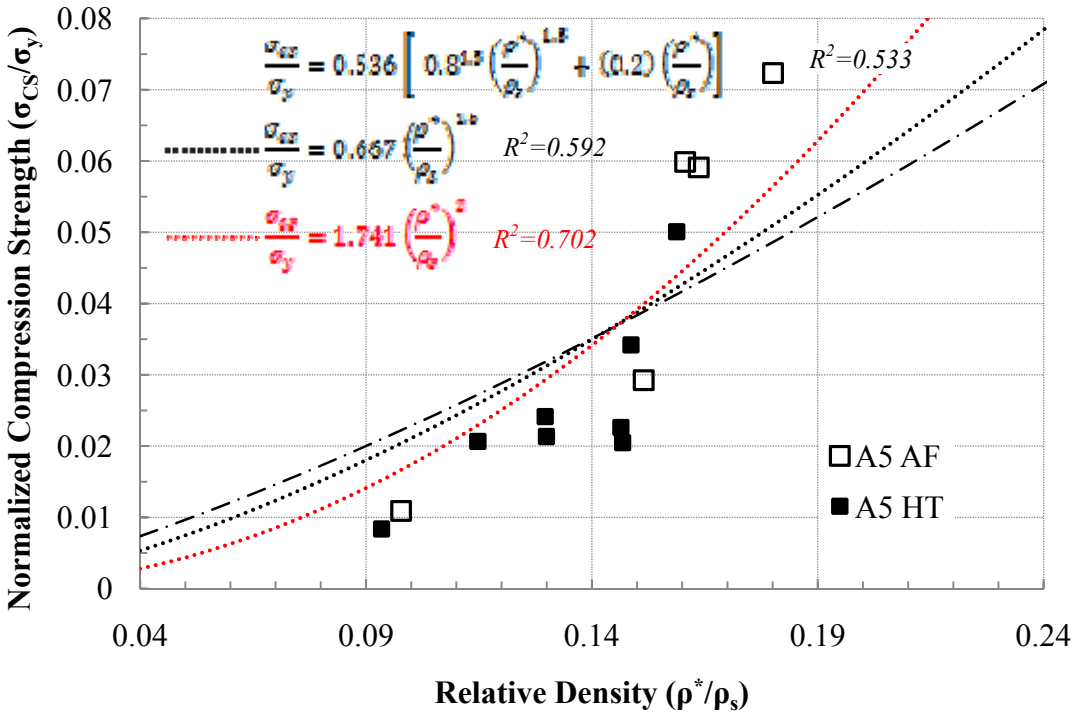

Figure 4.27. Normalized compression strength – relative density for A5 foams. The normalizing solid yield strengths are: 145 MPa (AF), 276 MPa (HT)

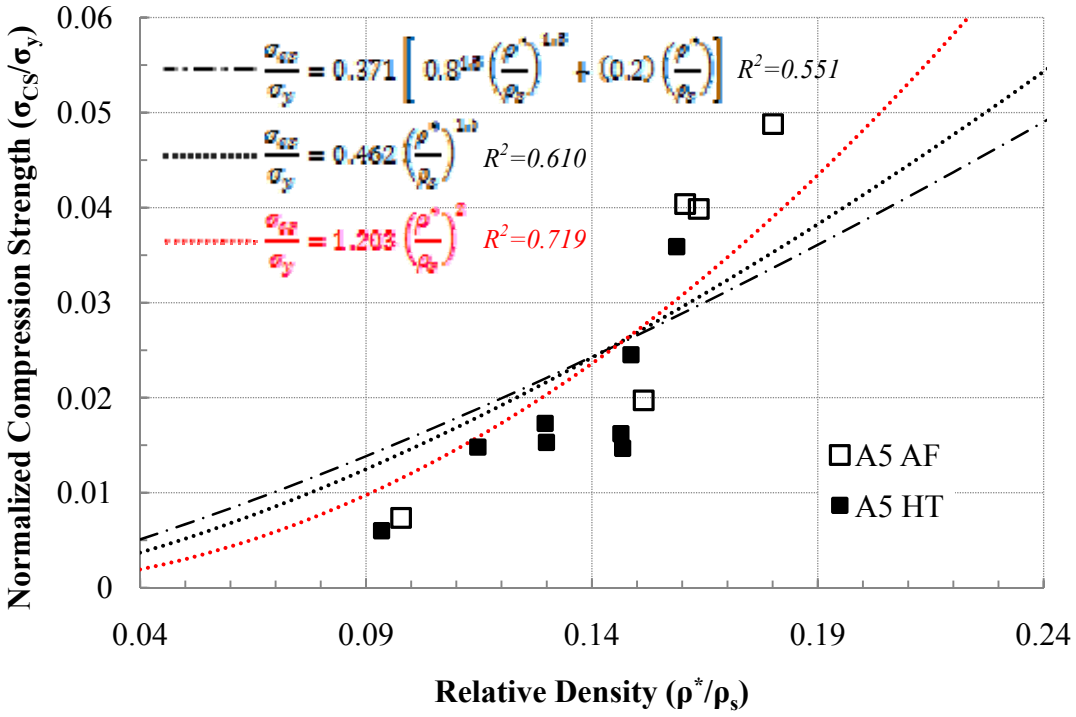

Figure 4.28. Normalized compression strength – relative density for A5 foams. The normalizing solid yield strengths are: 215 MPa (AF), 385 MPa (HT)

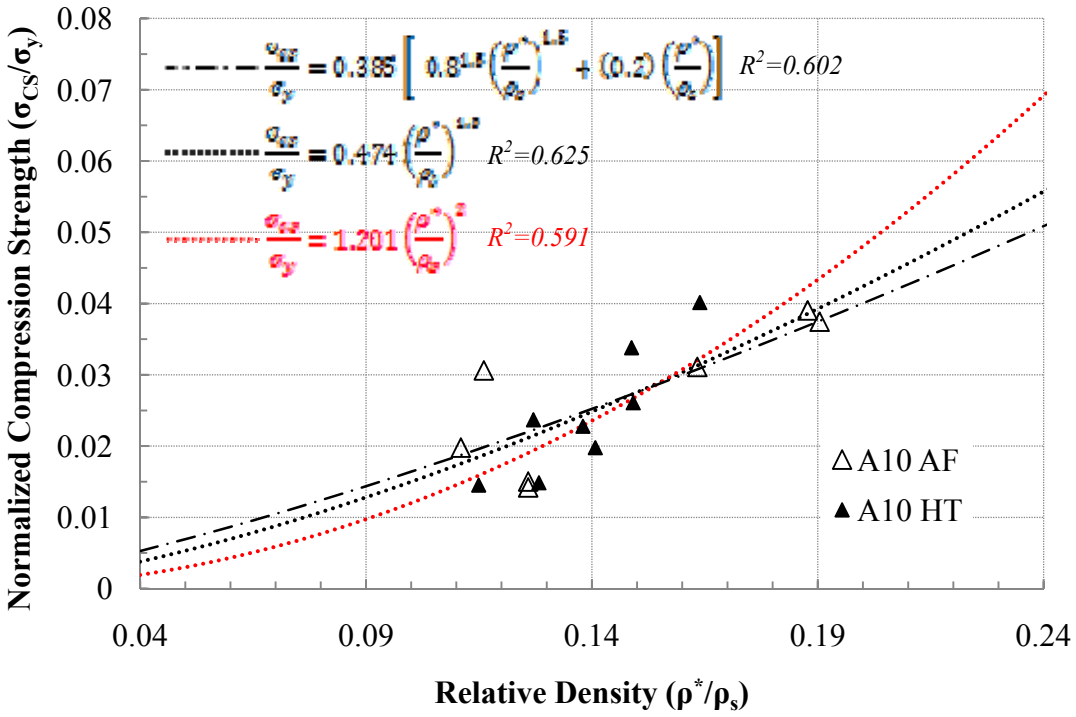

Figure 4.29. Normalized compression strength – relative density for A10 foams. The normalizing solid yield strengths are: 145 MPa (AF), 276 MPa (HT)

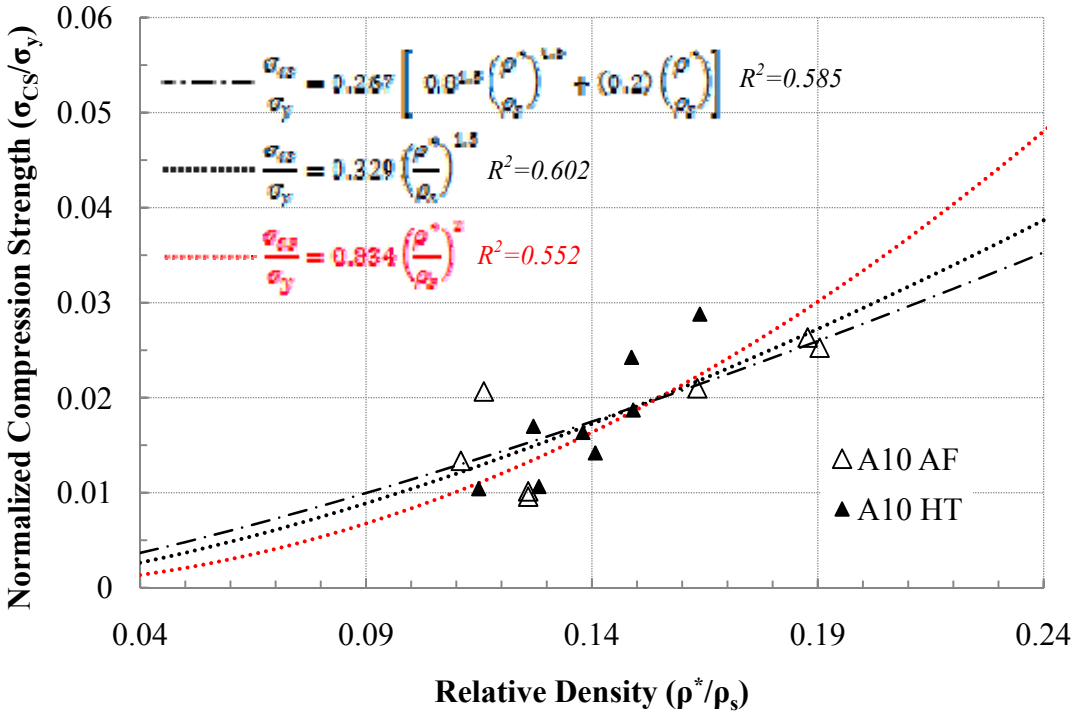

Figure 4.30. Normalized compression strength – relative density for A10 foams. The normalizing solid yield strengths are: 215 MPa (AF), 385 MPa (HT)

Correlations made according to the normalized experimental data with the best fit are given below for A0, A3, A5 and A10 foams respectively:

$$\frac{\sigma_{cs}}{\sigma_y} = 0.523\left(\frac{\rho^*}{\rho_s}\right)^{1.5}$$
$$\frac{\sigma_{cs}}{\sigma_y} = 0.364\left(\frac{\rho^*}{\rho_s}\right)^{1.5} \quad (4.14)$$

$$\frac{\sigma_{cs}}{\sigma_y} = 0.662\left(\frac{\rho^*}{\rho_s}\right)^{1.5}$$
$$\frac{\sigma_{cs}}{\sigma_y} = 0.453\left(\frac{\rho^*}{\rho_s}\right)^{1.5} \quad (4.15)$$

$$\frac{\sigma_{cs}}{\sigma_y} = 1.741\left(\frac{\rho^*}{\rho_s}\right)^{2}$$
$$\frac{\sigma_{cs}}{\sigma_y} = 1.203\left(\frac{\rho^*}{\rho_s}\right)^{2} \quad (4.16)$$

$$\frac{\sigma_{cs}}{\sigma_y} = 0.474\left(\frac{\rho^*}{\rho_s}\right)^{1.5}$$
$$\frac{\sigma_{cs}}{\sigma_y} = 0.329\left(\frac{\rho^*}{\rho_s}\right)^{1.5} \quad (4.17)$$

where first terms in each equation are the normalized values with the solid yield strength of 145 MPa (AF) and 276 MPa (HT) and the second terms are the normalized values with the solid yield strength of 215 MPa (AF) and 385 MPa (HT).

As seen in the correlations given above, for the same relative density, stiffness values A0, A3 and A5 foams are close to each other and these foams are stiffer than A10 foams.

When the relative density is above 0.15, A5 foams have higher strength values. Compression strength of A10 foams is lower than the others because of the imperfect cell structure and high density gradient observed in these foams. In addition, the micrographs of the cell walls of the composite foams showed that while a fraction of ceramic particles were embedded inside the metal matrix some were pushed to the interface between the gas and liquid during foaming or solidification. This probably decreased the extent of strengthening effect expected on the mechanical properties of composite foams.

The results also showed that foams behaved essentially as open cell foams. This was also evident in the SEM examinations where voids and cracks on the cell faces could be observed. As seen in Figure 4.10 and Figure 4.11 the cell faces of the foams have a corrugated structure or the remains of prior powder boundaries. The overall deformation behavior of the AlMgSi and composite foams might be dominated by the cell edges mostly because of these defects and the topology of the cell faces.

4.2. Manufacturing of MMC_p Foams from Extruded Powder Compacts

4.2.1. Powder Compaction by Extrusion

During extrusion of the green compacts, pressure increases linearly with ram displacement as the green compact upsets to fill the container and reaches a maximum value as the workpiece starts to flow through die cavity. As the ram advances, a small decrease in pressure is observed indicating the decreasing frictional resistance as the contact area between the compact and container wall decreases. Manometer readings from extrusion press showed a significant increase in pressure with the addition of ceramic particles. Probably the presence of the ceramics increased shear strength and hence the necessary force for deformation. Increasing of reinforcement volume from five per cent to 10 per cent resulted in increased surface defects of the extrudes. The surface defects observed can be as a result of increased agglomeration of ceramics during blending or higher heat generation during the extrusion as a result of increased shear strength [67, 72]. For obtaining better quality surfaces the extrusion temperature and ram speed were lowered. Figure 4.31 shows the deformation and compaction of powders during extrusion. Powder mixture is first compacted and then deformed through the extrusion die. Original powder boundaries diminish after extrusion indicating a high level of deformation and welding of powders together with fresh interfaces. The microstructures of CA1, CA3 and CB mixtures after compaction are shown in Figure 4.32.

4.2.2. Foaming Time

Foaming time was considerably reduced by ceramic particle addition. Since specific heats and densities of the ceramics and Al are comparable to each other, comparison of thermal conductivities and thermal diffusivities is necessary (Table 4.2). To predict the effects of ceramic addition on the foaming time, an example calculation can be done for Al_2O_3 addition to Al. Table 4.3 gives thermal conductivity values for both materials with increasing temperature. Assuming heat transfer to all precursors by convection and radiation is the same inside the furnace, it can be shown that Al_2O_3 particle addition should slow down heat flow inside the material, hence retard foaming.

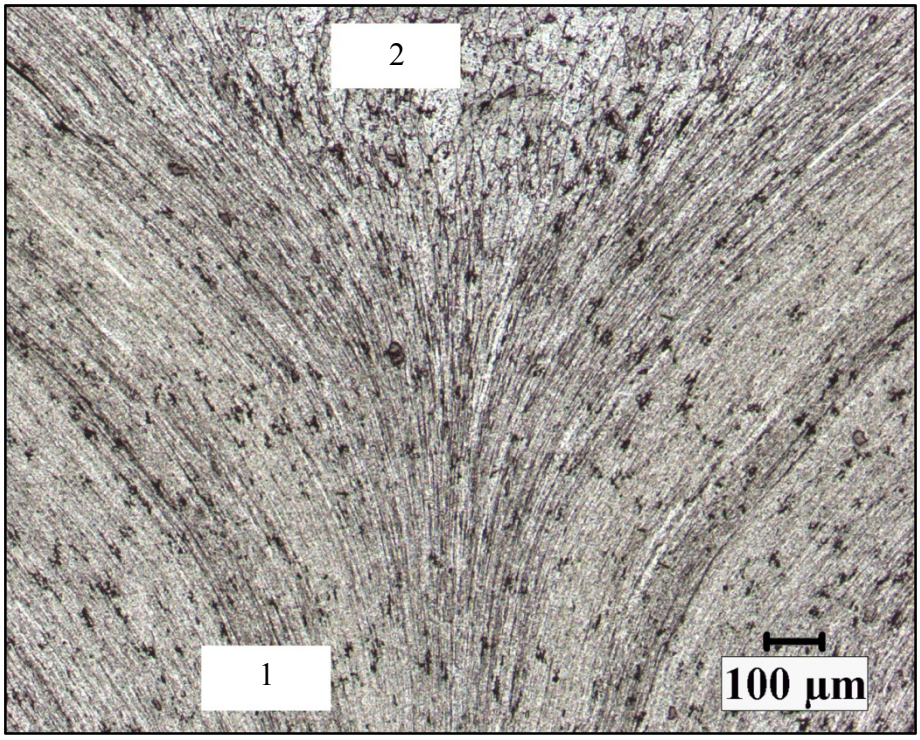

(a)

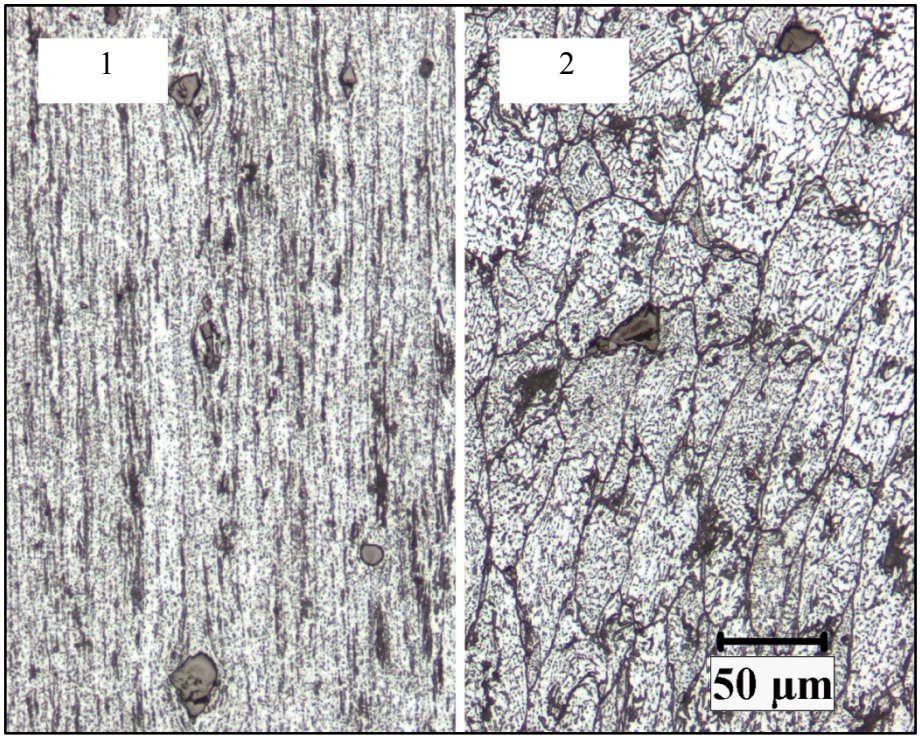

(b)

Figure 4.31. Microstructure of powder metal compact during extrusion (moderately etched): (a) extrusion die entrance zone, flow of the material to the die orifice, (b) original powder grains are compacted and then extruded

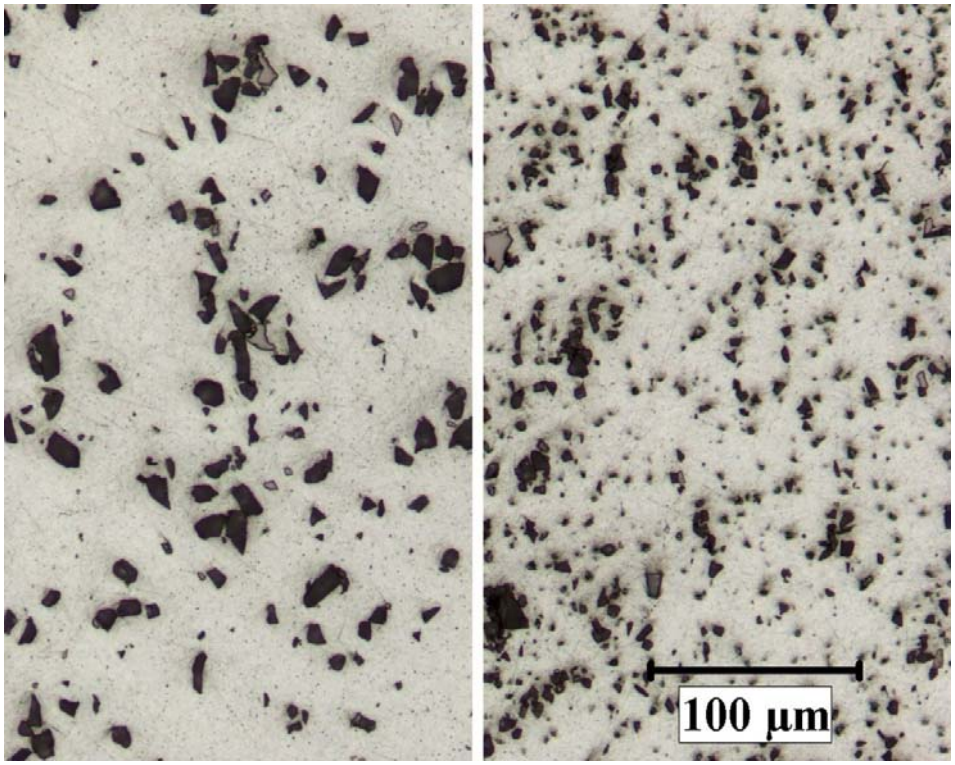

(a)

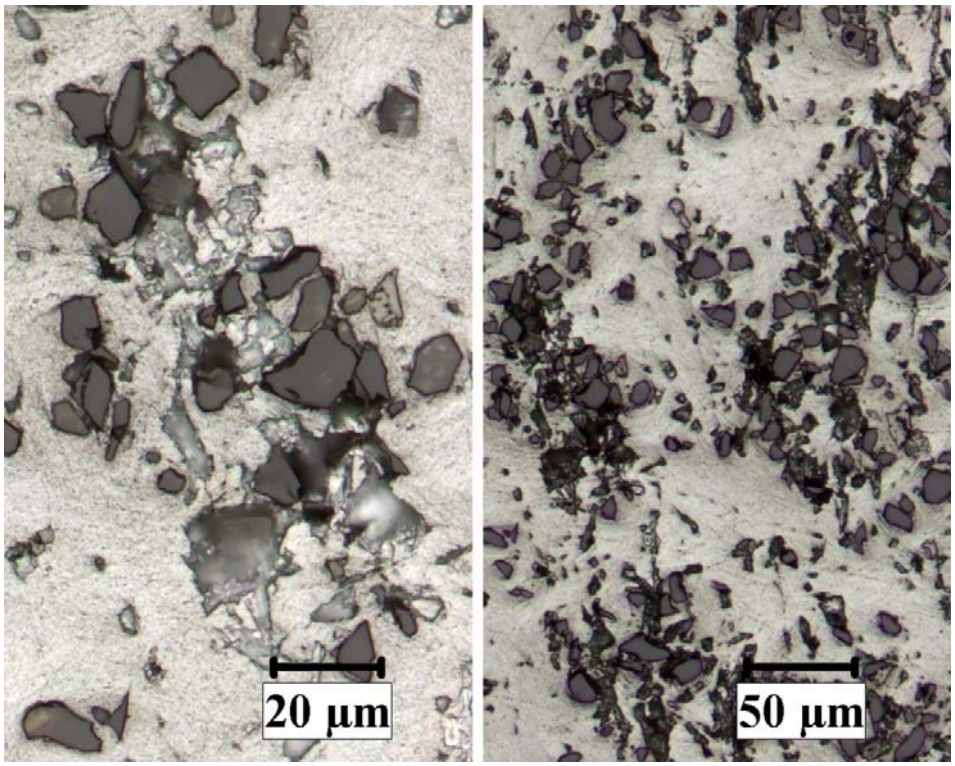

(b)

Figure 4.32. Extruded powder compacts (slightly etched): (a) CA3 compact on the left and CA1 compact on right handside, (b) CB compact

A simple rule of mixtures calculation [69] for the precursor material with five vol. per cent Al_2O_3 addition gives 0.89-0.915 W/cm•K and ≈0.99 cm^2/s at 800 °C which is approximately five to eight per cent below thermal conductivity and thermal diffusivity of pure Al.

In a pure liquid with no impurities, the surface tension is generally too strong and viscosity is lower. Assuming bulk viscosity change by 5 to 10 vol. per cent ceramic addition is small and neglecting viscous and inertia forces acting on every bubble representing the initiation of foaming, pressure equilibrium at the gas-liquid interface can be written as:

$$P_B = P_a + \rho g h + \frac{2\sigma}{R} \tag{4.18}$$

where g is the gravity constant, P_a is the ambient pressure, P_B is the bubble pressure, h is the depth of the bubble, σ, is the surface tension and R is the radius of the bubble. Considering the equation, the pressure contribution resulting from surface energies for all precursors seems to be the deciding parameter in initiation of foaming. Ceramic particle addition generally increases viscosity and reduces surface tension at the gas-liquid interface. It seems for the particular composition the reduction in surface tension is more effective than the increase in viscosity and slower heat conduction within the material. Here it must be noted that specimens foamed were small and the surface area over volume ratio was also small. If higher volume or bulk precursors are to be foamed, the decreased thermal conductivity and diffusivity of the precursor can be more effective. As a result of inhomogeneous heating and temperature distribution through the material the quality of the foam can be poor.

Another possibility for earlier expansion of the composite foams can be the change of the hydrogen generation from the blowing agent caused by the broken oxide layers during extrusion in the presence of hard ceramic particles.

Table 4.2. Comparison of thermal properties of Al, Al_2O_3, SiC and B_4C [72, 73]

Reinforcement	**Specific heat, (J/g·°C)**	**Thermal conductivity, (W/cm·K)**	**Density, (g/cm^3)**	**Thermal Diffusivity, (cm^2/s)**
Al_2O_3	0.71	0.30	3.96	0.11
SiC	0.67	0.52	3.20	0.24
B_4C	0.84	0.26	2.51	0.12
Matrix				
Al	0.82	2.37	2.7	1.07

Table 4.3. Thermal conductivities of Al and Al_2O_3 at different temperatures [73]

Temperature (°C)		**Room temp.**	**300**	**500**	**800**
Thermal Conductivity (W/cm·K)	Al	2.37	2.32	2.2	(0.96)
	Al_2O_3	0.25	0.155	0.146	0.063-0.071

4.2.3. Cell Structures

Simple free foaming experiments showed that ceramic addition significantly increases expansion of foams. The macrographs of the precursor and the cell structures of Al and Al composite foams are shown in Figure 4.33. Al foam had small number of cells, which were larger. Thick cell walls and drainage at the bottom was observable. When the foaming temperature was increased from 800 °C to 850 °C a slight increase in expansion was seen (Figure 4.33b). Composite foams had high number of cells with thinner cell walls. Cells were smaller and relatively homogeneously distributed. There was no significant drainage at the bottom. Maximum expansion was achieved with CA3, CA4 and CB composite foams. However, the cell size differences were higher when compared with CA1 and CA2 foams. The most homogeneous cell size distribution was achieved with CA1

and CA2 foams. The geometry and cell faces of CB foams were quite smooth. A reaction between Al and B_4C had resulted in an enhanced wetting of the ceramic particles by the liquid matrix during foaming. An evidence for the reaction was the change in the color of the CB foams. Particle size of Al_2O_3 had a little effect on expansion. When the amount was increased from five to 10 vol. per cent larger cells were formed and thicker cell walls were observed. This behavior was less significant in CA2 when compared with CA4 foams.

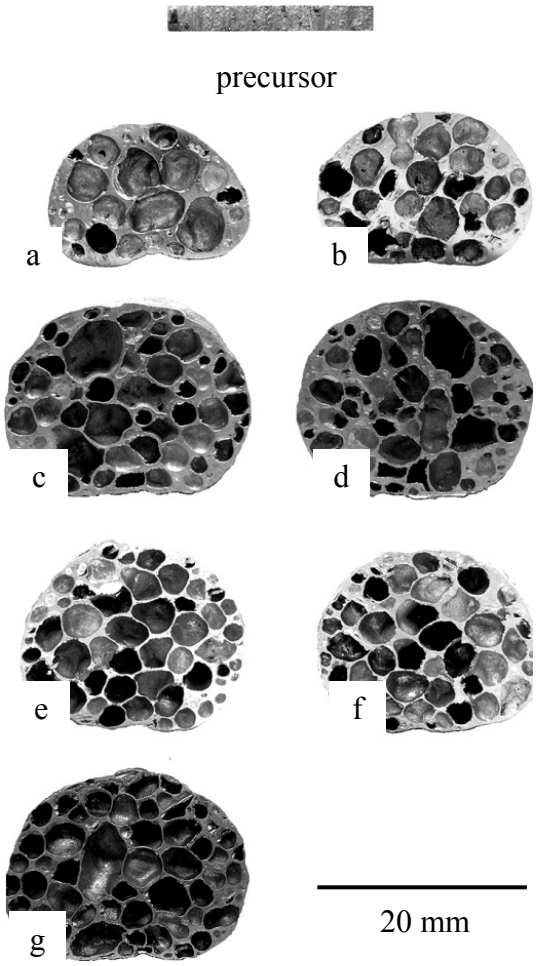

Figure 4.33. The cell structures: (a) Al (f.t., 800 °C), (b) Al (f.t., 850 °C), (c) CA3, (d) CA4, (e) CA1, (f) CA2, (g) CB foams

4.2.4. Microstructures

Enhanced foaming behavior and improved stabilization of composite foams are believed to be as a result of ceramic particles addition. Microstructures of fractured cell walls and cell faces are studied by SEM for a better understanding of the experimental results. Al foam cell faces had corrugated cell wall topography (Figure 4.34a). Körner *et al.* [39] explained the reason for this topography with the entrapment of solid particles between two opposing interfaces. Solid particles were formed during foaming as oxide networks and the oxides were coming from the oxide skin of the Al powders. The structure of the fractured cell wall indicated a ductile rupture took place. The cells of the foams manufactured by PCM method usually contains cracks or holes on the cell faces. Most of the powders retain their original boundaries during foaming and solidification. These boundaries are the weak points where cracks may initiate during expansion or contraction of the cell face (Figure 4.34c). Figure 4.35, Figure 4.36, Figure 4.37 and Figure 4.38 are the fractured cell wall Plateau region, fractured cell wall and cell wall faces of CA1, CA2, CA3 and CB foams respectively. The fracture surfaces of the composite foams either had a large cavity or highly agglomerated ceramic particles. Decohesive rupture at the surfaces with voids or ceramic agglomerates, and ductile shear lips at the soft Al matrix was observable. The majority of large ceramic particles in CA3 and CB foams were observed on the cell faces while small ceramic particles in CA1 and CA2 foams were observed equally both on the cell faces and in the cell walls (Figure 4.36).

BSE micrographs of CA3 and CA2 foam showed the remains of the blowing agent TiH_x particles were also attached to the cell face and partially wetted by the Al matrix. Although TiH_2 is heat treated and oxidized to retard hydrogen release the particle observed in Figure 4.39d indicated that during extrusion or foaming they crack and the new oxide free surfaces can result in earlier decomposition. Ceramic particles had sharp edges and as seen in Figure 4.40d. They could be the source of rupture or cell coalescence by tearing the cell faces during the expansion of foams.

Ceramic particles were generally distributed homogeneously on the cell walls. A ceramic particle layer was formed between the metal and gas interface. A closer look to the surface one can see that these particles are poorly wetted (Figure 4.41b). B_4C particles

were larger and segregated between the metal and gas interface. However a closer look to the walls showed that wetting of B_4C particles were better than Al_2O_3 particles (Figure 4.42b). The wetting behavior of different ceramics by the Al matrix changes the topography of the cells as observed in Figure 4.43.

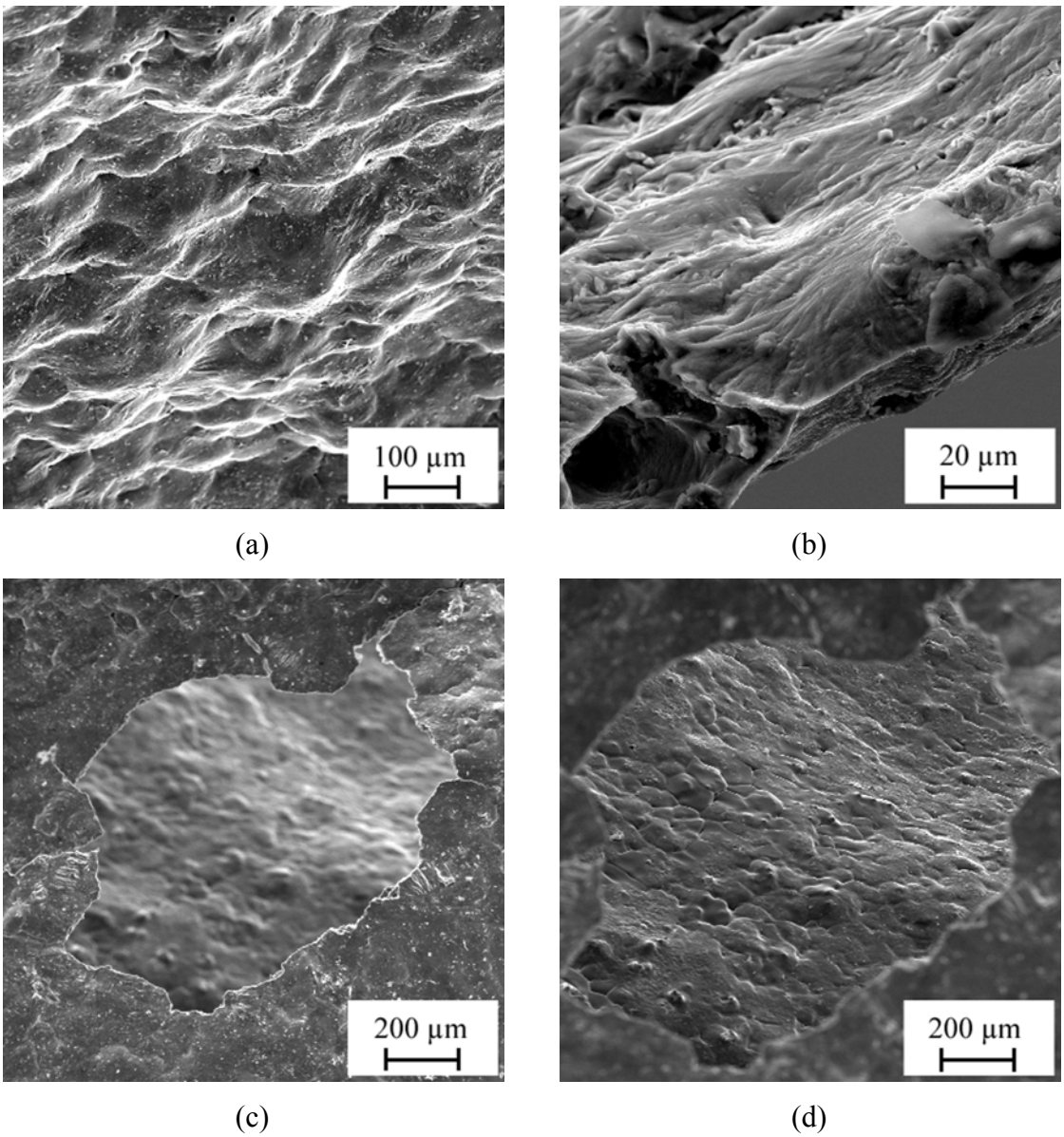

Figure 4.34. SEM micrographs of Al foam: (a) cell face with wavy surface, (b) cell face and shear lip on the fractured cell wall, (c) cell face rupture during expansion or solidification of the foam, (d) cell face through the ruptured neighboring cell face revealing the prior boundaries of the powders after foaming

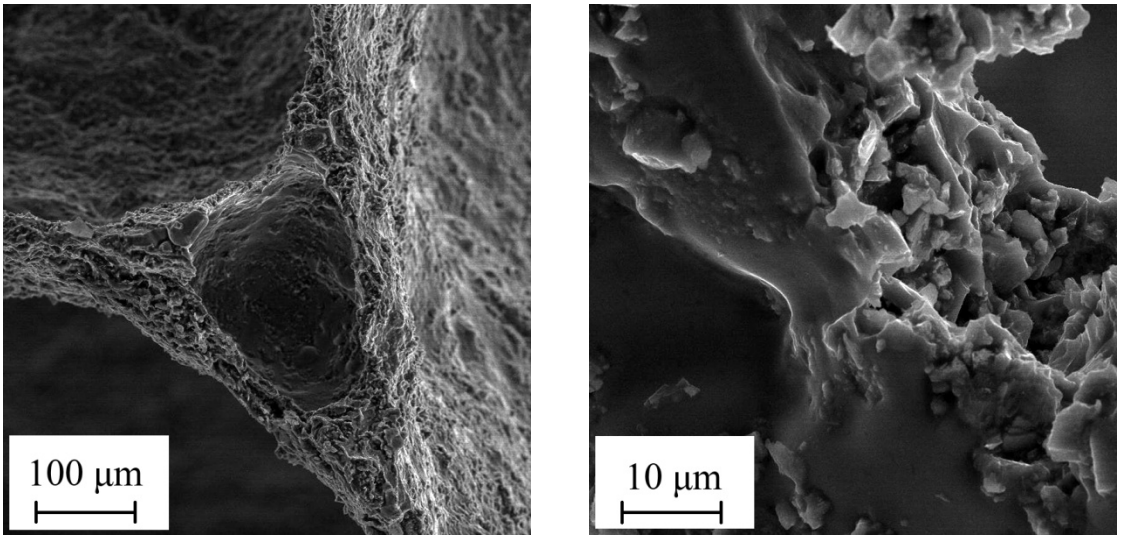

(a) (b)

Figure 4.35. SEM micrographs of CA1 foam: (a) fracture surface of cell wall Plateau region with a large void at the center, (b) cell face and fractured cell wall by decohesive rupture through the surfaces with Al_2O_3 agglomerates

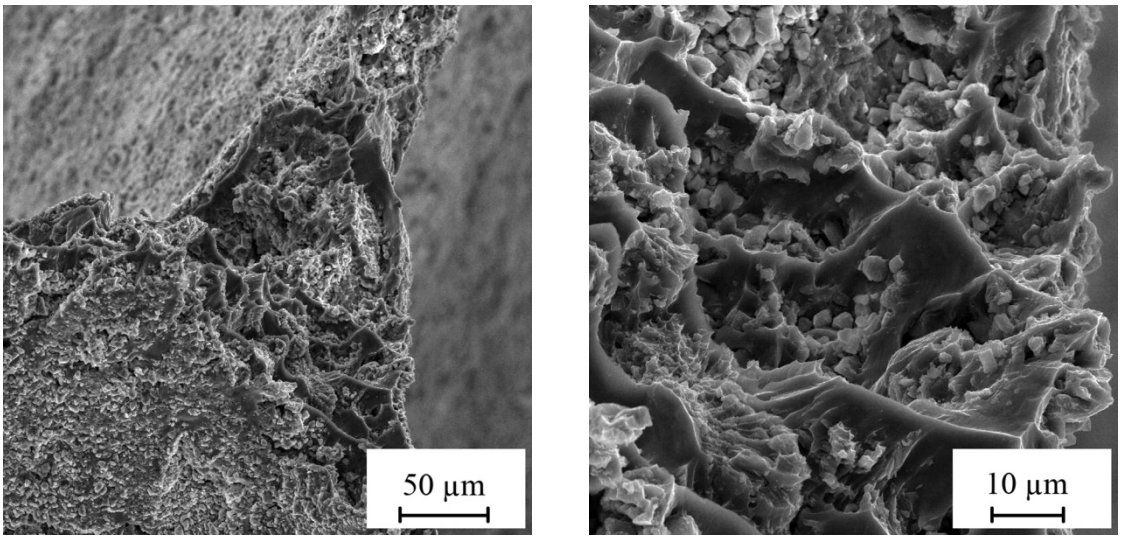

(a) (b)

Figure 4.36. SEM micrographs of CA2 foam: (a) fracture surface of cell wall Plateau region with white Al_2O_3 particles on cell faces and in the cell wall, (b) fractured cell wall showing the decohesive rupture through Al_2O_3 agglomerates and shear lips formed during ductile deformation of the soft Al matrix

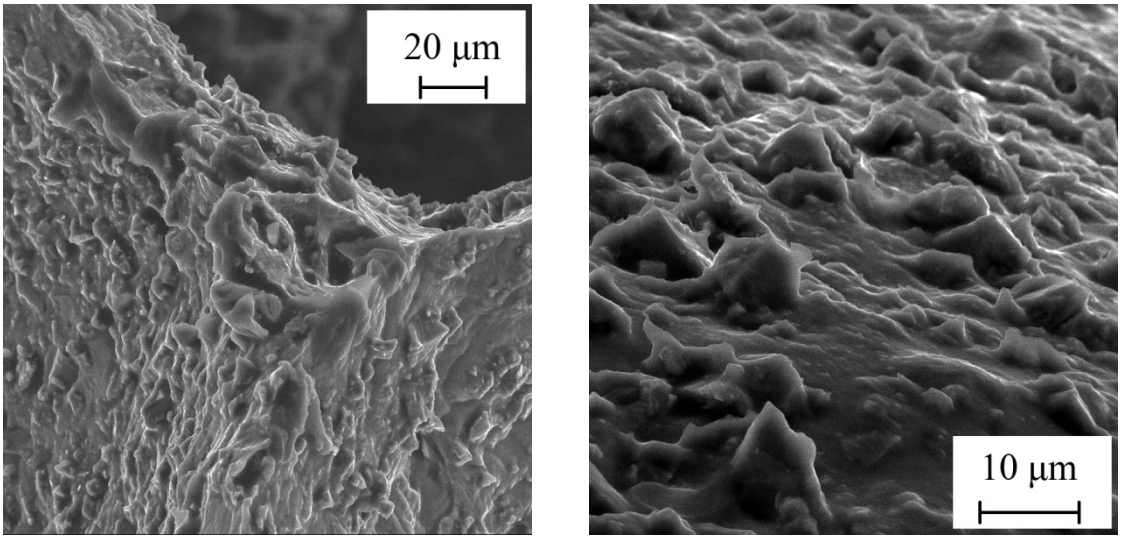

(a) (b)

Figure 4.37. SEM micrographs of CA3 foam: (a) fracture surface of cell wall Plateau region with large Al_2O_3 particles on cell faces, (b) cell face with partially wetted Al_2O_3 particles

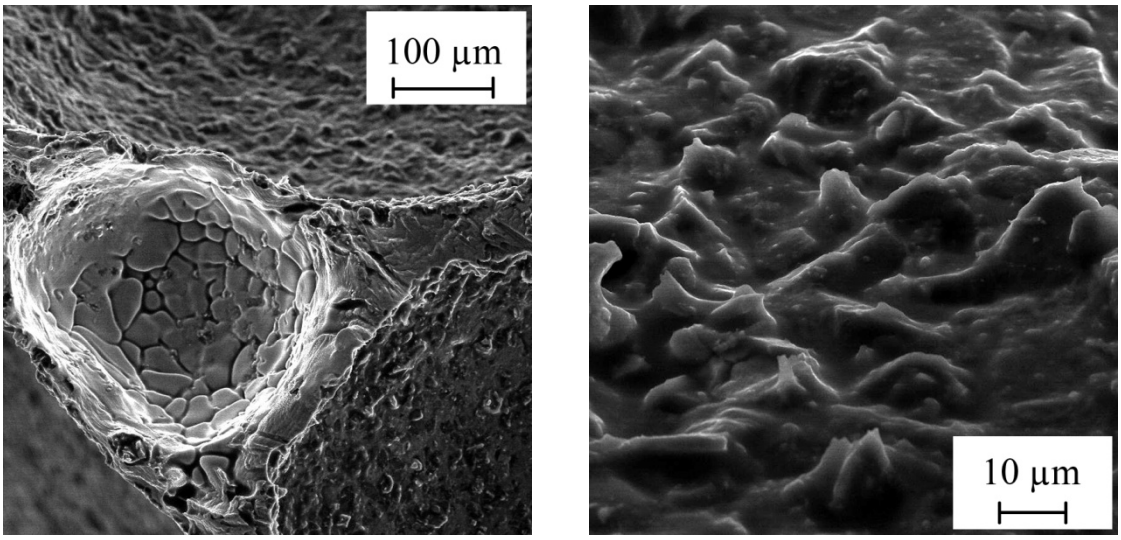

(a) (b)

Figure 4.38. SEM micrographs of CB foam: (a) fracture surface of cell wall Plateau region with a large void at the center, the prior powder boundaries retained after foaming, dark B_4C particles are embedded to the cell faces, (b) cell face with partially wetted B_4C particles

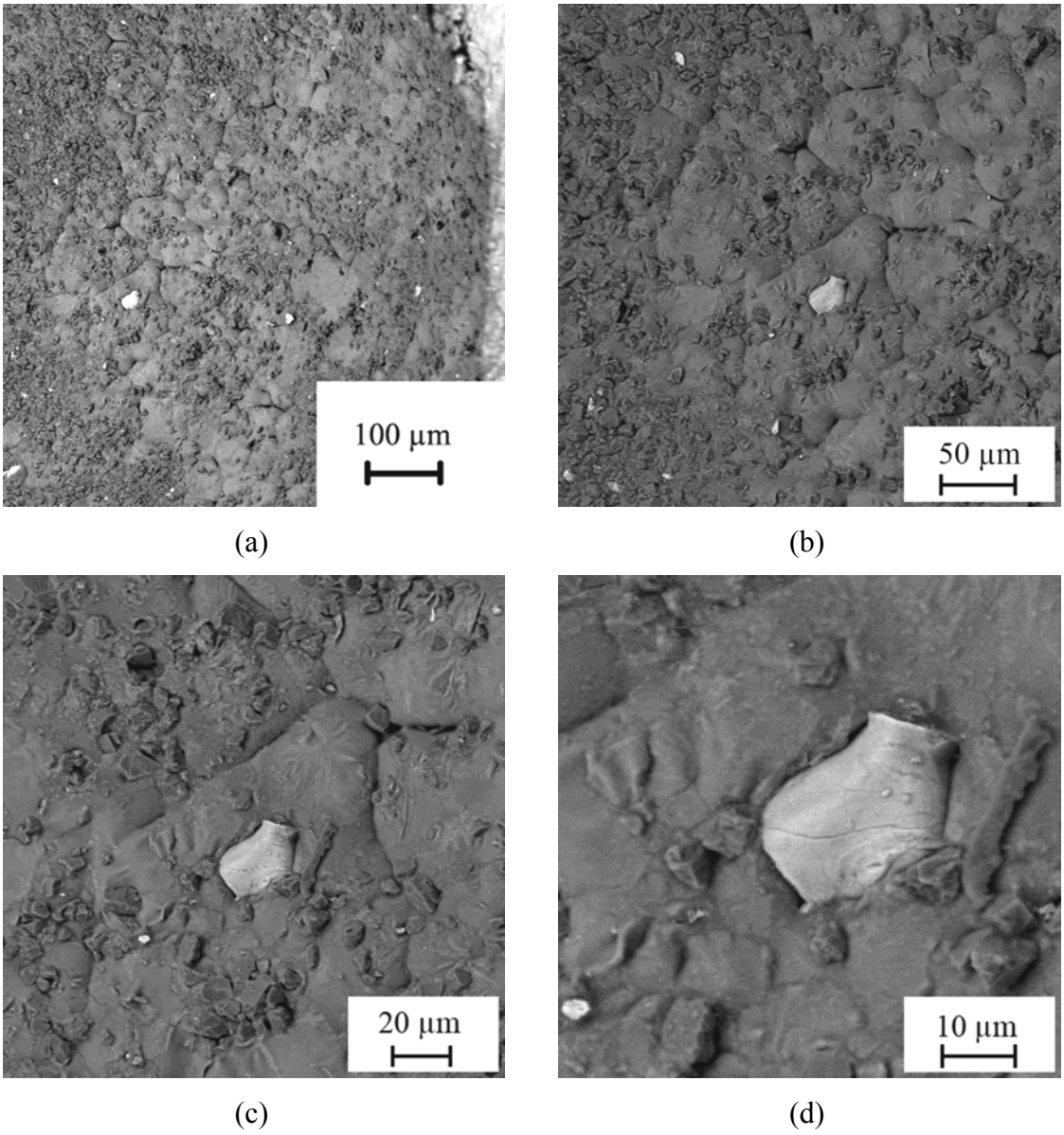

Figure 4.39. BSE micrographs of CA3 foam: (a) general view of a cell face showing the distribution of Al_2O_3 (dark gray) and TiH_x (white), (b) prior Al particle boundaries are retained after foaming, (c) Al_2O_3 and TiH_x particles are partially wetted by the aluminum matrix, (d) TiH_x particle cracked during extrusion or during decomposition of hydrogen

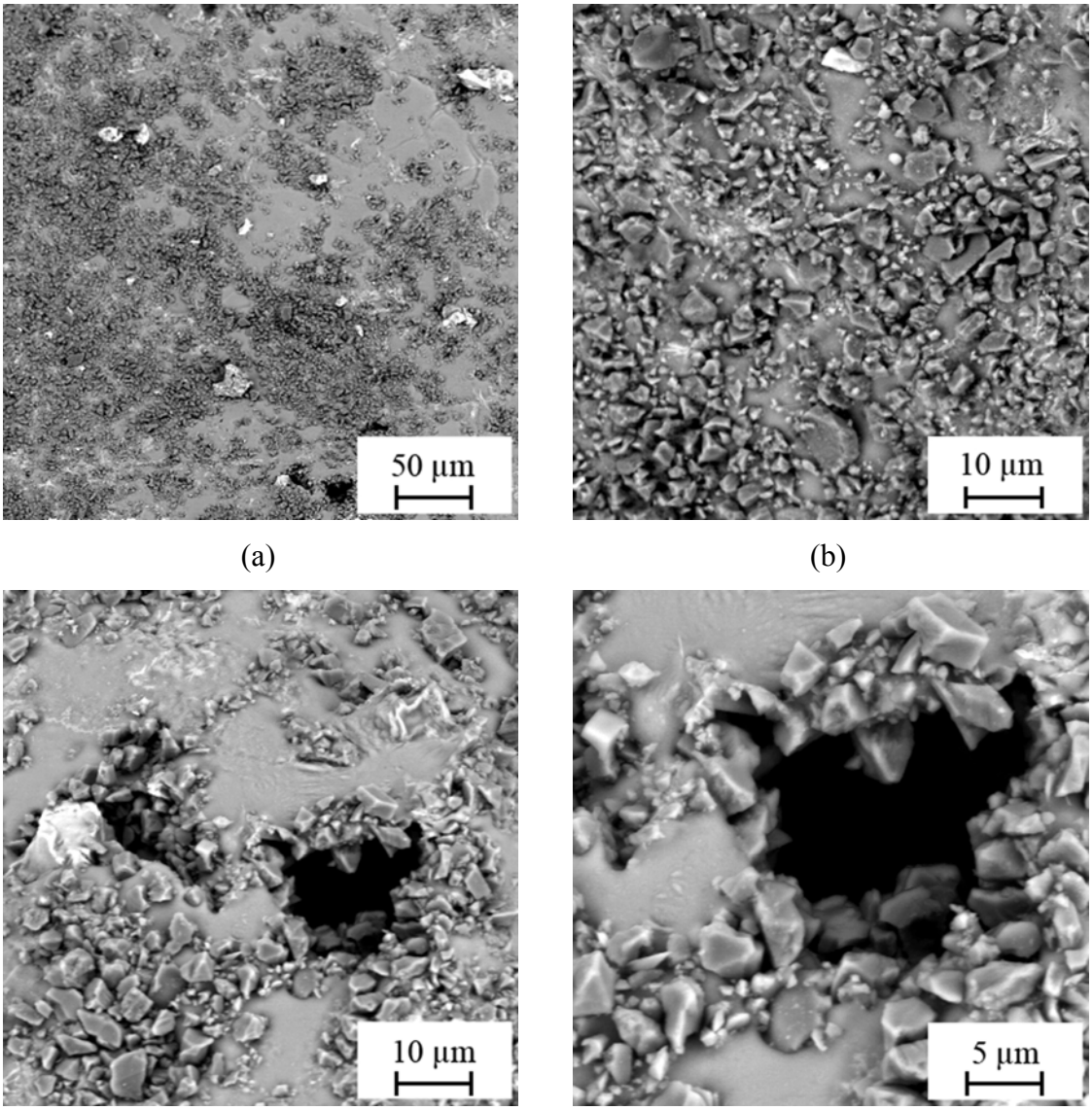

Figure 4.40. BSE micrographs of CA2 foam: (a) general view of the cell face of a coalesced cell showing the inhomogeneous distribution of Al_2O_3 (gray) and TiH_x (white) particles, (b) Al_2O_3 particles are agglomerated and wetting by the Al matrix is poor, (c) two openings on the cell face one with TiH_x particle and agglomerates other with Al_2O_3 agglomerates only, (d) Al_2O_3 around the opening indicating the rupture reason may be the sharp edges of the ceramics

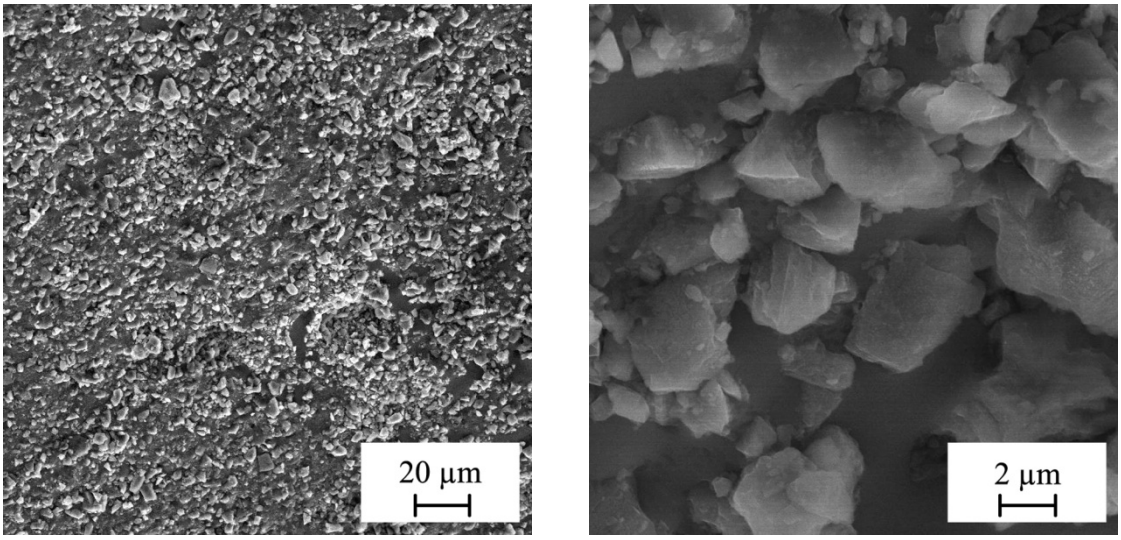

(a) (b)

Figure 4.41. SEM micrograph of CA1 foam: (a) homogeneous distribution of Al_2O_3 particles on the cell face, (b) ceramic particles are poorly wetted

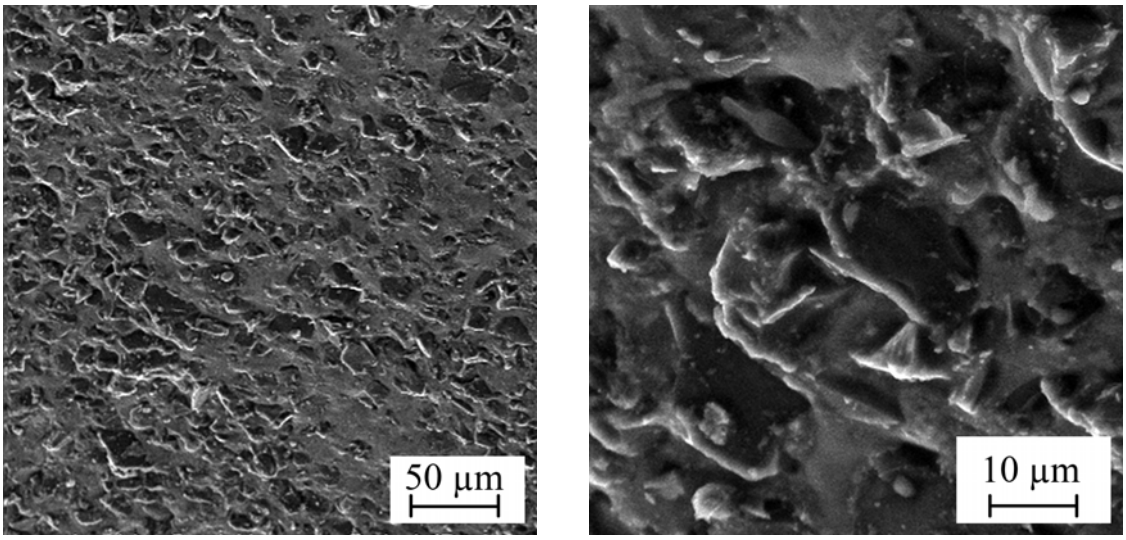

(a) (b)

Figure 4.42. SEM micrograph of CB foam: (a) homogeneous distribution of B_4C particles on the cell face, (b) ceramic particles are partially wetted

4.3. Mechanical Properties of AlSi Foams Manufactured by Using PCM Method

4.3.1. Macrostructure of the Foams

The macrographs of AlSi foams in Figure 4.43 show from left to right early stages of foaming, foam at 60 mm height and foam at 70 mm height. All the samples shown have the same weight. At the beginning of the expansion, pores are elongated perpendicular to the compaction direction. The pores become more spherical or polyhedral when fully foamed. The overall structure seems to be homogeneous except the few large cells at the bottom of the foams. As the expansion increases cell size also increases.

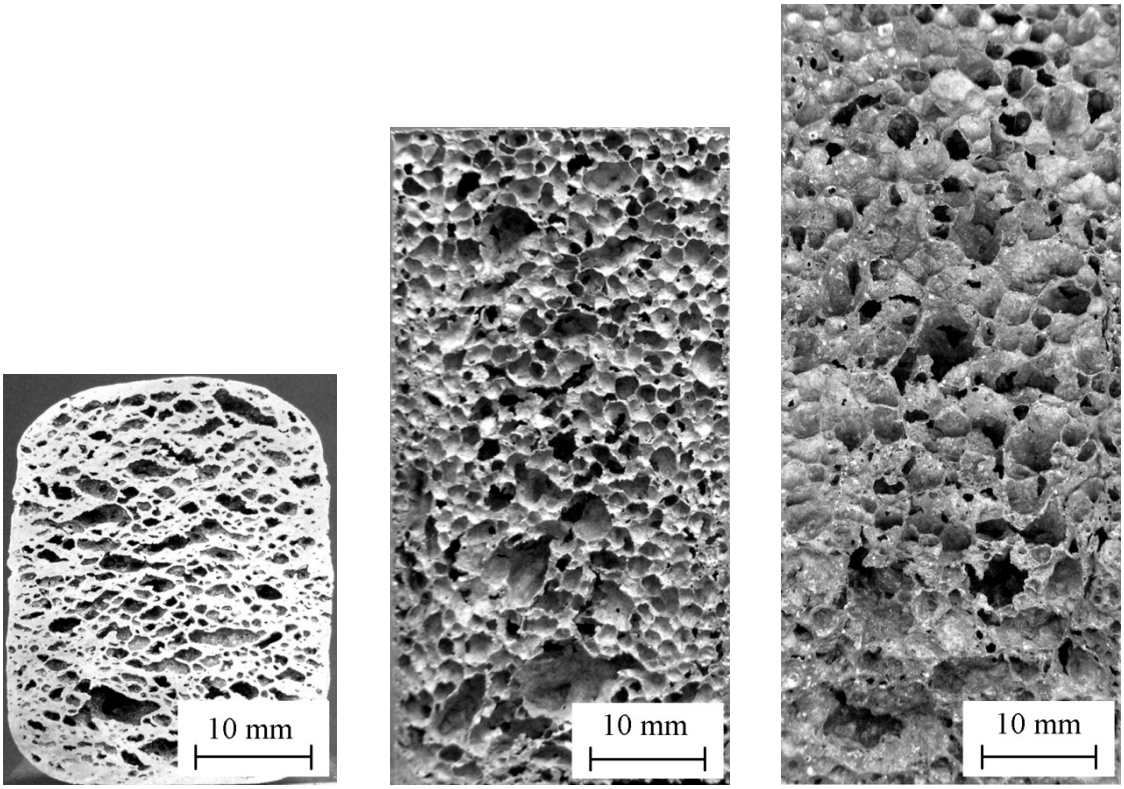

Figure 4.43. Macrostructure of AlSi foams: (a) earlier stages of foaming, (b) foamed to 60 mm height, (c) foamed to 70 mm height

4.3.2. Microstructure of the foams

The important features of the microstructures of AlSi foams are shown in Figure 4.44 to Figure 4.48. As already mentioned, first phase that crystallizes from the hypereutectic AlSi melt is primary Si (see Figure 2.18). During solidification, primary Si particles nucleate and grow. The remaining liquid behaves as the hypoeutectic AlSi alloy and produces aluminum and eutectic silicon. Foaming temperatures of AlSi foams were as high as 780 °C and the powder compact was melted as the expansion reached its maximum value. The microstructure of the foams obtained after cooling is shown in Figure 4.44. The primary Si particles were large and had an angular geometry. The eutectic Si phases were small and had a plate like geometry. After SHT at 530 °C the morphology of the eutectic Si-phases became a more spherical (Figure 4.45). The sharp edges of primary silicon particles were also rounded off. This unsharpness of primary silicon particles and round morphology of eutectic silicon crystals may have reduced the stress concentration at particle-matrix interface, thereby increasing the stress required to nucleate a void at the particle matrix interface. This morphology is favorable from the tensile strength and ductility point of view.

Heat treatment did not affect the size of primary silicon crystals. The morphology of primary silicon crystals depends considerably on solidification parameters such as freezing rate, temperature gradient in the liquid, and composition of the liquid [74]. Foams were not stable in the liquid state and could not be soaked into water. To maintain its shape inside the foaming mold, they were carefully taken out from the furnace and cooled by blowing air. Hence, the cooling rate of the AlSi melt was quite slow. Refinement of primary silicon can be achieved by addition of phosphorous (P) in casting alloys. However, its effect on foaming behavior is not known and therefore it was not added to the powder mixture.

Mg and Cu are employed in the AlSi family to improve strength and hardness of the Al alloy. Microhardness measurements showed that the hardness of SHT and SHT + Aged AlSi foams did not change significantly. Measured hardness values were HV 100 for annealed samples and HV 120 for the others. Casting alloys are generally solution heat treated for longer times when compared with wrought alloys. Al foams were subjected to SHT for approximately two hours and some of them were aged afterwards.

An interesting feature observed under optical microscope is shown in Figure 4.46. After SHT, surfaces of the etched matrix have reflected a colorful image. These different colors are presumably showing the different oxidation levels of the matrix, which contains copper. The pictures were taken after application of Keller's agent for one minute.

SEM micrographs taken from the cell walls of the as foamed and heat treated AlSi foams revealed the intermetallics precipitated at the grain boundaries (Figure 4.47). Al_2Cu intermetallic, agglomerated primary Si particles and spheroidized eutectic Si particles are observed. During solidification, primary Si particles are first crystallized and these particles are surrounded by liquid until the eutectic point. The agglomeration of Si particles may be because of the push by the solidification front and bubble movements during the expansion of the foam. Figure 4.47c shows three large Si particles that are very close to each other but not in contact. Spectrum analyses of AlSi foam without the blowing agent performed along the cell wall showed the presence of Al, Si, Cu and Mg elements (Figure 4.48). The percentage of the elements is shown in Table 4.4. Fracture surfaces of AlSi foams are shown in Figure 4.49. Cell walls fractured from their weak points; voids present in the cell wall, prior powder boundaries and from the surfaces with primary Si particles as seen in the figure. The cell wall Plateau border is the region where three cell wall boundaries of the cells meet. The Plateau regions are important since the drainage or flow of liquid with gravity forces to the bottom of the foam is from the cell walls through the cell wall Plateau borders. The cell wall of the foams was as thin as 60 μm, which was very close to the size of primary Si particles observed in optical and SEM micrographs of AlSi cell walls.

Table 4.4. Spectrum analysis of AlSi foam cell wall (see Figure 4.48)

Element	**O K**	**Mg K**	**Al K**	**Si K**	**Cu K**	**Totals**
Weight (%)	4.83	0.58	50.23	39.40	4.96	100
Atomic (%)	8.23	0.65	50.75	38.25	2.13	100

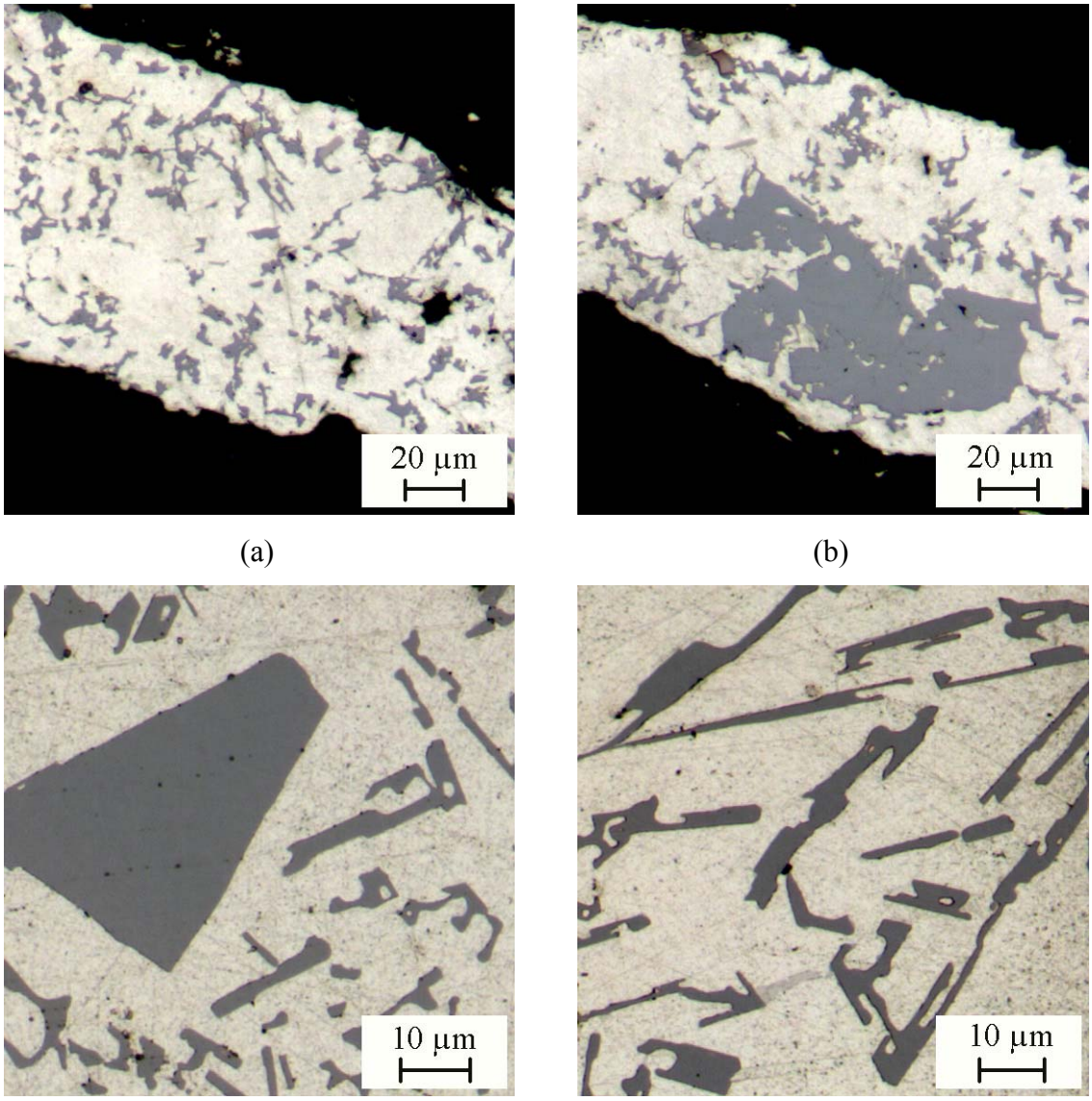

Figure 4.44. Optical micrographs showing the cross sections of cell walls: AlSi foam; (a) cell wall with eutectic Si particles only, (b) cell wall with primary and eutectic Si particles, there is an agglomeration of three or more primary Si particles, AlSi foam without the blowing agent; (c) a single angular primary Si and eutectic Si particles, (d) eutectic Si particles with sharp edges, most of them are in contact with each other

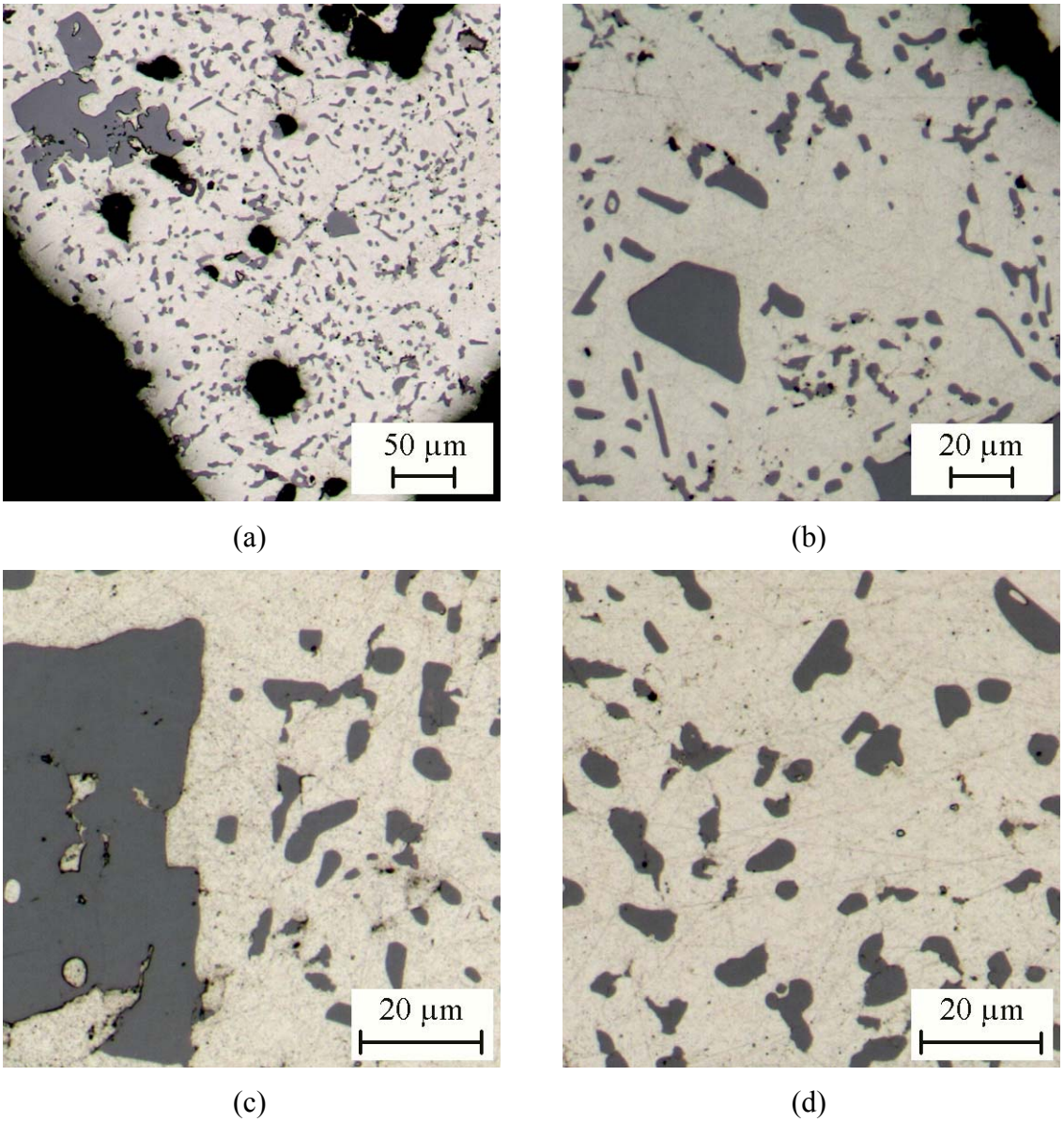

Figure 4.45. Optical micrographs showing the cross sections of cell walls: AlSi foam without the blowing agent after SHT; (a) three or more primary silicon particles agglomerated during solidification seen on the top left hand side, (b) an individual primary Si particle with rounded edges after SHT heat treatment, (c) the size difference of primary and secondary silicon particles is shown, (d) spheroidizing of secondary Si particles is clearly seen after SHT heat treatment

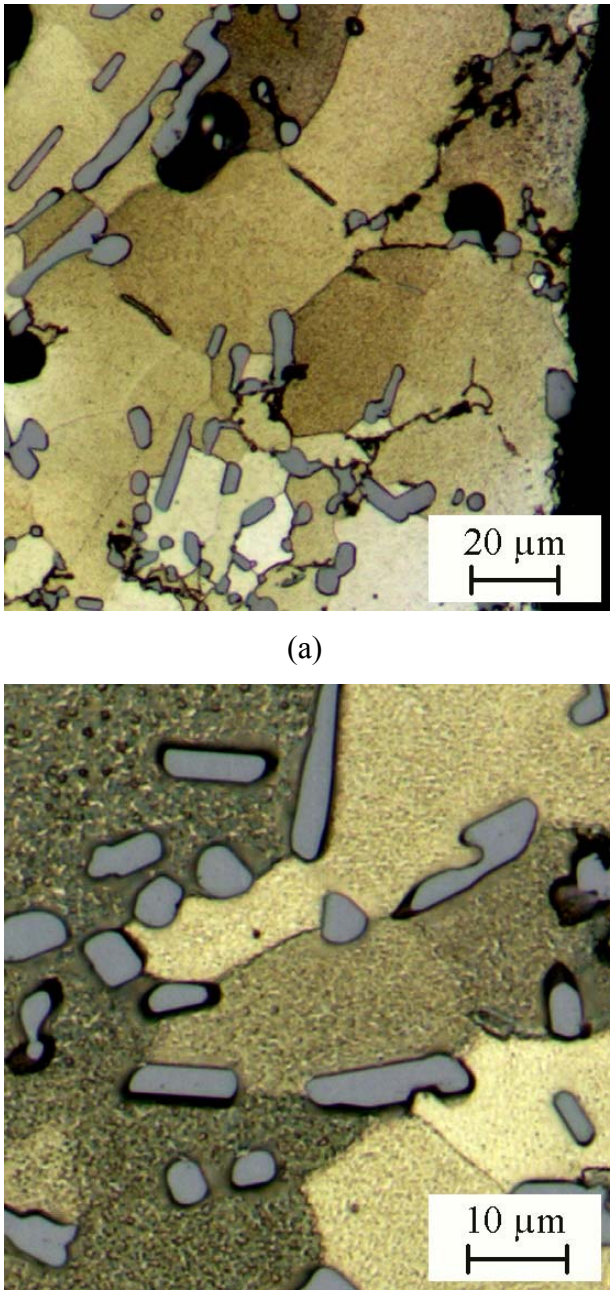

Figure 4.46. Brightfield (no polarization) optical micrographs showing the cross sections of cell walls: AlSi foam without the blowing agent after SHT (1h) and etching; (a) gray eutectic silicon particles surrounded by colored Al alloy matrix, (b) spheroidized Si

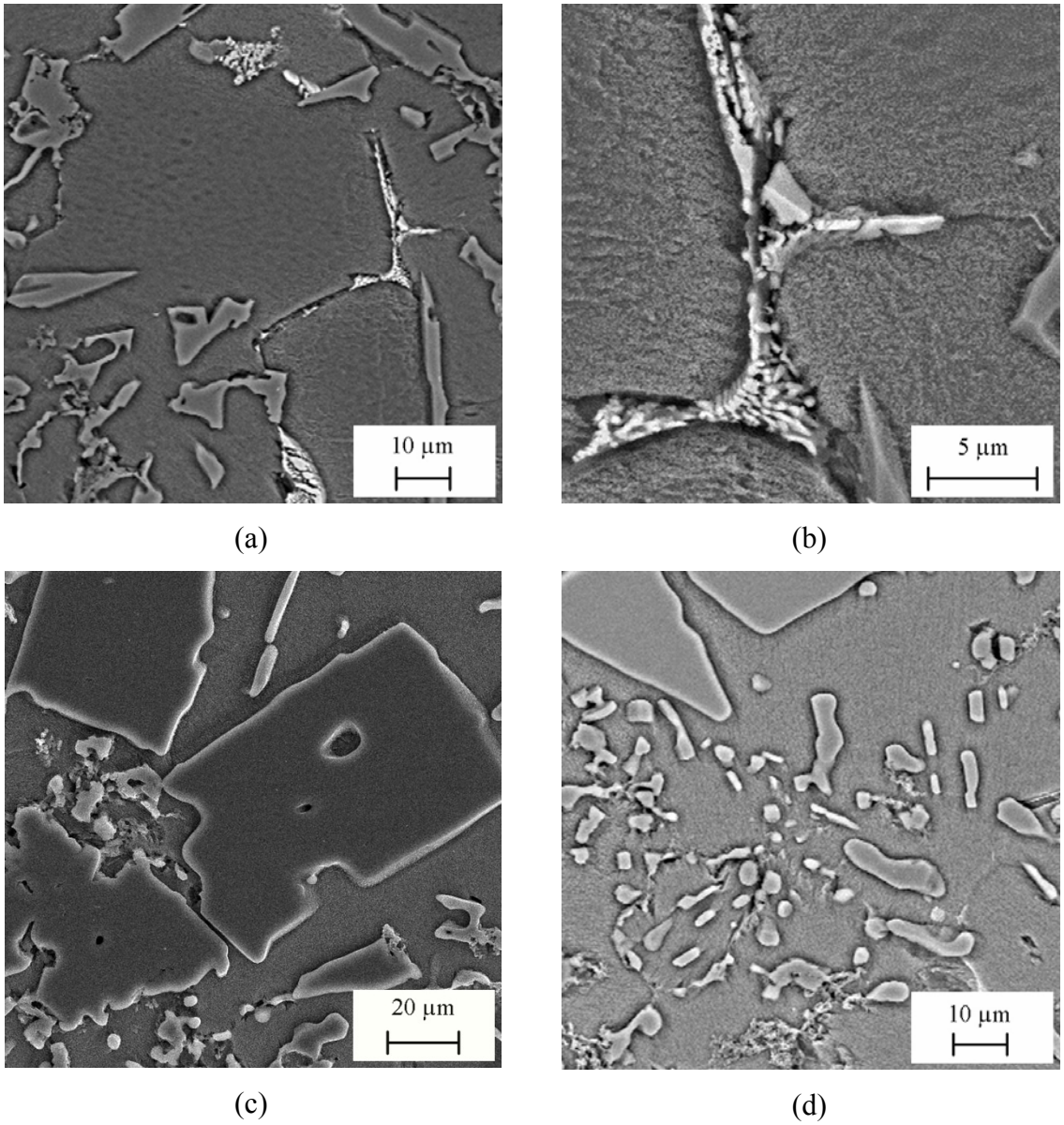

Figure 4.47. SEM micrographs of cross section of cell walls: AlSi foam without the blowing agent; (a) eutectic Si particles and intermetallics precipitated at the grain boundaries, (b) Al_2Cu intermetallic, AlSi foam after SHT (1h); (c) agglomerated primary Si particles, particles are not in contact, (d) spheroidized eutectic Si particles and primary Si particles with rounded edges

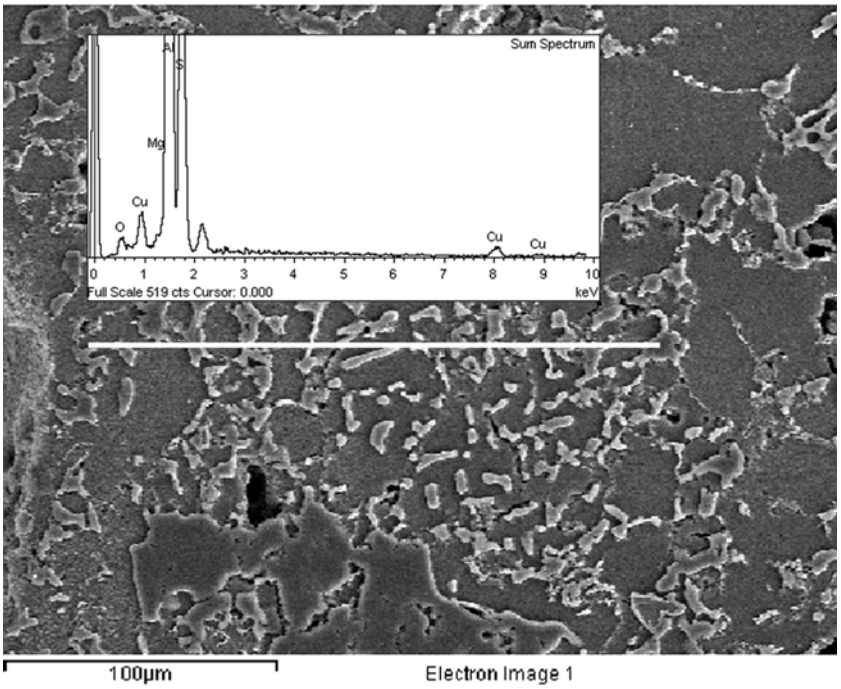

(a)

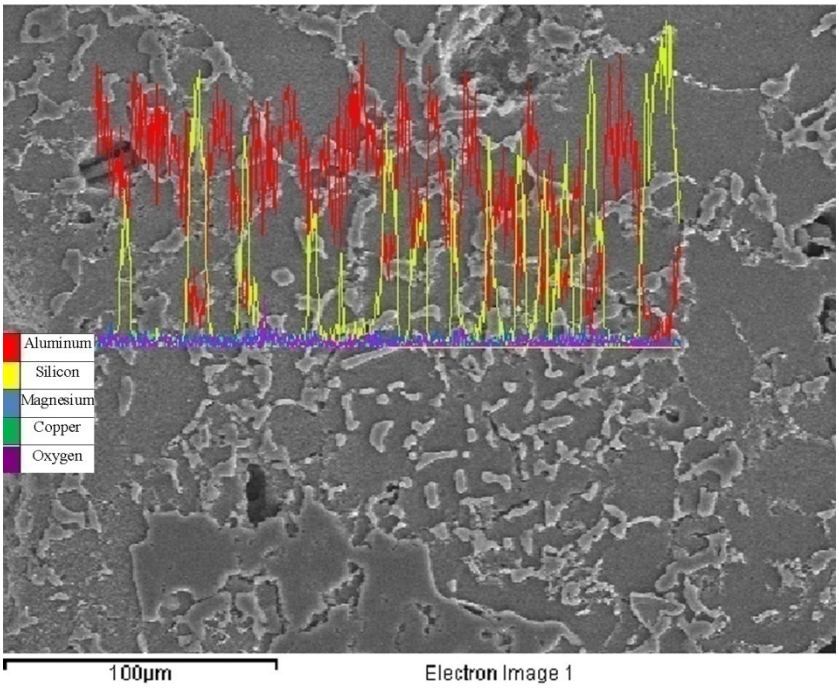

(b)

Figure 4.48. Spectrum analyses of AlSi foam without the blowing agent: (a) analysis is performed along the white line showing the presence of Al, Si, Cu and Mg elements, (b) distribution of the elements along the same line, note the yellow and red peaks on the line as it crosses the eutectic Si and Al on the matrix

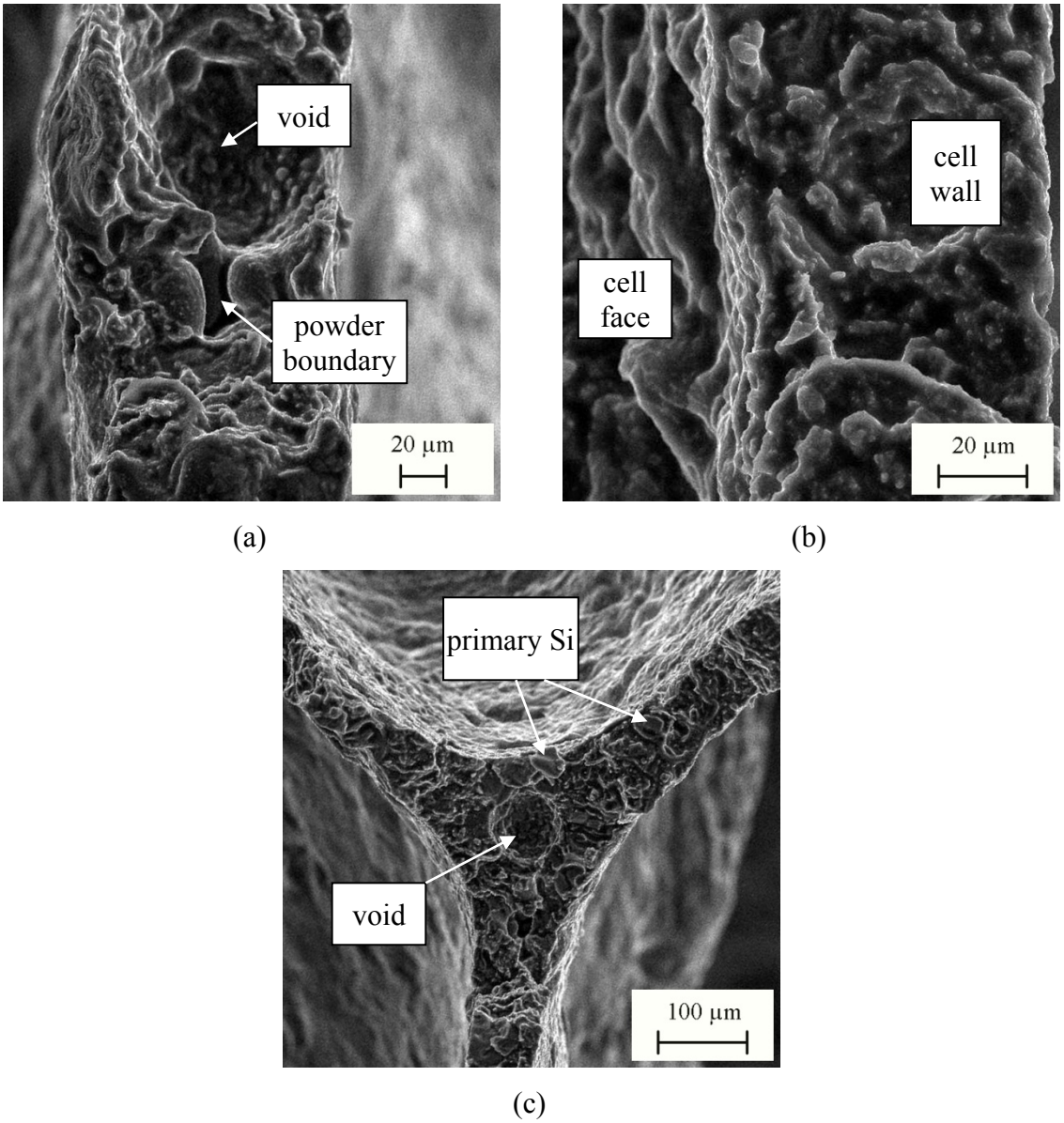

Figure 4.49. SEM micrographs of fractured cell walls of AlSi foam after moderate etching: (a) decohesive rupture from retained powder boundaries and voids, (b) cell wall and cell face, cell wall thickness is approximately 60 μm, (c) Plateau region, primary Si particles and voids are seen at the fracture interface

4.3.3. Compression behavior of the foams

The stress-strain curves of AlSi foams are shown in Figure 4.50. For comparison of the behavior after full heat treatment, foams with similar relative densities were selected. The curves for the foams are characteristic for brittle foams. First, they show a stress peak when strained up to two per cent. There is a drop in stress after the peak, followed by a wavy curve where the stress goes up and down sharply around an average value. This behavior continues with increasing strain and the deformation is in a brittle manner. When cell walls fracture and do not bend plastically, their contribution to densification decreases. Foam material either fell off to the compression plate after crushing or become like powder and fill the empty cells of the foam. The deformation observed was progressive. It started from the low-density regions at the top of the foam and continued up to 40 per cent without any collapse at the bottom of the foam. This behavior can be better understood with the two examples given in Figure 4.51. The black region at the top of the macrographs represents the initial height of the foams. First foam was compressed to 25 per cent and second foam to 40 per cent. After deformation, the foams were cut from the center in order to observe the cross sections. Most of the deformed metal was lost during cutting but still a deformed layer, which is quite dense, can be observed at the top of the foams. No evidence of collapse is observed below the deformation area. Generally, for closed cell foams, it is expected that, after a high deformation (40-60 per cent) stress will raise, since density of the foam is also increasing continuously. However, as seen in Figure 4.50b, AlSi foams can be crushed to as high as 80 per cent deformation without any significant hardening behavior. This can be an advantage for energy absorption applications, e.g. automobile crash-boxes, where the requirement for constant deceleration can be achieved.

After heat treatment, collapse stress of the foam increased approximately 50 per cent (Figure 4.53). However, this could not be verified by microhardness measurements. There was no significant increase in hardness of the matrix, indicating the increased strength of the foam is not primarily because of heat treatment only. The strengthening may also be because of spheroidizing and the strains induced during quenching of the foam in SHT.

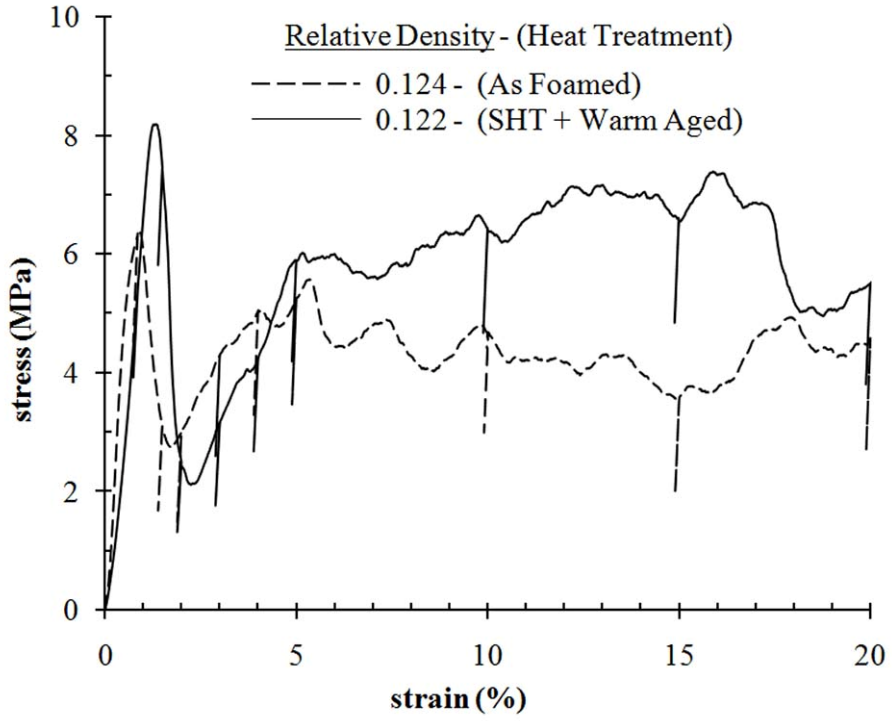

(a)

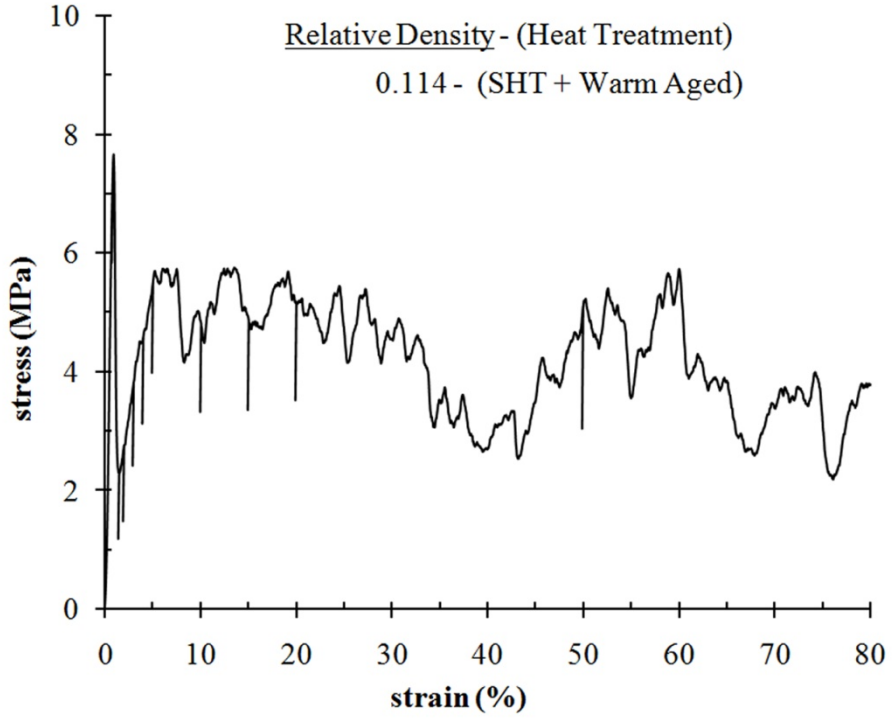

(b)

Figure 4.50. Compression stress-strain curves: (a) heat treated and as foamed hypereutectic AlSi foams, (b) compression behavior of heat treated hypereutectic AlSi foam up to 80 per cent strain

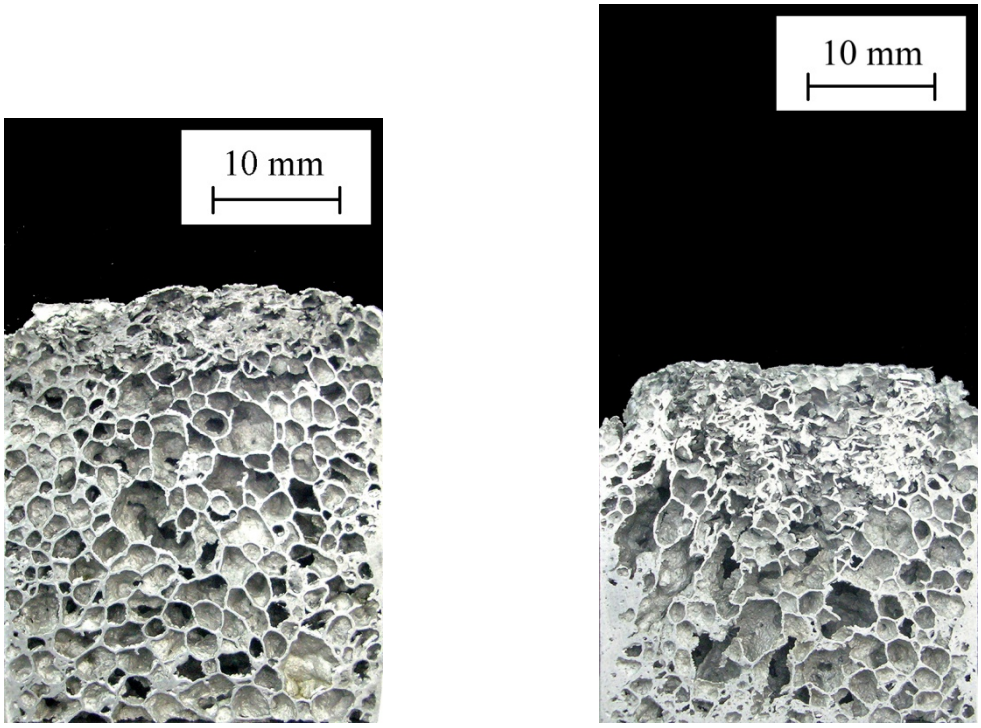

(a) (b)

Figure 4.51. Progressive collapse behavior of AlSi foams, black areas represent initial foam height: (a) 20 per cent deformation, (b) 50 per cent deformation

As expected, collapse stress and stiffness increased with increasing density (Figure 4.52 and Figure 4.53). These two values are well described by scaling relations given by Gibson and Ashby [1, 3] according to:

$$E^* = 77.82\left(\frac{\rho^*}{\rho_s}\right)^2 \tag{4.19}$$

where E^* is the stiffness and ρ^*/ρ_s is the relative density of the foam. The collapse stress is related to the relative density by:

$$\sigma_{cs} = 363.8\left(\frac{\rho^*}{\rho_s}\right)^2 \tag{4.20}$$

where σ_{cs} is the compression strength of the foam.

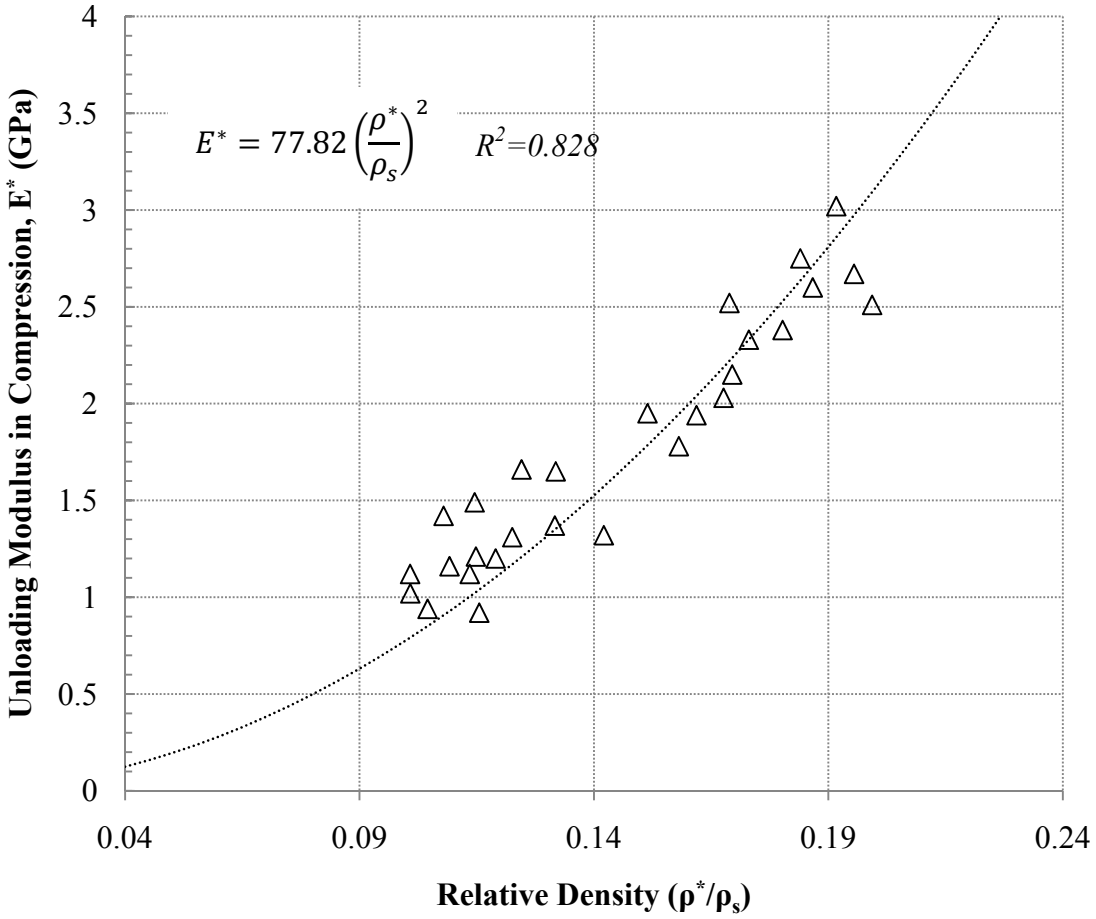

Figure 4.52. Effect of relative density on unloading modulus of hypereutectic AlSi foams

The density of the cell wall material was taken to be 2.7 gr/cm^3. An estimation of the yield strength of the solid material can be made by assuming $\sigma_y = HV/3$. For as foamed and heat treated samples this corresponds to $\sigma_y \approx 390$ MPa. If the modulus of the solid material is taken as 70 GPa and yield strength 390 MPa Eqs. 4.19 and 4.20 can be written as:

$$\frac{E^*}{E_s} = 1.112\left(\frac{\rho^*}{\rho_s}\right)^2 \tag{4.21}$$

$$\frac{\sigma_{cs}}{\sigma_y} = 0.933\left(\frac{\rho^*}{\rho_s}\right)^2 \tag{4.22}$$

which gives the normalized modulus and normalized compression strength of AlSi foams and hence allows for a comparison with the data of AlMgSi foams.

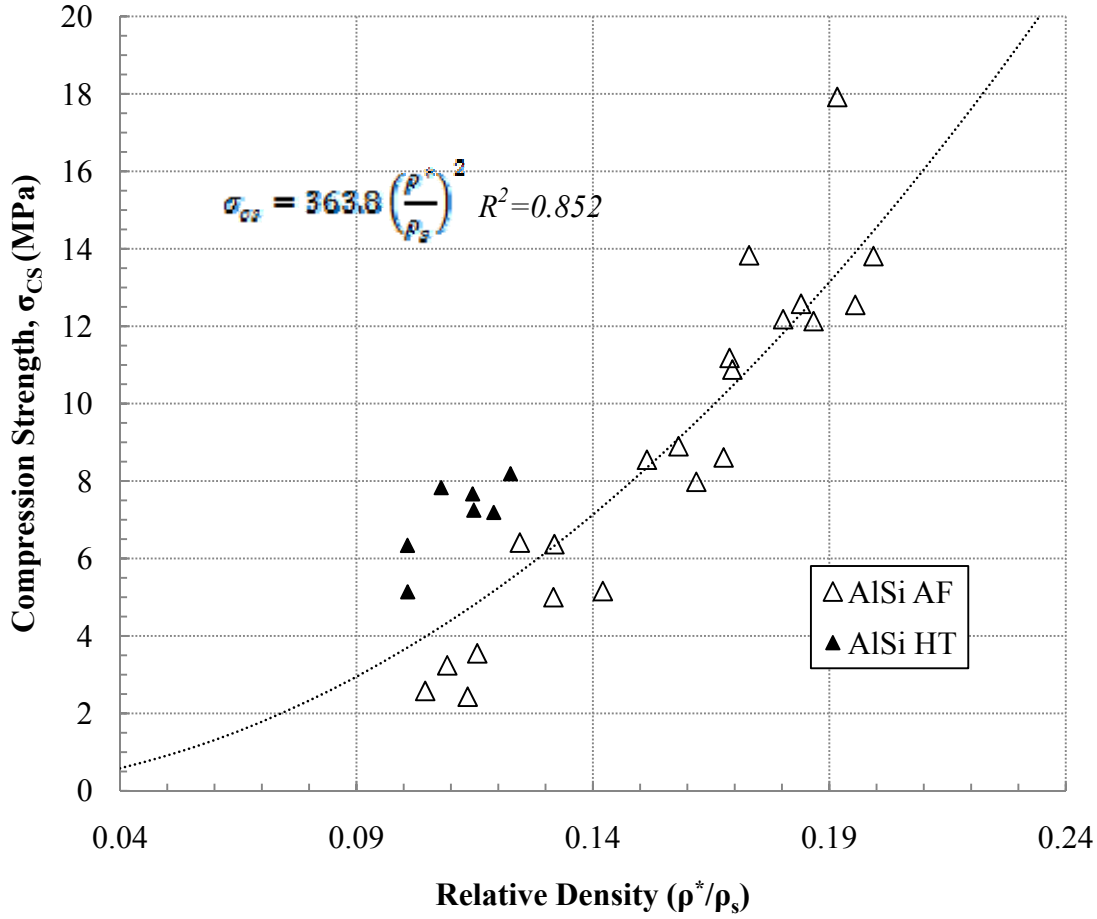

Figure 4.53. Effect of relative density and heat treatment on compression strength of hypereutectic AlSi foams

CONCLUSIONS

The role of ceramic particle addition and metallurgical condition of the matrix alloy on the mechanical properties of closed cell AlMgSi foams were studied. First, AlMgSi foams were manufactured by PCM method and their macro- and microstructural properties were investigated. Mechanical testing of the foams followed the metallographic analyses. Finally, a comparison of the results with applicable scaling models and similar studies on elastic stiffness and compression strength of the foams were presented.

Mechanical tests of AlMgSi foams and AlMgSi foams reinforced with increasing amounts of Al_2O_3 showed that both foams could be hardened by heat treatment. Hardness values of the foams could be increased from HV 66±9 (after foaming) to HV 117±9 (fully hardened). Compression strength and unloading moduli of the foams increased non-linearly with relative density. Increasing the amount of Al_2O_3 to 10 vol. per cent did not affect the compression strength and stiffness of the foams positively. However, for the same relative density, unloading moduli and compression strength increased with 3 and 5 vol. per cent Al_2O_3 additions. Correlations made relating the mechanical properties to relative density showed that the contribution of the cell faces to the mechanical properties of the foams was low hence the foams behaved essentially as open-cell foams.

Foamability of pure Al-TiH_2 powder compacts is low. Generally, low melting point Al alloy - TiH_2 powder compacts are foamed by using PCM method. In an effort to increase the foamability and structural quality of Al foams, different ceramic particles (Al_2O_3 and B_4C) were added to the Al - TiH_2 mixtures. Precursors were prepared by powder extrusion at elevated temperatures below the decomposition temperature of TiH_2. Powder extrusion was found to be a suitable method for precursor manufacturing since powders were both compacted and shaped before foaming. Addition of ceramic particles increased foam expansion. The particles were generally attached to the cell walls forming a surface layer at the liquid-gas interface. Composite foams had higher number of cells with thinner cell walls. Cells were smaller and relatively homogeneously distributed. There was no significant drainage at the bottom in contrast to Al foams. Ceramic particles not only increased foam expansion but also increased the stabilization during foaming and the

subsequent cooling stage. Degree of wetting for particles in Al-B_4C system was better than Al-Al_2O_3. However, in both systems wetting was generally poor. The relation between wetting and stabilization was not fully clear but partial wetting seemed to give stabilization to the composite foams.

A different Al alloy - TiH_2 system with hypereutectic composition was successfully foamed by PCM technique. The interesting feature observed in the microstructure of the foams was the spheroidization of the plate like eutectic Si after SHT. Primary Si particles remained essentially unchanged but the edges were rounded. The behavior of the foams in compression was similar to brittle foams owing to the high Si content of the alloy. During deformation, no significant increase in forces was observed up to 80 per cent deformation although the foams were closed cell. Compression strength and unloading modulus of the foams were higher than AlMgSi foams. By heat treatment compression strength of these foams was increased up to 50 per cent while the stiffness remained unchanged.

REFERENCES

1. Gibson, L. J. and M. F. Ashby, *Cellular Solids, Structure and Properties, Second Edition*, Cambridge University Press, 1999.

2. Curran, D., *Metal Foams*, http://www.msm.cam.ac.uk/mmc/people/old/dave/dave.html, 2005.

3. Ashby, M. F., A. G. Evans, N. A. Fleck, L. J. Gibson, J. W. Hutchinson and H. N. G. Wadley, *Metal Foams: A Design Guide*, Butterworth Heineman, 2000.

4. Sosnick, B., *Process for Making Foamlike Mass of Metal*, United States Patent No. 2,434,775, 1948.

5. Banhart, J., "Manufacture, Characterisation and Application of Cellular Metals and Metal Foams", *Progress in Materials Science,* Vol. 46, pp. 559-632, 2001.

6. Elliott, J. C., *Method of Producing Metal Foam*, United States Patent No. 2,751,289, 1956.

7. Alen, B. C., *Method of Making Foamed Metal*, United States Patent No. 3,087,807, 1963.

8. Hardy, P. W. and G. W. Peisker, *Method of Producing a Lightweight Foamed Metal*, United States Patent No. 3,300,296, 1967.

9. Niebyski, L. M., C. P. Jarema and T. E. Lee, *Preparation of Metal Foams with Viscosity Increasing Gases*, United States Patent No. 3,816,952, 1974.

10. Speed, S.E., *Foaming of Metal by the Catalyzed and Controlled Decomposition of Zirconium Hydride and Titanium Hydride*, United States Patent No. 3,981,720, 1976.

11. Akiyama, S., H. Ueno, K. Imagawa, A. Kitahara, S. Nagata, K. Morimoto, T. Nishikawa and M. Itoh, *Foamed Metal and Method of Producing Same*, United States Patent No. 4,713,277, 1987.

12. Jin, I., L. D. Kenny and H. Sang, *Method of Producing Lightweight Foamed Metal*, Unites States Patent No. 4,973,358, 1990.

13. Jin, I., L. D. Kenny and H. Sang, *Stabilized Metal Foam Body*, Unites States Patent No. 5,112,697, 1992.

14. Baumeister, J. and H. Schrader, *Methods for Manufacturing Foamable Metal Bodies*, United States Patent No. 5,151,246, 1992.

15. Jin, I., L. D. Kenny and H. Sang, *Lightweight Metal with Isolated Pores and Its Production*, United States Patent No. 5,221,324, 1993.

16. Kenny, L. D. and M. Thomas, *Process for Shape Casting of Particle Stabilized Metal Foam*, United States Patent No. 5,281,251, 1994.

17. Sang, H., L. D. Kenny and I. Jin, *Process for Producing Shaped Slabs of Particle Stabilized Foamed Metal*, United States Patent No. 5,334,236, 1994.

18. Wörz, H. and H. P. Degischer, *Process for the Production of Foamable Metal Elements*, United States Patent No. 5,393,485, 1995.

19. Thomas, M., D. Kenny and H. Sang, *Particle-Stabilized Metal Foam and Its Production*, United Stated Patent No. 5,622,542, 1997.

20. Schörghuber, F., F. Simancik and E. Hartl, *Method of Producing Molded Bodies of a Metal Foam*, United States Patent No. 5,865,237, 1999.

21 Banhart, J., *Metal Foam Info*, http://www.metalfoam.net/, 2008.

22. Thomas, V., A. Poellmann, K. Mueller and U. Bahrke, *Apparatus and Process for Making Cut Extruded Hollow Profiles*, United States Patent No. 5,927,129, 1999.

23. Seeliger, H. W. and W. Bunsmann, *Component Made From a Metallic Foam Material*, United States Patent No. 6,090,232, 2000.

24. ERG Materials and Aerospace Corporation, *ERG Duocel Reticulated Carbon, Ceramic and Metal Foam*, http://ergaerospace.com/, 2008.

25. Rioja, R. J., M. G. Chu, G. J. Hildeman, D. D. Leon and R. J. Kozarek, *Method and Apparatus for Producing A Porous Metal via Spray Casting*, United States Patent No. 6,250,362, 2001.

26. Yu, C. J., H. H. Eifert, J. Banhart and J. Baumeister, "Metal Foaming by A Powder Metallurgy Method: Production, Properties and Applications", *Materials Research Innovations*, Vol. 2, No. 3, pp. 181-188, 1998.

27. Duarte, I. and J. Banhart, "A Study of Aluminium Foam Formation - Kinetics and Microstructure", *Acta Materialia*, Vol. 48, pp. 2349-2362, 2000.

28. Baumgartner, F., I. Duarte and J. Banhart, "Industrialization of Powder Compact Foaming Process", *Advanced Engineering Materials*, Vol. 2, No. 4, pp. 168-174, 2000.

29. Matijasevic, B and J. Banhart, "Improvement of Aluminium Foam Technology by Tailoring of Blowing Agent", Sc*ripta Materialia*, Vol. 54, pp. 503-508, 2006.

30. Körner, C., F. Berger, M. Arnold, C. Stadelmann, and R. F. Singer, "Influence of Processing Conditions on Morphology of Metal Foams Produced from Metal Powder", *Materials Science and Technology*, Vol. 16, No. 7/8, pp. 781-784, 2000.

31. Elzey, D. M. and H. N. G. Wadley, “The Limits of Solid-State Foaming”, *Acta Materilia*, Vol. 49, pp. 849-859, 2001.

32. Elbir, S., S. Yılmaz, A. K. Toksoy, M. Güden, and I. W. Hall, "SiC-particle Aluminum Composite Foams Produced by Powder Compacts: Foaming and Compression Behavior", *Journal of Materials Science*, Vol. 38, pp. 4745-4755, 2003.

33. Kennedy, A. R. and S. Asavavisithchai, "Effects of TiB_2 Particle Addition on the Expansion, Structure and Mechanical Properties of PM Al Foams", *Scripta Materialia*, Vol. 50, pp. 115-119, 2004.

34. Kennedy, A. R. and S. Asavavisithchai, "Effect of Ceramic Particle Additions on Foam Expansion and Stability in Compacted Al-TiH_2 Powder Precursors", *Advanced Engineering Materials*, Vol. 6, No. 6, pp. 400-402, 2004.

35. Asavavisithchai, S., A. R., Kennedy, "The Effect of Mg Addition on the Stability of Al-Al_2O_3 Foams Made by A Powder Metallurgy Route", *Scripta Materialia,* Vol. 54, pp. 1331-1334, 2006.

36. Esmaeelzadeh, S., A. Simchi and D. Lehmus, "Effect of Ceramic Particle Addition On the Foaming Behavior, Cell Structure and Mechanical Properties of P/M AlSi7 Foam", *Materials Science and Engineering A*, Vol. 424, pp. 290-299, 2006.

37. Haibel, A., A. Rack and J. Banhart, "Why Are Metal Foams Stable?", Applied Physics Letters, Vol. 89, No. 154102, pp. 1-3, 2006.

38. Haesche, M., J. Weise, F. G. Moreno and J. Banhart, "Influence of Particle Additions on the Foaming Behavior of AlSi11/TiH_2 Composites Made by Semi-Solid Processiong", *Materials Science and Engineering A*, Vol. 480, pp. 282-288, 2008.

39. Körner, C., M. Arnold and R. F. Singer, "Metal Foam Stabilization by Oxide Network Particles", *Materials Science and Engineering A*, Vol. 396, pp. 28-40, 2005.

40. Asavavisithchai, S., A. R. Kennedy, "Effect of Powder Oxide Content on the Expansion and Stability of PM-Route Al Foams", *Journal of Colloid and Interface Science*, Vol. 297, pp. 715-723, 2006.

41. Banhart, J., "Metal Foams: Production and Stability", *Advanced Engineering Materials*, Vol. 8, No. 9, pp. 781-794, 2006.

42. Dudka, A., F. G. Moreno, N. Wanderka and J. Banhart, "Structure and Distribution of Oxides in Aluminium Foam", *Acta Materialia*, Vol. 56, pp. 3990-4001, 2008.

43. Kennedy, A. R., "Effects of Foaming Configuration on Expansion", *Journal of Materials Science*, Vol. 39, pp. 1143-1145, 2004.

44. Banhart, J., "Manufacturing Routes for Metallic Foams", *JOM*, Vol. 52, No. 12, pp. 22-27, 2000.

45. Mathers, G., *The Welding of Aluminium and its Alloys,* CRC Press LLC, 2000.

46. Von Zeppelin, F., M. Hirscher, H. Stanzick and J. Banhart, "Desorption of Hydrogen from Blowing Agents Used for Foaming Metals", *Composite Science and Technology*, Vol. 63, pp. 2293-2300, 2003.

47. Kennedy, A. R., "The effect of TiH_2 Heat Treatment on Gas Release and Foaming in Al- TiH_2 Preforms", *Scripta Materialia*, Vol. 47, pp. 763-767, 2002.

48. Bhosle, V., E. G. Baburaj, M. Miranova and K. Salama, "Dehydrogenation of TiH_2", *Materials Science and Engineering A*, Vol. 356, pp. 190-199, 2003.

49. Lehmhus, D. and G. Rausch, "Tailoring Titanium Hydride Decomposition Kinetics by Annealing in Various Atmospheres", *Advanced Engineering Materials*, Vol. 6, No. 5, pp. 313-330, 2004.

50. Matijasevic-Lux, B, J. Banhart, S. Fiechter, O. Görke and N. Wanderka, "Modification of Titanium Hydride for Improved Aluminium Foam Manufacture", *Acta Materialia*, Vol. 54, pp. 1887-1900, 2006.

51. Moreno, F. G., N. Babcsan and J. Banhart, “X-ray Radioscopy of Liquid MetalfoamsÇ Influence of Heating Profile, Atmosphere and Pressure”, *Colloids and Surfaces A*, Vol. 263, pp. 290-294, 2005.

52. Kaptay, G., “Interfacial Criteria for Stabilization of Liquid Foams by Solid Particles”, *Colloids and Surfaces A*, Vol. 230, pp. 67-80, 2004.

53. Wübben, T., H. Stanzick, J. Banhart and S. Odenbach, “Stability of Metallic Foams Studied Under Microgravity”, *Journal of Physics: Condensed Matter*, Vol. 15, pp. 427-433, 2003.

54. Wübben, T. and S. Odenbach, “Stabilisation of Liquid Metallic Foams by Solid Particles”, *Colloids and Surfaces* A, Vol. 266, pp. 207-213, 2005.

55. Koza, E., M. Leonowicz, S. Wojciechowski and F. Simancik, “Compressive strength of aluminum foams”, *Material Letters,* Vol. 58, pp. 132-135, 2003.

56. Kriszt, B., B. Foroughi, K. Faure and H. P. Degischer, “Behavior of Aluminium Foam Under Uniaxial Compression”, Materials Science and Technology, Vol. 16, pp. 792-796, 2000.

57. Andrews, E., W. Sanders and L. J. Gibson, “Compressive and Tensile Behavior of Aluminum Foams”, Materials Science and Engineering A, Vol. 270, pp. 113-124, 1999.

58. Bart-Smith, H., A. F. Bastawros, D. R. Mumm, A. G. Evans, D. J Sypeck and H. N. G. Wadley, “Compressive Deformation and Yielding Mechanisms in Cellular Al Alloys Determined Using X-ray Tomography and Surface Strain Mapping”, *Acta Materialia*, Vol. 46, No. 10, pp. 3583-3592, 1998.

59. Banhart, J.and J. Baumeister, “Deformation Characteristics of Metal Foams”, *Journal of Materials Science*, Vol. 33, pp. 1431-1440, 1998.

60. Gergely, V. and B. Clyne, "The FORMGRIP Process: Foaming of Reinforced Metals by Gas Release in Precursors", *Advanced Engineering Materials*, Vol. 2, No. 4, pp. 175-178, 2000.

61. Lehmhus, D. and M. Busse, "Potential New Matrix Alloys for Production of PM Aluminium Foams", *Advanced Engineering Materials*, Vol. 6, No. 6, pp. 391-396, 2004.

62. Lehmhus, D. and J. Banhart, "Properties of heat-treated aluminium foams", *Materials Science and Engineering A*, Vol. 349, pp. 98-110, 2003.

63. Degischer, H. P. and B. Kriszt, eds., *Handbook of Cellular Metals: Production, Processing, Applications*, Wiley-VCH Verlag GmbH & Co. KGaA, 2002.

64. Gergely, V., H. P. Degischer and T.W. Clyne, "Chapter 3.30 Recycling of MMCs and production of metallic foams", *Comprehensive Composite Materials*, Vol. 3, pp. 797-829, 2000.

65. Baker, H., ed., *ASM Handbook: Volume 3: Alloy Phase Diagrams*, ASM International, 10th edition, 1992.

66. Boz, K., *Control of Process Parameters in Squeeze Vasting of An Aluminum Piston*, M.S. Thesis, Boğaziçi University, 1996.

67. Mortensen, A., A. Needleman and S. Suresh, *Fundamentals of Metal-Matrix Composites*, Butterworth-Heinemann, 1993.

68. Çıtak, H. C., *Investigation of extrudability of different aluminum alloys by using the method of hot extrusion*, M.S. Thesis, Boğaziçi University, 2005.

69. Ashby, M.F., "Criteria for Selecting The Components of Composites", *Acta metallurgica et materialia*, Vol. 41., No. 5, pp. 1313-1335, 1993.

70. McCullough, K.Y.G., N.A. Fleck and M.F. Ashby, "Uniaxial Stress-Strain Behavior of Aluminium Alloy Foams", *Acta Materialia*, Vol. 47, No. 8, pp. 2323-2330, 1999.

71. Rooy, E. L., *ASM Handbook: Volume 2: Properties and Selection : Nonferrous Alloys and Special-Purpose Materials*, *Section: Introduction to Aluminum and Aluminum Alloys*, ASM International, 10th edition, 1992.

72. Donaldson, S. L. and D. B. Miracle, *ASM Handbook Composites Volume 21*, ASM International; 10th edition, 2001.

73. Shackelford, J. F. and W. Alexander, eds, *Materials Science and Engineering Handbook*, CRC Press LLC, 2001.

74. Totten, G. E., D. S. MacKenzie, eds., *Handbook of Aluminum, Vol. 1, Physical Metallurgy and Processes*, Marcel Dekker, Inc., 2003.